2

NASA CR-137467

APPLIED SCIENCE ASSOCIATES, INC.

105 EAST CHATHAM STREET
POST OFFICE BOX 949
APEX, NORTH CAROLINA 27502
PHONE (919) 362-7256

(NASA-CR-137467) OCEAN DYNAMICS STUDIES Final Report (Applied Science Associates, Inc., Apex, N.C.) 185 p HC $12.25 CSCL 08C G3/13 46528 Unclas N74-30842

OCEAN DYNAMICS STUDIES

Final Report
May, 1974

PRICES SUBJECT TO CHANGE

Prepared Under
NASA CONTRACT NO. NAS6-2307
for
NATIONAL AERONAUTICS AND SPACE ADMINISTRATION
WALLOPS STATION
WALLOPS ISLAND, VIRGINIA 23337

Reproduced by
NATIONAL TECHNICAL
INFORMATION SERVICE
US Department of Commerce
Springfield, VA. 22151

AUG 1974
RECEIVED
NASA STI FACILITY
ACQ BRANCH

185

FOREWORD

This report was prepared for the National Aeronautics and Space Administration by the Applied Science Associates under Contract NAS6-2307. J. T. McGoogan and H. R. Stanley, of NASA Wallops Station, acted as NASA coordinators.

The study was performed both at the Applied Science Associates and at North Carolina State University. N. E. Huang served as project director. The theoretical part was assisted by Professor C. C. Tung of the North Carolina State University at Raleigh as a conslultant, Dr. N. Guttman worked on the dispersive relation, and Mr. S. R. Long worked on the capillary gravity waves interaction with currents. The experimental part was carried out at the North Carolina State University through a sub-contract to Professor F. Y. Sorrell. G. V. Strum and S. R. Long also worked on the experiments.

ABSTRACT

This report presents the results of a one-year study of current-wave interactions. The subjects treated include both theoretical and experimental parts.

In the theoretical study, three problems are discussed. The first is the dispersive relation of a random gravity-capillary wave field. It is concluded that no universal relationship can be found for all the sea states. The second problem is on the changes of the statistical properties of surface waves under the influence of currents. The possibility of utilizing such changes for remote sensing of surface currents is also discussed. The third problem is on the interaction of capillary-gravity with the non-uniform currents.

The experimental study deals with the measurement of wave-current interaction and trying to establish the feasibility of using such measurements for remote sensing of surface currents. A laser probe was developed to measure the surface statistics. In a laboratory, the possibility of using current-wave interaction as a means of current measurement was demonstrated.

CONTENTS

PART I

THEORETICAL STUDIES

The theoretical study consists of three parts. The first part discusses the non-linear dispersive relation in a random gravity-capillary wave field. The result indicates that the dispersive relation is a function of the energy spectrum; therefore, a universal dispersive relationship seems impossible. The second part deals with the statistical properties of surface waves under the influence of currents. The changes due to currents can be used as an additional method to measure surface current. The third part dicusses the interaction of capillary-gravity waves with non-uniform current. A perturbation scheme is used to overcome the difficulty of multiple values of the dispersive relationship in this range of the wave spectrum.

1. Dispersive relation for gravity-capillary waves.

1.1 INTRODUCTION

Looking over the surface of the open ocean, a casual observer notices a seemingly endless moving succession of irregular humps and hollows, or waves. These surface waves are the most common motion at the air-sea interface. They form an oscillatory pattern and travel in all directions and at different speeds.

One characteristic of an oscillatory wave is its period. This quantity is the time interval between passages, at a fixed point, of a given phase of the oscillation. Its reciprocal is the wave frequency n. Since n is a function solely of time, it can be measured relatively easily from a point by noting the elapsed time between the passage of two crests.

Another characteristic is the wave length, or the distance between particles moving in the same phase of the oscillation. The reciprocal of this quantity is the wave number k. Since the wave travels on the two dimensional free surface $\underset{\sim}{x} = (x,y)$, the wave length and directional properties can be combined and represented by the vector wave number $\underset{\sim}{k} = \underset{\sim}{k}(\underset{\sim}{x})$. Measurement of the directional wave length at infinitely many points is necessary to obtain spatial correlations over the two dimensional wave number plane.

The velocity $\underset{\sim}{c}$ at which the wave travels is defined as

$$\underset{\sim}{c} \equiv \frac{n}{\underset{\sim}{k}} \tag{1}$$

Since the frequency n is non-directional and relatively easy to measure, and since the wave number $\underset{\sim}{k}$ is economically and logistically prohibitive to obtain over the free surface, it would be advantageous to find a relationship between n and $\underset{\sim}{k}$.

For a single gravity wave traveling in the x direction, such a relationship can be derived. Consider a two dimensional spatial coordinate system (x,z) where z is measured positively upward and the plane z = 0 represents the mean free surface level as shown in Figure 1. Assuming an incompressible, inviscid fluid, the motion can be regarded as irrotational and is thus controlled by Laplace's equation

$$\nabla^2 \phi\,(x,z,t) = 0 \tag{2}$$

where ϕ is the velocity potential and t is time. By requiring that no motion exist at z = -h, where h is the water depth, and that Bernoulli's linearized equation

$$g\zeta = \frac{\partial \phi}{\partial t} - \frac{p}{\rho} \tag{3}$$

hold at the free surface, (2) can be solved for ϕ. In (3), g is the gravitational acceleration, p is the pressure at the interface, ρ is the density of the water, and ζ is the oscillatory surface elevation

$$\zeta(x,t) = a\cos(kx - nt) \tag{4}$$

where a is the wave amplitude. Bernoulli's equation has been linearized under the assumption that terms of the order of the square of the velocity components are negligible compared to other terms.

The solution to (2) is

$$\phi = -ca\,\frac{\cosh[k(z+h)]}{\sinh(kh)}\sin(kx - nt)\ . \tag{5}$$

Substituting (5) into (3), using (1), and assuming that $k\zeta \ll 1$, i.e., a small wave amplitude assumption,

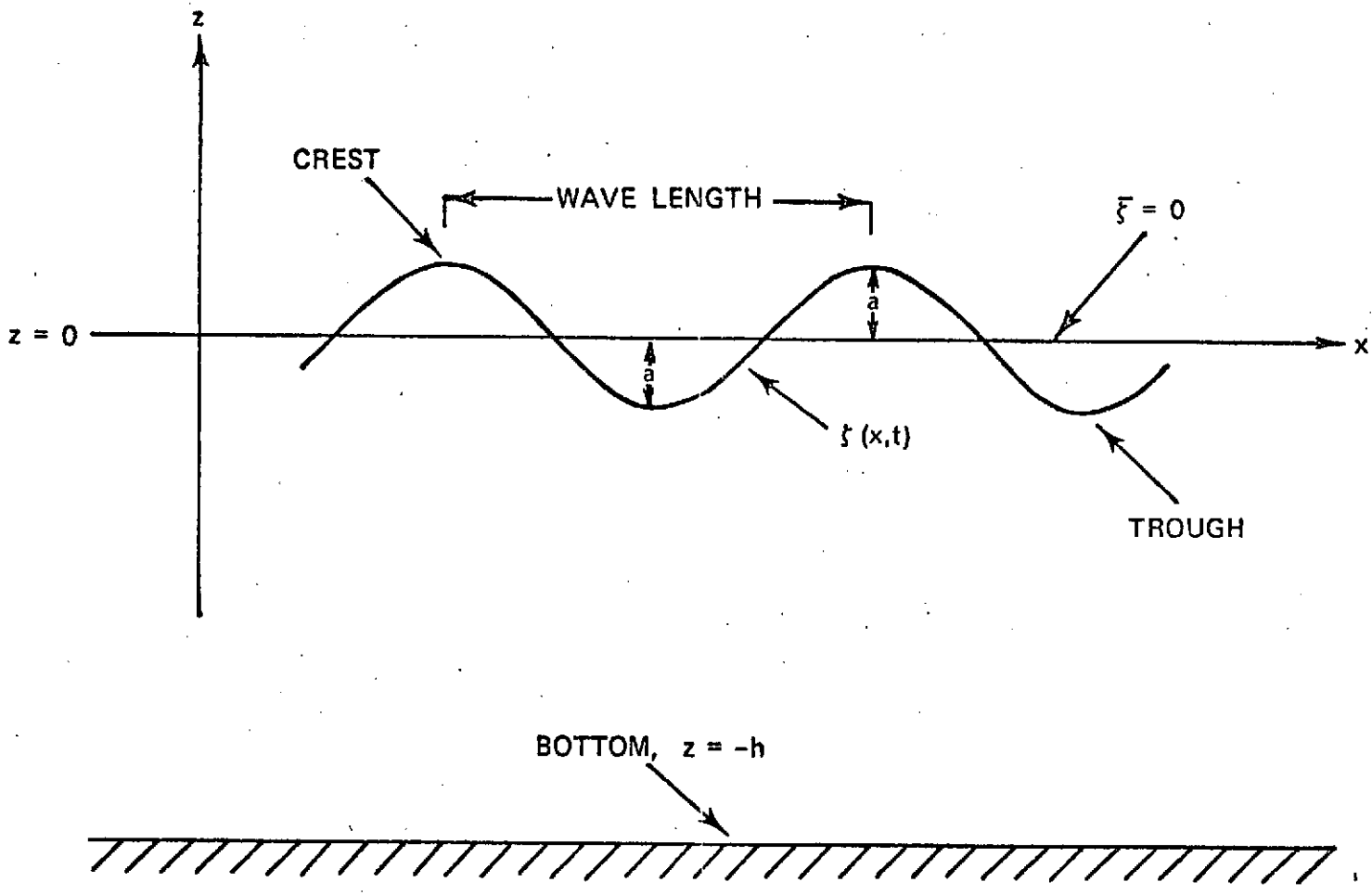

Figure 1. Representation of a single wave

$$[g - c^2 k \coth(kh)]\zeta = - \frac{p}{\rho} \Big|_{\zeta=z} . \qquad (6)$$

If capillary waves are also included, the effect of surface tension must be considered. The difference between the water pressure p and the atmospheric pressure p_a at the interface is a result of surface tension such that

$$p = p_a - \rho\gamma \frac{\partial^2 \zeta}{\partial x^2} \qquad (7)$$

where γ is the ratio of the surface tension to the water density. Equation (7) has been linearized by considering terms of the order of the square of the gradient of the surface elevation in the representation of the surface curvature to be negligible compared to other terms. The atmospheric pressure is assumed to be constant, and the free surface $\zeta = 0$ is taken as a reference level at which $p = 0$. In this situation $p_a = 0$ since the surface tension term vanishes. Thus,

$$p = - \rho\gamma \frac{\partial^2 \zeta}{\partial x^2} . \qquad (8)$$

Substituting (4) into (8) and then (8) into (6) and rearranging,

$$g + \gamma k^2 = c^2 k \coth(kh) . \qquad (9)$$

For deep water waves, h is large and asymptotically

$$\coth(kh) = 1 \qquad (10)$$

so that

$$\frac{g}{k} + \gamma k = c^2 . \qquad (11)$$

Equation (11) is the linearized relationship for the speed of a single wave under the restoring influences of gravity and surface tension.

It is depicted graphically in Figure 2. The speed is a function of the wave length and thus represents the dispersion of the wave. Substituting (1) into (11) results in the dispersive relationship as a function of n and k,

$$n^2 = gk + \gamma k^3 . \qquad (12)$$

Equation (12) is graphically depicted in Figure 3.

It is important to note that (12) is in reality only approximately true since just linear terms are considered. Cole (1968) discusses the general case of periodic motions of slightly non-linear oscillations. He treats various physical problems that are characterized by the presence of a small disturbance which acts over a long time. He shows in his non-linear asymptotic expansion of the solution to these oscillatory problems that a frequency shift from the linear solution will occur, and that this shift is generally a function of the amplitude of the oscillation.

Becoming more specific, Kinsman (1965) discusses the non-linear expansions of the phase speed for single gravity and capillary waves. For gravity waves, the third order expansion includes a perturbation on the linear phase speed that is a function of the square of the amplitude. The capillary wave higher order solution also includes a perturbation on the linear phase speed that is a function of the square of the amplitude. Using (1) to transform these results into frequencies, it is found that even though the restoring forces to the oscillatory waves are different, both the gravity and capillary wave frequencies will exhibit shifts from the linear solution that are dependent upon the square of the amplitude of the waves.

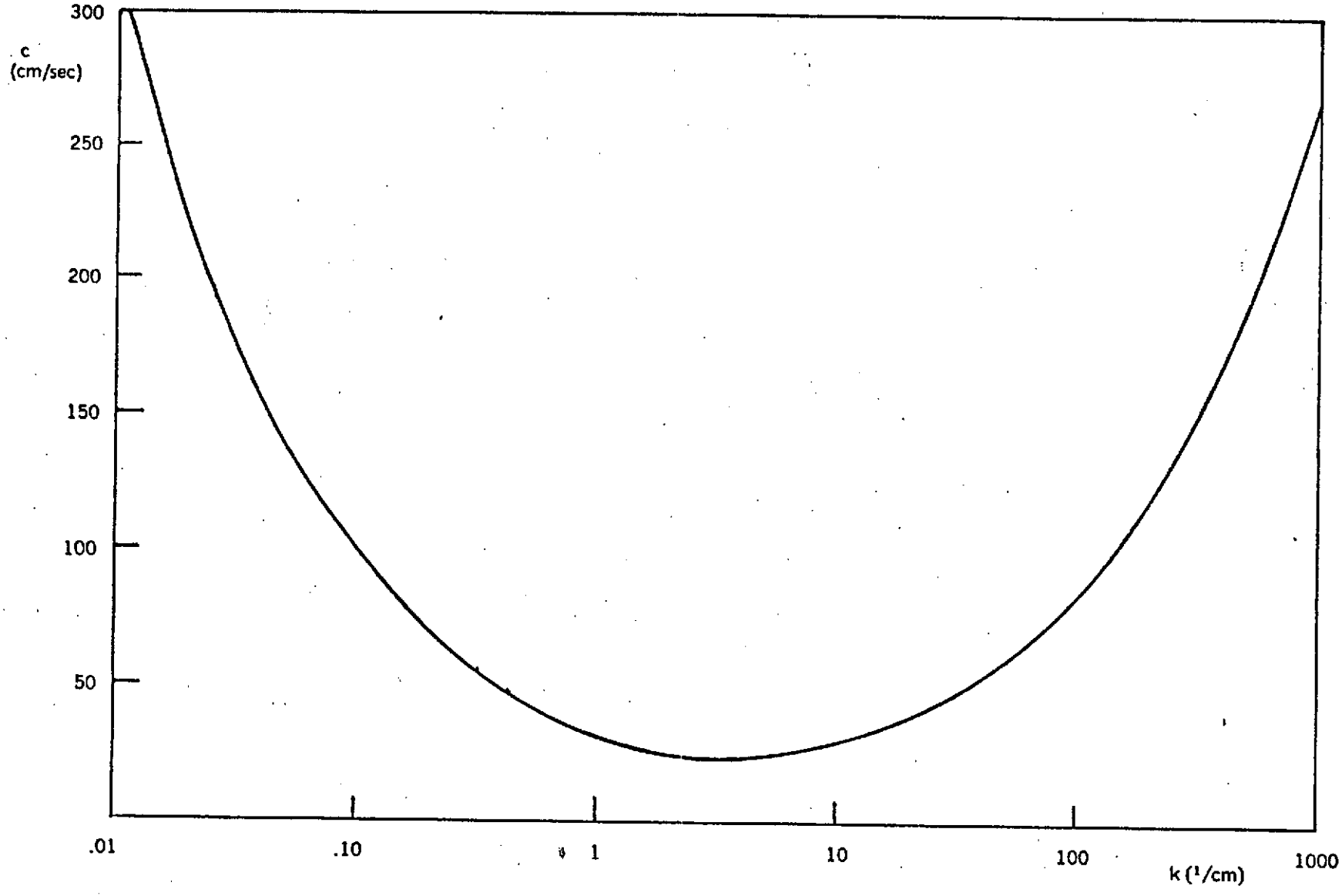

Figure 2. Phase speed c vs. wave number k

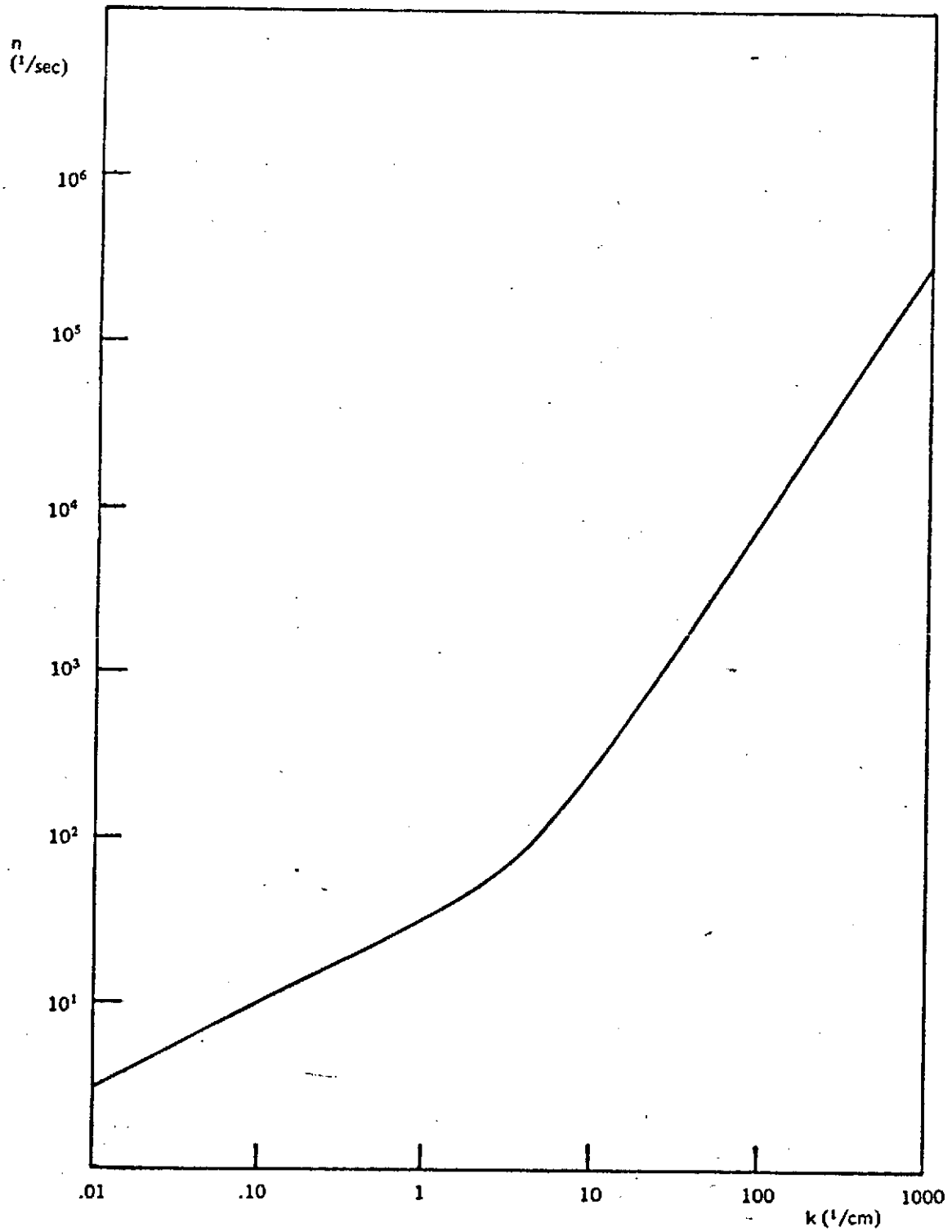

Figure 3. Frequency n vs. wave number k

Comparison of the linear dispersion with observed data was made by Longuet-Higgins et al. (1963) for gravity waves with frequencies up to 4 rad sec^{-1}. They found that the waves appeared a little shorter than those predicted by linear theory. The mean increase in the observed wave number is about 10 percent. The authors note, however, that they are skeptical of the calibration of the instruments. In addition, the buoy used has a diameter that is about one-third the shortest wave length. When the buoy is located near the crest or trough of the shorter waves in the range of the experiment, it will not completely rest on the water surface and slope measurements may be inaccurate. The resulting wave numbers may therefore be inaccurate. These possible errors cast some doubt on the validity of the 10 percent difference between the observed wave numbers and those suggested by linear theory.

Yefimov and Khristoforov (1971) also compared the linear dispersion with observed data for gravity waves with frequencies up to 4 rad sec^{-1}. Their comparison is based on measurements of the velocity spectra at 1 m and 3 m below the surface. They show that for frequencies below 2.5 rad sec^{-1} the waves are slightly shorter than those suggested by linear theory. Above 2.5 rad sec^{-1}, the waves are longer than suggested by linear theory. They emphasize, however, that small deviations from the linear relationship in the low frequency range can be caused by the recording by the measuring equipment of harmonics of the principal oscillation. Additionally, the authors point out that the large deviations between the observed data and the linear theory at frequencies near 4 rad sec^{-1} are the result of the high frequency turbulent regime of the velocity spectra.

Grose (1971) and Grose et al. (1972) measured wave heights relative to a buoy for gravity waves with frequencies up to about 4 rad sec^{-1}. It is shown in these papers that the linear dispersion suggests wave numbers that are too large when compared to values computed from the wave height measurements. In other words, the observed wave numbers are smaller than those predicted by linear theory. The authors state, however, that the measuring technique does not differentiate between fundamental waves and harmonics. All wave components are treated as fundamentals so that errors in the observed dispersive relationship do exist.

Comparison between the linear and observed dispersion in the capillary wave range has, unfortunately, not been made. Experimentation in this area needs to be accomplished and should provide very worthwhile results.

Linearizing the governing equations and boundary conditions decreases the reality of the surface motion but greatly simplifies the mathematics since the principle of superposition is applicable. Any linear combination of solutions to the equations is itself a solution. For example, consider two waves of equal amplitude but slightly differing frequencies and wave numbers traveling in the same direction. Mathematically,

$$\zeta_1 = a \cos(k_1 x - n_1 t) \tag{13}$$

$$\zeta_2 = a \cos(k_2 x - n_2 t) \tag{14}$$

$$k_1 \approx k_2, \quad n_1 \approx n_2 \tag{15}$$

$$k_1 - k_2 \ll k_1, \quad n_1 - n_2 \ll n_1 \ . \tag{16}$$

Each wave travels at its own phase speed. When they meet, however, they interact to form a new wave.

$$\zeta_3 = \zeta_1 + \zeta_2$$

$$= 2a \cos\left[\frac{(k_2-k_1)x}{2} - \frac{(n_2-n_1)t}{2}\right] \cos\left[\frac{(k_1+k_2)x}{2} - \frac{(n_1+n_2)t}{2}\right] \ . \tag{17}$$

From (15) and (16), the argument of the first cosine function of (17) will be small. This term thus serves as a slowly varying amplitude modulator of the second cosine function or basic wave. Writing

$$a' = 2a \cos\left[\frac{(k_2-k_1)x}{2} - \frac{(n_2-n_1)t}{2}\right] \tag{18}$$

and

$$k_3 = \frac{k_1+k_2}{2}, \quad n_3 = \frac{n_1+n_2}{2} \ . \tag{19}$$

(17) can be restated as

$$\zeta_3 = a' \cos(k_3 x - n_3 t) \ . \tag{20}$$

Since k_3 and n_3 must satisfy the dispersion depicted in Figure 3,

$$n_3^2 = gk_3 + \gamma k_3^3 \tag{21}$$

or

$$\left(\frac{n_1+n_2}{2}\right)^2 = g\left(\frac{k_1+k_2}{2}\right) + \gamma\left(\frac{k_1+k_2}{2}\right)^3 . \qquad (22)$$

Obviously, from (22), even though the new wave was produced from the sum of ζ_1 and ζ_2, it will not be dispersed according to the summation relationship

$$n_1^2 + n_2^2 = g(k_1+k_2) + \gamma(k_1^3+k_2^3) . \qquad (23)$$

The addition of the two sinusoids as seen in Figure 4 begins to show some of the properties of ocean waves. By adding together a large number of sinusoids and by considering the directional properties of the waves over the two dimensional sea surface plane, the irregular pattern of the ocean surface can be approximated. The true random surface, however, must be described by considering both the linear and the non-linear parts of the governing equations.

The importance of non-linear interactions for gravity waves was discussed by Phillips (1960a, 1969). He showed that the interaction of three primary waves can cause a resonance condition to exist so that secondary waves will be generated. A weak energy transfer from the primary to the secondary waves will also occur. McGoldrick (1965) studied interactions among capillary and among capillary and gravity waves and found that resonance and thus secondary wave generation and corresponding energy transfer occur with certain triads of waves. Longuet-Higgins (1963a) explained the non-linear mechanism for the formation of capillary waves on the forward face of gravity waves. He related this process to the generation of waves by wind.

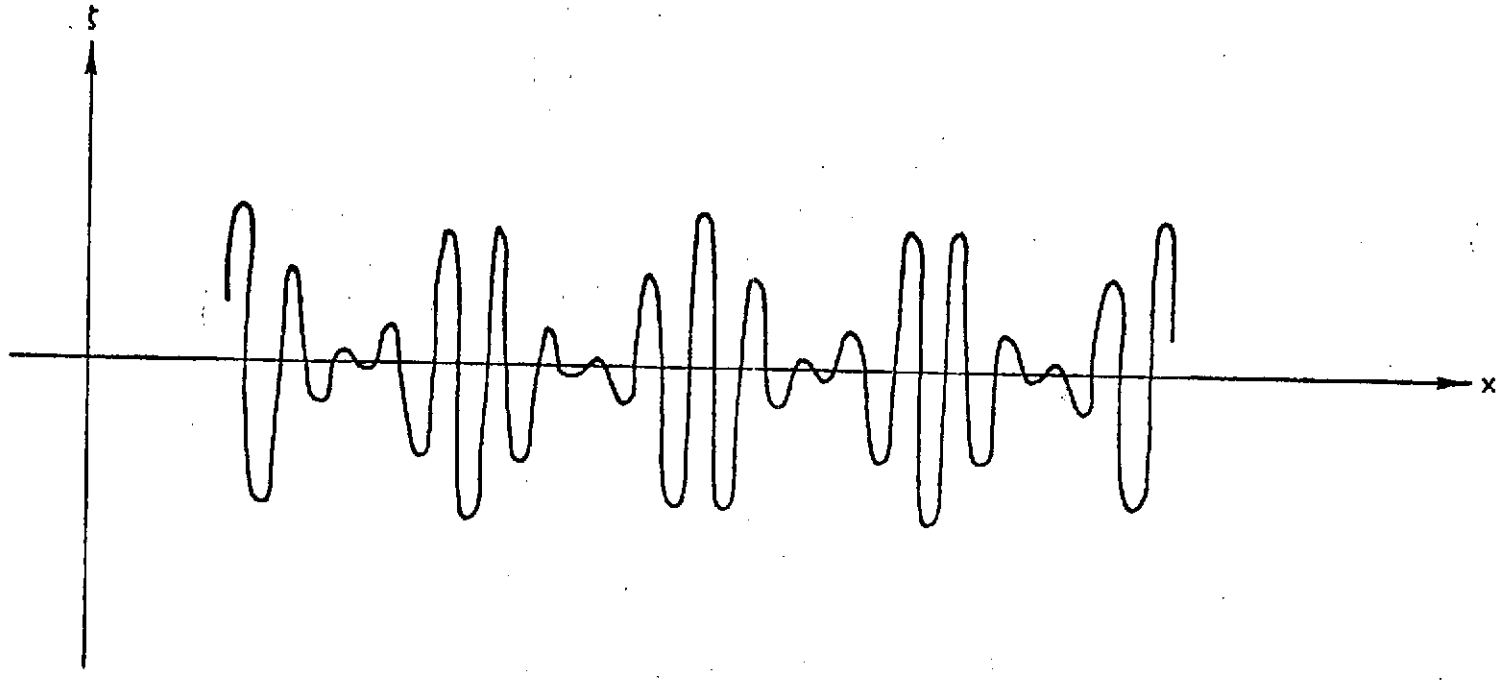

Figure 4. Addition of two sinusoids with different wave numbers at time of t = 0

All of the above studies are important contributions to the understanding of surface waves. They all concern non-linear interactions, but the development of each theory relies on the assumption of the validity of the linear dispersive relationship (12). The resonance models in particular are critically dependent upon this assumption. The reliance upon the linear dispersion is true not only for the three papers cited, but for virtually all studies involving non-linear interactions. If (12) is not a good representation of the true dispersion, then all of these papers--some of which are major contributions--may be improved.

The present study investigates the dispersion of non-linearly interacting random pelagic gravity and capillary surface waves. A quantitative analysis is given, and the deviation from linear theory is examined in terms of the non-linear interactions.

Not only is the non-linear dispersion important in the assessment of major theories that lead to the understanding of random waves, but it is also important in determining the transformations between wave number and frequency spectra. An accurate transformation is necessary in view of the economical and logistical problems of wave number measurement in the random ocean and of the relative ease of frequency measurements.

The discussion so far has related to wave-wave interactions. Wave-current interactions, however, also affect the dispersion. The change in wave number and amplitude when short waves ride on long swells was rigorously calculated by Longuet-Higgins and Stewart (1960). The changes in wave characteristics when waves interact with currents was also noted by Whitham (1960, 1962). Since an accurate transformation between wave number

and frequency spectra is desired, the present study additionally describes the modification needed in the dispersion when the waves are under the influence of current. Although the modification is given only for a single wave, the logic of the derivation is valid for random waves.

1.2 SPECIFICATION OF THE RANDOM SEA

The detailed pattern of the waves on the sea surface is random in the sense that it varies without regularity in both space and time. The motion of the waves obeys certain known dynamical and kinematical restrictions. The randomness, however, must be treated statistically. The statistical measures of the motion can then be used to ascribe some order to the surface structure. It is necessary, therefore, to specify the dynamical, kinematical, and statistical properties of the random sea surface.

Consider a rectangular coordinate system with the z-axis measured positive vertically upward with the plane $z = 0$ at the mean free surface level. Any point in this system can be described by z and a horizontal position vector $\underset{\sim}{x} = (x,y)$. Under the standard assumptions of an incompressible, inviscid fluid, the motion can be approximated as irrotational. This motion is governed by Laplace's equation

$$\nabla^2 \phi(\underset{\sim}{x},z,t) = 0 \tag{24}$$

where $\phi(\underset{\sim}{x},z,t)$ is the velocity potential as a function of $\underset{\sim}{x}$,z and time t. If it is further assumed that the random wave field is statistically stationary with respect to both time and space and that there is no motion at $z = -\infty$, Phillips (1960a) showed that the solution to (24) is

$$\phi(\underset{\sim}{x},z,t) = \iint_{\underset{\sim}{k}n} dA(\underset{\sim}{k},n)\exp[|\underset{\sim}{k}|z]\exp[i(\underset{\sim}{k}\cdot\underset{\sim}{x} - nt)] \tag{25}$$

where $dA(\underset{\sim}{k},n)$ is any complex valued random function of the horizontal wave number vector $\underset{\sim}{k}$ and frequency n. The velocity potential is represented as a Fourier-Stieltjes integral with the integration over all wave number-frequency space.

Under the same assumptions Phillips (1960a) showed that the surface elevation $\zeta(\underset{\sim}{x},t)$ can be represented as

$$\zeta(\underset{\sim}{x},t) = \iint_{\underset{\sim}{k}n} dB(\underset{\sim}{k},n)\exp[i(\underset{\sim}{k}\cdot\underset{\sim}{x} - nt)] \tag{26}$$

where ζ is the displacement from the mean free surface $\overline{\zeta} = 0$ and $dB(\underset{\sim}{k},n)$ is another complex valued random function. Since $\zeta(\underset{\sim}{x},t)$ is real,

$$\begin{aligned}\zeta(\underset{\sim}{x},t) &= \iint_{\underset{\sim}{k}n} dB(\underset{\sim}{k},n)\exp[i(\underset{\sim}{k}\cdot\underset{\sim}{x} - nt)] \\ &= \iint_{\underset{\sim}{k}n} dB^*(\underset{\sim}{k},n)\exp[-i(\underset{\sim}{k}\cdot\underset{\sim}{x} - nt)] \\ &= \iint_{\underset{\sim}{k}n} dB^*(-\underset{\sim}{k},-n)\exp[i(\underset{\sim}{k}\cdot\underset{\sim}{x} - nt)] \end{aligned} \tag{27}$$

where $dB^*(\underset{\sim}{k},n)$ is the complex conjugate of $dB(\underset{\sim}{k},n)$.

A relationship exists between $dB(\underset{\sim}{k},n)$ and the directional wave energy spectrum $X(\underset{\sim}{k},n)$ such that

$$\overline{dB(\underset{\sim}{k}_i,n_i)dB^*(\underset{\sim}{k}_j,n_j)} = \begin{cases} X(\underset{\sim}{k}_i,n_i)d\underset{\sim}{k}_i\,dn_i & \text{if } i = j \\ 0 \text{ otherwise} \end{cases} \tag{28}$$

where the overbar indicates an ensemble average. The spectral function is perhaps the most common representation of the wave field. In order to relate quantities other than the surface elevation to the wave spectrum, it is necessary to find a relationship between $dA(\underset{\sim}{k},n)$ and $dB(\underset{\sim}{k},n)$. This can be done from the kinematic boundary condition at the free surface.

If the position of the free surface is specified by ζ, the total derivative of ζ is

$$\frac{d\zeta}{dt} = \frac{\partial \zeta}{\partial t} + \underset{\sim}{q}_{\zeta} \cdot \nabla_h \zeta \tag{29}$$

where $\nabla_h = (\partial/\partial x, \partial/\partial y)$ is the horizontal gradient operator, $\underset{\sim}{q}$ is the horizontal velocity vector, and the subscript ζ indicates measurement at the free surface. For irrotational flow (29) becomes

$$\frac{\partial \zeta}{\partial t} = (\partial\phi/\partial z)_{\zeta} - (\nabla_h \phi)_{\zeta} \cdot \nabla_h \zeta \ . \tag{30}$$

Equation (30) represents the free surface kinematic boundary condition.

Substituting (25) and (26) into (30),

$$\iint_{\underset{\sim}{k}n} -in dB(\underset{\sim}{k},n)\exp[i(\underset{\sim}{k}\cdot\underset{\sim}{x} - nt)] = \iint_{\underset{\sim}{k}n} |\underset{\sim}{k}|\, dA(\underset{\sim}{k},n)\exp[|\underset{\sim}{k}|\zeta]\exp[i(\underset{\sim}{k}\cdot\underset{\sim}{x} - nt)]$$

$$+ \iiint_{\underset{\sim}{k}n\underset{\sim}{k}_1 n_1} \underset{\sim}{k}\cdot\underset{\sim}{k}_1 dA(\underset{\sim}{k},n)dB(\underset{\sim}{k}_1,n_1)\exp[|\underset{\sim}{k}|\zeta]\exp\{i[(\underset{\sim}{k}+\underset{\sim}{k}_1)\cdot\underset{\sim}{x} - (n + n_1)t]\} \tag{31}$$

The exponential term in (31) involving the surface slope $|k|\zeta$ can be expanded in a Taylor series around $\zeta = 0$ such that

$$\exp[|\underset{\sim}{k}|\zeta] = 1 + |\underset{\sim}{k}|\zeta + \frac{1}{2}[|\underset{\sim}{k}|\zeta]^2 + \ldots \frac{1}{j!}[|\underset{\sim}{k}|\zeta]^j + \ldots + R. \tag{32}$$

The convergence of the series for gravity waves can be determined by noting that the maximum steepness a gravity wave can have before it breaks is .142. This value was determined by Stokes (1880), and according to Kinsman (1965), it may be taken as an established value. In terms of wave slope, the maximum value is one half the maximum steepness, or

.071. Terminating (32) after only two terms results in a maximum error R

$$R = \frac{1}{2}(.071)^2 \exp(.071) = .003 \ . \tag{33}$$

This error is negligible.

For capillary waves, Crapper (1957) found that the maximum steepness can be .730. The maximum slope is therefore .365. The maximum error if only the first two terms of (32) are used is then

$$R = \frac{1}{2}(.365)^2 \exp(.365) = .096 \ . \tag{34}$$

If the first three terms are used,

$$R = (1/6)(.365)^3 \exp(.365) = .012 \ . \tag{35}$$

Although these errors are larger than that for gravity waves, they are still small.

Using the series expansion for $\exp[|\underset{\sim}{k}|\zeta]$ truncated after the first three terms, the relationship between $dA(\underset{\sim}{k},n)$ and $dB(\underset{\sim}{k},n)$ is found by successive approximations. Details of the operation, following the method developed by Huang (1971) in his second order study of Stokes drift in a deep water random gravity wave field, are in Appendix A. To the third order the relationship is

$$dA(\underset{\sim}{k},n) = -\frac{in}{|\underset{\sim}{k}|} dB(\underset{\sim}{k},n) + i\int_{\underset{\sim}{k}_1} \int_{n_1} \left[\frac{\underset{\sim}{k}\cdot(\underset{\sim}{k} - \underset{\sim}{k}_1)}{|\underset{\sim}{k}||\underset{\sim}{k} - \underset{\sim}{k}_1|}\right](n - n_1)dB(\underset{\sim}{k} - \underset{\sim}{k}_1, n - n_1)$$

$$dB(\underset{\sim}{k}_1,n_1) + i \int_{\underset{\sim}{k}_1} \int_{n_1} \int_{\underset{\sim}{k}_2} \int_{n_2} \frac{(n - n_1 - n_2)}{|\underset{\sim}{k}|} \left[\frac{1}{2}(\underset{\sim}{k} + \underset{\sim}{k}_1 - \underset{\sim}{k}_2)\right.$$

$$\cdot(\underset{\sim}{k} - \underset{\sim}{k}_1 - \underset{\sim}{k}_2) - \frac{\cdot \underset{\sim}{k}\cdot(\underset{\sim}{k} - \underset{\sim}{k}_1)(\underset{\sim}{k} - \underset{\sim}{k}_1)\cdot(\underset{\sim}{k} - \underset{\sim}{k}_1 - \underset{\sim}{k}_2)}{|\underset{\sim}{k} - \underset{\sim}{k}_1||\underset{\sim}{k} - \underset{\sim}{k}_1 - \underset{\sim}{k}_2|} \Bigg]$$

$$dB(\underset{\sim}{k} - \underset{\sim}{k}_1 - \underset{\sim}{k}_2,\ n-n_1 - n_2)dB(\underset{\sim}{k}_1, n_1)dB(\underset{\sim}{k}_2, n_2) \qquad (36)$$

A dynamic boundary condition on the free surface is imposed by the requirement that the pressure on the two sides of the surface differ only as a result of surface tension. From Bernoulli's non-linear equation, the pressure in the water at the free surface is given by

$$\frac{p}{\rho} + g\zeta + (\partial\phi/\partial t)_\zeta + \frac{1}{2}(\nabla\phi)_\zeta^2 = 0 \ . \qquad (37)$$

The difference in pressure resulting from the surface tension can be written as

$$p = p_a - \rho\gamma(\nabla_h^2\zeta)[1 + (\nabla_h\zeta)^2]^{-(3/2)} \qquad (38)$$

where the second term on the right represents the contribution from the surface tension. As in the linearized equations, the atmospheric pressure is assumed to be constant. If the free surface $\zeta = 0$ is taken as a reference level at which $p = 0$, then $p_a = 0$ since the surface tension component vanishes. The resulting dynamical free surface boundary constraints on the wave motion are

$$g\zeta = -(\partial\phi/\partial t)_\zeta - \frac{1}{2}(\nabla\phi)_\zeta^2 + \gamma(\nabla_h^2\zeta)[1 + (\nabla_h\zeta)^2]^{-(3/2)} \ . \qquad (39)$$

1.3 MATHEMATICAL DERIVATION AND PHYSICS OF THE DISPERSIVE RELATIONSHIP

It has been stated that the dispersive relationship is one particular property of gravity and capillary waves relating wave number and frequency and that several investigators use the relationship in a form derived from linear theory for a single wave. The present analysis describes the mean deviation and the scattering from the simple dispersion for the more realistic random, non-linearly interacting waves. The analytical derivation makes use of the full non-linear equations for a capillary and gravity surface random wave field and is an extension of the study by Huang (1972) on gravity waves.

The free surface dynamical boundary constraints yield an identity from which the dispersion for a single wave train was found. They also provide a corresponding relation for a random wave field. Looking at (39), the term raised to the -3/2 power can be expanded into the binomial series

$$[1 + (\nabla_h \zeta)^2]^{-3/2} = 1 - (3/2)(\nabla_h \zeta)^2 + (15/8)(\nabla_h \zeta)^4 + \ldots$$

$$+ \frac{[-(3/2) - j + 1][-(3/2) - j + 2] \ldots [-(3/2) - 1]\,(-3/2)}{j!}$$

$$(\nabla_h \zeta)^{2j} + \ldots + R \quad . \tag{40}$$

Equation (40) is valid for

$$|(\nabla_h \zeta)^2| < 1 \quad . \tag{41}$$

This condition is always satisfied in light of the maximum wave slopes permitted before breaking occurs. Truncating (40) after the first two terms yields a maximum error

$$R = (15/8)(\nabla_h \zeta)^4 \quad . \tag{42}$$

Since the maximum gradient is small in order to retain the wave stability, the maximum error after a two term truncation is minute.

Substituting the first two terms of the binomial series (40) and the first three terms of the Taylor series (32) in (39) and then using (25) and (26) to substitute for ϕ and ζ, an expression is obtained in terms of $dA(\underset{\sim}{k},n)$ and $dB(\underset{\sim}{k},n)$ such that

$$\begin{aligned}
\iint_{\underset{\sim}{k}n} g\,dB(\underset{\sim}{k},n)\exp[i(\underset{\sim}{k}\cdot\underset{\sim}{x}-nt)] = {} & \iint_{\underset{\sim}{k}n} in[1 + |\underset{\sim}{k}|\zeta + \tfrac{1}{2}|\underset{\sim}{k}|^2\zeta^2]\,dA(\underset{\sim}{k},n)\exp[i(\underset{\sim}{k}\cdot\underset{\sim}{x} - nt)] \\
& - \tfrac{1}{2}\iiint_{\underset{\sim}{k}n}\int_{\underset{\sim}{k}_1 n_1} (|\underset{\sim}{k}||\underset{\sim}{k}_1| - \underset{\sim}{k}\cdot\underset{\sim}{k}_1)[1 + (|\underset{\sim}{k}| + |\underset{\sim}{k}_1|)\zeta] \\
& dA(\underset{\sim}{k},n)\,dA(\underset{\sim}{k}_1,n_1)\exp\{i[(\underset{\sim}{k} + \underset{\sim}{k}_1)\cdot\underset{\sim}{x} - (n + n_1)t]\} \\
& - \gamma\iint_{\underset{\sim}{k}n}|\underset{\sim}{k}|^2\,dB(\underset{\sim}{k},n)\exp[i(\underset{\sim}{k}\cdot\underset{\sim}{x} - nt)] - \gamma(3/2) \\
& \iiint_{\underset{\sim}{k}n}\int_{\underset{\sim}{k}_1 n_1}\int_{\underset{\sim}{k}_2 n_2} |\underset{\sim}{k}|^2\,\underset{\sim}{k}_1\cdot\underset{\sim}{k}_2\,dB(\underset{\sim}{k},n)\,dB(\underset{\sim}{k}_1,n_1)\,dB(\underset{\sim}{k}_2,n_2) \\
& \exp\{i[(\underset{\sim}{k} + \underset{\sim}{k}_1 + \underset{\sim}{k}_2)\cdot\underset{\sim}{x} - (n + n_1 - n_2)t]\}
\end{aligned} \tag{43}$$

Substitution of (36) in (43) results in the non-linear third order dispersive relationship for random gravity and capillary waves

$$g + \gamma|\underset{\sim}{k}|^2 - \frac{n^2}{|\underset{\sim}{k}|} = \int_{\underset{\sim}{k}_1}\int_{n_1} f_1 dB(\underset{\sim}{k}_1, n_1)\exp[i(\underset{\sim}{k}\cdot\underset{\sim}{x} - n_1 t)]$$

$$- \int_{\underset{\sim}{k}_1}\int_{n_1}\int_{\underset{\sim}{k}_2}\int_{n_2} f_2 dB(\underset{\sim}{k}_1, n_1)dB(\underset{\sim}{k}_2, n_2)\exp\{i[(\underset{\sim}{k}_1 + \underset{\sim}{k}_2)$$

$$\cdot\underset{\sim}{x} - (n_1 + n_2)t]\} - \frac{1}{2}\int_{\underset{\sim}{k}_1}\int_{n_1}\int_{\underset{\sim}{k}_2}\int_{n_2} f_3 dB(\underset{\sim}{k}_1 - \underset{\sim}{k}_2, n_1 - n_2)$$

$$dB(\underset{\sim}{k}_2, n_2)\exp[i(\underset{\sim}{k}_1\cdot\underset{\sim}{x} - n_1 t)] \qquad (44)$$

where

$$f_1 = n^2 - \frac{\underset{\sim}{k}\cdot(\underset{\sim}{k} + \underset{\sim}{k}_1)}{|\underset{\sim}{k}||\underset{\sim}{k} + \underset{\sim}{k}_1|} n(n + n_1) + \frac{1}{2}\left(1 - \frac{\underset{\sim}{k}\cdot\underset{\sim}{k}_1}{|\underset{\sim}{k}||\underset{\sim}{k}_1|}\right)nn_1 \qquad (45)$$

$$f_2 = \frac{n(n + n_1 + n_2)}{|\underset{\sim}{k} + \underset{\sim}{k}_1 + \underset{\sim}{k}_2|}\left[\frac{1}{2}(\underset{\sim}{k} + 2\underset{\sim}{k}_1)\cdot\underset{\sim}{k} - \frac{(\underset{\sim}{k} + \underset{\sim}{k}_1 + \underset{\sim}{k}_2)\cdot(\underset{\sim}{k} + \underset{\sim}{k}_2)(\underset{\sim}{k} + \underset{\sim}{k}_2)\cdot\underset{\sim}{k}}{|\underset{\sim}{k} + \underset{\sim}{k}_2||\underset{\sim}{k}|}\right]$$

$$+ \frac{(\underset{\sim}{k} + \underset{\sim}{k}_1)\cdot\underset{\sim}{k}}{|\underset{\sim}{k}|} n(n + n_1) - \frac{1}{2} n^2|\underset{\sim}{k}| - \frac{1}{2}\left[1 - \frac{\underset{\sim}{k}\cdot\underset{\sim}{k}_1}{|\underset{\sim}{k}||\underset{\sim}{k}_1|}\right]$$

$$(|\underset{\sim}{k}| + |\underset{\sim}{k}_1|)nn_1 + \frac{1}{2}\left[1 - \frac{(\underset{\sim}{k} + \underset{\sim}{k}_2)\cdot\underset{\sim}{k}_1}{|\underset{\sim}{k} + \underset{\sim}{k}_2||\underset{\sim}{k}_1|}\right]\frac{(\underset{\sim}{k} + \underset{\sim}{k}_2)\cdot\underset{\sim}{k}}{|\underset{\sim}{k}|} nn_1$$

$$+ (3/2)\gamma|\underset{\sim}{k}|^2\underset{\sim}{k}_1\cdot\underset{\sim}{k}_2 \qquad (46)$$

$$f_3 = \left[1 - \frac{\underset{\sim}{k}\cdot\underset{\sim}{k}_1}{|\underset{\sim}{k}||\underset{\sim}{k}_1|}\right]\frac{\underset{\sim}{k}_1\cdot(\underset{\sim}{k}_1 - \underset{\sim}{k}_2)}{|\underset{\sim}{k}_1 - \underset{\sim}{k}_2|} n(n_1 - n_2) \qquad (47)$$

Details of the mathematics of the derivation are given in Appendix B.

Equation (44) is the most general form of the dispersive relationship for a random sea surface through third order interactions. It is a function of both space and time. If all the non-linear terms on the right hand side are neglected, and if only a single wave train is considered, the frequently used simple relationship (12) is recovered.

The deviation from the linear theory is given by the right hand side of (44). The mean deviation is easily computed by taking the mean of each term of the deviation. The first term represents a random scattering of the surface elevation and has a zero mean.

It is seen from (27) that

$$dB(\underset{\sim}{k},n) = dB^*(-\underset{\sim}{k},-n) \tag{48}$$

The mean Fourier-Stieltjes components in the third term can then be written as

$$\overline{dB(\underset{\sim}{k}_1 - \underset{\sim}{k}_2, n_1 - n_2)dB(\underset{\sim}{k}_2, n_2)} = \overline{dB(\underset{\sim}{k}_1 - \underset{\sim}{k}_2, n_1 - n_2)dB^*(-\underset{\sim}{k}_2, -n_2)} \tag{49}$$

and from (28)

$$\overline{dB(\underset{\sim}{k}_1 - \underset{\sim}{k}_2, n_1 - n_2)dB^*(-\underset{\sim}{k}_2, -n_2)} = \begin{cases} X(\underset{\sim}{k}_2, n_2)d\underset{\sim}{k}_2 dn_2 & \text{if } \underset{\sim}{k}_1 = n_1 = 0 \\ 0 \quad \text{otherwise.} \end{cases} \tag{50}$$

If $\underset{\sim}{k}_1 = n_1 = 0$, then (47) becomes zero. The mean of this third term therefore vanishes.

Equations (48) and (28) can be used to determine the mean of the second term. Thus,

$$\overline{dB(\underset{\sim}{k}_1,n_1)dB^*(-\underset{\sim}{k}_2,-n_2)} = \begin{cases} X(\underset{\sim}{k}_1,n_1)d\underset{\sim}{k}_1 dn_1 & \text{if } \underset{\sim}{k}_1 + \underset{\sim}{k}_2 = n_1 + n_2 = 0 \\ 0 & \text{otherwise .} \end{cases} \tag{51}$$

Substituting $\underset{\sim}{k}_1 = -\underset{\sim}{k}_2$, $n_1 = -n_2$ into (46) yields a non-zero term

$$f_2' = \frac{n^2}{|\underset{\sim}{k}|}\left[\frac{1}{2}(\underset{\sim}{k} + 2\underset{\sim}{k}_1)\cdot\underset{\sim}{k} - \frac{\underset{\sim}{k}\cdot(\underset{\sim}{k} - \underset{\sim}{k}_1)(\underset{\sim}{k} - \underset{\sim}{k}_1)\cdot\underset{\sim}{k}}{|\underset{\sim}{k} - \underset{\sim}{k}_1||\underset{\sim}{k}|}\right] + \frac{(\underset{\sim}{k} + \underset{\sim}{k}_1)\cdot\underset{\sim}{k}}{|\underset{\sim}{k}|} n(n + n_1)$$

$$- \frac{1}{2}n^2|\underset{\sim}{k}| - \frac{1}{2}\left[1 - \frac{\underset{\sim}{k}\cdot\underset{\sim}{k}_1}{|\underset{\sim}{k}||\underset{\sim}{k}_1|}\right](|\underset{\sim}{k}| + |\underset{\sim}{k}_1|)nn_1$$

$$+ \frac{1}{2}\left[1 - \frac{(\underset{\sim}{k} - \underset{\sim}{k}_1)\cdot\underset{\sim}{k}_1}{|\underset{\sim}{k} - \underset{\sim}{k}_1||\underset{\sim}{k}_1|}\right]\frac{(\underset{\sim}{k} - \underset{\sim}{k}_1)\cdot\underset{\sim}{k}}{|\underset{\sim}{k}|} nn_1 - \frac{3}{2}\gamma|\underset{\sim}{k}|^2|\underset{\sim}{k}_1|^2. \tag{52}$$

It is seen that the mean of the second term is therefore non-zero.

The resulting mean non-linear dispersion is

$$g + \gamma|\underset{\sim}{k}|^2 - \frac{n^2}{|\underset{\sim}{k}|} = -\int_{\underset{\sim}{k}_1}\int_{n_1} f_2' X(\underset{\sim}{k}_1,n_1)d\underset{\sim}{k}_1 dn_1. \tag{53}$$

The right hand side of (53) represents the mean non-linear deviation from linear theory in terms of the spectral function. This expression is greatly simplified if only unidirectional waves are considered. Equation (23) reduces to

$$g + \gamma k^2 - \frac{n^2}{k} = -\int_{k_1}\int_{n_1} [3n^2 k_1 + nn_1(k + k_1) - (3/2)\gamma k^2 k_1^2]$$

$$X(k_1,n_1)dk_1 dn_1. \tag{54}$$

Since the spectral function is even and n_1, k_1 are odd functions, (54) becomes

$$g + \gamma k^2 - \frac{n^2}{k} = -\int_{k_1}\int_{n_1} [nn_1 k_1 - (3/2)\gamma k^2 k_1^2] X(k_1,n_1)dk_1 dn_1 . \tag{55}$$

The mean squared random error is a measure of the variability of the random scattering about the mean deviation. The right hand side of (44) represents the deviation ε from the linear theory. The mean of its square $\overline{\varepsilon^2}$, is the mean squared random error. The computation of $\overline{\varepsilon^2}$ to the third order requires that we consider only the first term on the right hand side of (44) as inclusion of the other terms will yield higher than third order results. Thus,

$$\varepsilon = \int_{\underset{\sim}{k}_1}\int_{n_1} f_1 dB(\underset{\sim}{k}_1,n_1)\exp[i(\underset{\sim}{k}_1\cdot\underset{\sim}{x} - n_1 t)] . \tag{56}$$

The mean squared random error is arrived at by once again using (48) and (28) to compute the mean of the square of (56). The resulting expression is

$$\overline{\varepsilon^2} = \int_{\underset{\sim}{k}_1}\int_{n_1} f_1^2 X(\underset{\sim}{k}_1,n_1)d\underset{\sim}{k}_1 dn_1 . \tag{57}$$

For unidirectional waves, (57) reduces to

$$\overline{\varepsilon^2} = n^2\int_{k_1}\int_{n_1} n_1^2 X(k_1,n_1)dk_1 dn_1. \tag{58}$$

Anticipating the results of the next section, the behavior of the mean deviation and root mean squared random error can be schematically visualized as in Figure 5. The ratio of the linear dispersion to the non-linear dispersion is plotted against the wave frequency. It is seen that as n increases from the low frequency gravity waves through the high frequency capillary waves, the mean deviation and random scattering first increase in magnitude and then decrease in magnitude. The inflection points of the curves are found in the transition zone between the gravity and capillary wave ranges.

The reversal of the mean effects can be seen by looking at the term in brackets in (55). The first component dominates in the gravity wave range since in this range the square of the wave number is much less than the wave number itself. In the capillary wave range, however, the wave number is large so that its square is even larger. The second term therefore dominates in this range. Since the two terms are of opposite sign, their effects will be opposite.

The random fluctuations are a function of the quasi-Eulerian velocity components. The schematic depiction shows that these random fluctuations are maximized in the transition zone between the gravity and capillary waves. This curve is based in part on measurements of velocity spectra by Yefimov and Khristoforov (op.cit.). These authors show that in the gravity wave range the random, turbulent type velocity components become increasingly stronger as the transition zone is approached. No measurements of velocity spectra have been made in the capillary wave range, but Phillips (1969) discusses integrated frequency spectra in this

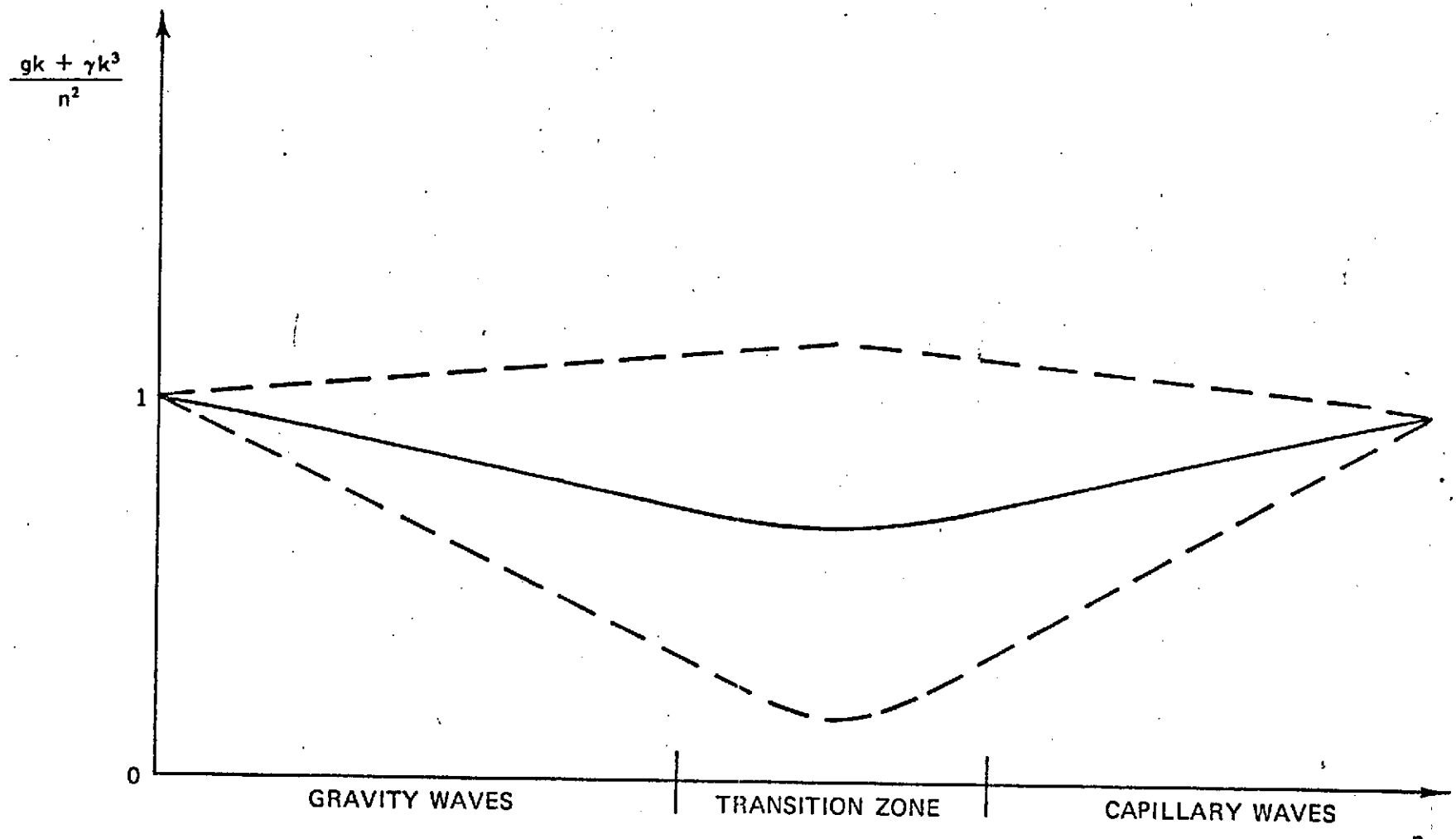

Figure 5. Schematic of the effect on the linear dispersion of the non-linear mean deviation (——) and root mean squared random error (— —)

range. He states that the maximum spectral values occur in the lowest frequencies, or those frequencies near the transition zone. At higher frequencies, the spectral values decrease rapidly because of the increased effect of viscous dissipation of the capillary waves. Thus, as the frequency increases, the wave energy becomes less and therefore the velocity components decrease in magnitude.

The dispersion by definition relates the velocity at which a wave travels to the wave length. This has the effect of sorting the waves as they travel. For simplicity, consider three gravity waves of differing lengths propagating unidirectionally from a point x_o at time t_o. Since the waves are traveling at different speeds, at a later time t_1 the fastest wave will at at x_1, the next fastest at $x_2<x_1$, and the slowest at $x_3<x_2<x_1$. It is therefore seen that even though the three waves started traveling from the same point at the same time, they will be sorted at t_1.

The linear dispersion (11) shows that the square of the phase speed is indirectly proportional to the wave number when the wave is restored to the mean free surface level by gravity and directly proportional to the wave number when the wave is restored by surface tension. The effect of non-linear wave-wave interactions can be readily seen by looking at the simplified case of unidirectional waves. Using (1), the mean non-linear dispersion (55) can be rewritten as

$$c^2 = \frac{g}{k} + \gamma k + \int_{k_1}\int_{n_1}\left[\frac{n}{k} n_1 k_1 - (3/2)\gamma k k_1^2\right]X(k_1,n_1)\,dk_1\,dn_1$$

$$= c_0^2 \left[1 + \frac{c}{c_0^2} \int_{k_1} \int_{n_1} n_1 k_1 X(k_1, n_1) dk_1 dn_1 - (3/2) \frac{\gamma k}{c_0^2} \right.$$

$$\left. \int_{k_1} \int_{n_1} k_1^2 X(k_1, n_1) dk_1 dn_1 \right] \qquad (59)$$

where c_0^2 represents the linear dispersion. If interactions did not occur, c^2 would be coincident with c_0^2 and the linear theory would suffice. Physically, then, the third order mean non-linearities behave in the sense of a deviation from the linear dispersion. They thus affect the dispersion by changing the phase speed c_0 that results from linear theory.

Looking at the mean deviation, the first integral on the right hand side of (59) is an expression for the mean random ocean quasi-Eulerian velocity as derived by Phillips (1960b). This velocity is the mean of the horizontal component of the fluid velocity at the free surface for a fixed point (x,y). It is a quasi-Eulerian quantity in that it is measured at a fixed point on the projection of the free surface, but the vertical coordinate is allowed to move up and down with the free surface. A similar formula was derived by Longuet-Higgins and Phillips (1962) from a generalization of the interactions between two waves. The difference between the two expressions is a factor of two. Phillips (1960b), however, showed that the mean Eulerian velocity is one-half the Stokes drift. The Stokes drift is the mean velocity following a fluid particle and is by definition a Lagrangian property. Since the present study is based on an Eulerian reference frame, the first integral appears reasonable.

The second integral in (59) represents the mean square of the ratio of the surface elevation to the wave length. It is multiplied by the surface tension and is thus important in the capillary wave range. This term also appears reasonable in view of Crapper's (op.cit.) exact solution to the finite amplitude non-linear single capillary wave problem. He showed that the square of the phase speed is influenced, as in the present study, by a term proportional to the square of the ratio of the surface elevation to the wave length.

1.4 QUANTITATIVE ESTIMATES OF THE NON-LINEAR DISPERSION

The effect of the mean non-linear deviation can be quantitatively assessed if the spectral function is known. An order of magnitude estimate can be obtained by using the equilibrium range spectrum. For gravity waves assume the equilibrium spectrum given by Phillips (1958).

$$X(k,n) = \frac{\beta g^2}{n^5}\,\delta\left(k - \frac{n^2}{g}\right) \tag{60}$$

for

$$k \ll k_\gamma = (g/\gamma)^{1/2},\quad n \ll n_\gamma = (4g^3/\gamma)^{1/4} \tag{61}$$

where β is a universal constant and δ is the Dirac delta function. The constant β has been measured experimentally by Pierson (1960), Burling (1959) and Longuet-Higgins et al. (op.cit.). An average value is 1.2×10^{-2}. For capillary waves Phillips (1969) gave an equilibrium spectrum based on dimensional considerations such that

$$X(k,n) = \frac{\beta' \gamma^{2/3}}{n^{7/3}}\,\delta\left(k^3 - \frac{n^2}{\gamma}\right) \tag{62}$$

for

$$k_\gamma \ll k \ll k_\nu\ ,\quad n_\gamma \ll n \ll n_\nu \tag{63}$$

where β' is another constant, and k_ν and n_ν are the cut-off wave number and frequency, respectively, at which viscous effects dominate. Cox (1958) measured a constant for frequency spectra of the wave slope. Phillips (1969) showed that this constant could be used to approximate β' as 10^{-2}. Wu (1972), however, showed that this value may be in error by a factor of two.

In the gravity wave range the surface tension is unimportant compared to gravity so that after substituting (60) into (59)

$$c^2 = c_o^2\left[1 + \frac{c\beta g^2}{c_o^2} \int\int k_1 n_1 n_1^{-4} k_1 \, dk_1 \, dn_1\right] \tag{64}$$

where

$$n_1^2 = gk_1 \quad . \tag{65}$$

Using (65) and integrating (64) over the gravity wave range and noting that

$$c_o^2 = g/k \tag{66}$$

then

$$c^2 = c_o^2\left[1 + \frac{c\beta g}{c_o^2 n_1}\right]$$

$$= c_o^2 \left[1 + \beta n/n_1\right] \quad . \tag{67}$$

Equation (67) shows that the mean phase speed of interacting waves will be less than that predicted by linear theory, and that the difference will depend on the ratio n/n_1.

Examining this result in terms of wave number and frequency, substitute (1) and (66) into (67) and rearrange so that

$$gk = n^2[1 + (\beta n/n_1)]^{-1} \quad . \tag{68}$$

Expanding the multiplier of n^2 in a truncated binomial series,

$$[1 + (\beta n/n_1)]^{-1} = 1 - \beta n/n_1 \quad . \tag{69}$$

Hence

$$gk \approx n^2\left(1 - \beta\frac{n}{n_1}\right) \quad . \tag{70}$$

The error in (69) is negligible since n and n_1 are of the same order and β is small. Equation (70) clearly shows that for interacting gravity waves, an increase in wave number results from an increase in frequency below that predicted by linear theory. Furthermore, the effect of the interactions increases as the ratio n/n_1 increases. This result agrees with Huang (1972) and is consistent with Stokes' (1847) theoretical solution for gravity waves. Additionally, the result agrees with the observed data discussed earlier.

In the capillary wave range the gravity terms are unimportant compared to the surface tension terms so that after substituting (62) into (59),

$$c^2 = c_o^2\{1 + (\beta'/c_o^2)\int_{k_1}\int_{n_1}[c\gamma^{2/3}n_1^{-4/3}k_1 - (3/2)\gamma^{5/3}kn_1^{-7/3}k_1^2]$$

$$dk_1dn_1\} \tag{71}$$

where

$$n_1^2 = \gamma k_1^3 \quad . \tag{72}$$

Using (72) and integrating (71) over the capillary wave range,

$$c^2 = c_o^2\{1 - (\beta'/c_o^2)\,[(3/2)\gamma k \ln n_1 - 3c\gamma^{1/3}n_1^{1/3}]\} \quad . \tag{73}$$

The mean effect of the interactions on the phase speed can be assessed after the sign of

$$(3/2)\gamma k \ln n_1 - 3c\gamma^{1/3} n_1^{1/3} \tag{74}$$

is determined. Using (1), dividing by 3γ and rearranging (74) is re-written as

$$\frac{1}{2} n_1^{-1/3} \ln n_1 - \frac{n}{\gamma^{2/3} k^2} \quad . \tag{75}$$

The capillary wave range in which the equilibrium spectrum is valid begins at $n_\gamma \approx 100$ sec^{-1} as shown by Phillips (1969) and at $k_\gamma \approx 3.6$ cm^{-1} as shown by Wu (op.cit.). The upper limit to the range is determined by the energy dissipation resulting from molecular viscosity. Wu (op.cit.) showed that the cut-off wave number $k_\nu \approx 13$ cm^{-1}. The corresponding cut-off frequency $n_\nu \approx 1{,}000$ sec^{-1}. Additionally, n_1 is the lower bound of the equilibrium range so that n_1 is always less than or equal to n. Using these limiting values, the first term in (75) varies from .50 to .35 as n_1 increases and the second term varies from .44 to .34 as n increases. Equation (75) and therefore (74) is thus positive. It should be noted, however, that as the viscous dissipation of the wave energy becomes more pronounced, i.e., at the upper limits of the range for which the equilibrium spectrum is valid, the difference between the two terms becomes smaller and smaller. Since (74) is positive, the square of the phase speed c^2 in (73) will be less than that for the situation in which no interactions are involved, but only by a small amount.

In terms of wave number and frequency, for capillary waves

$$c_0^2 = \gamma k \quad . \tag{76}$$

Substituting (1) and (76) into (73) and rearranging,

$$\gamma k^3[1 - (3/2)\beta' \ln n_1] + \gamma^{1/3} k(3\beta' n n_1^{1/3}) - n^2 = 0 \quad . \tag{77}$$

This equation is a cubic expression of $\gamma^{1/3}k$ and can be solved in terms of n by using the formulas and procedures analogous to those outlined in Appendix C. Cubing the solution results in

$$\gamma k^3 = 2r + 3[(r + D^{1/2})^{2/3}(r - D^{1/2})^{1/3} + (r + D^{1/2})^{1/3}(r - D^{1/2})^{2/3}] \tag{78}$$

where

$$r = \frac{1}{2} n^2[1 - (3/2)\beta' \ln n_1]^{-1} \tag{79}$$

and

$$D = \beta'^3 n^3 n_1[1 - (3/2)\beta' \ln n_1]^{-3} + \frac{1}{4} n^4[1 - (3/2)\beta' \ln n_1]^{-2} \quad . \tag{80}$$

Since β' is such a small quantity, the first term in (80) is negligible compared to the second term. Thus, D is approximated by

$$D \approx \frac{1}{4} n^4[1 - (3/2)\beta' \ln n_1]^{-2} \quad . \tag{81}$$

Rewriting (78) and using the approximated value for D,

$$\gamma k^3 = 2r + 3(r^2 - D)^{1/3}[(r + D^{1/2})^{1/3} + (r - D^{1/2})^{1/3}]$$

$$= n^2[1 - (3/2)\beta' \ln n_1]^{-1} - 3\beta' n n_1^{1/3}[1 - (3/2)\beta' \ln n_1]^{-1}$$

$$[(r + D^{1/2})^{1/3} + (r - D^{1/2})^{1/3}]$$

$$\approx n^2[1 - (3/2)\beta'\ln n_1]^{-1} - 3\beta' n^{5/3} n_1^{1/3}[1 - (3/2)\beta'\ln n_1]^{-4/3}$$

$$= n^2\{[1 - (3/2)\beta'\ln n_1]^{-1} - 3\beta'(n_1/n)^{1/3}[1 - (3/2)\beta'\ln n_1]^{-4/3} \tag{82}$$

Expanding the terms in brackets into binomial series which are truncated so that only terms of the order of β' or larger are retained,

$$\gamma k^3 \approx n^2[1 + (3\beta'/2)\ln n_1 - 3\beta'(n_1/n)^{1/3}] \quad . \tag{83}$$

The error from the truncation of the binomial series is of the order of β'^2. This is negligible compared to the other terms in (83). It has already been ascertained that

$$\frac{1}{2}\ln n_1 - (n_1/n)^{1/3} > 0 \tag{84}$$

since in the capillary wave range the logarithmic part will always be greater than unity while the ratio will always be less than or equal to unity. Therefore, from (83) it is seen that if the frequency is increased, the non-linear interactions will have the mean effect of increasing the wave number above that which is predicted by linear theory. Furthermore, the effect becomes greater as n_1 and the ratio n/n_1 increase.

The mean squared random scattering defined by (58) can be interpreted as a measure of the random deviation about the mean scattering. It is analogous to a variance in the statistical sense. Its square root is analogous to a standard deviation. A large value indicates a wide spread of data points about the mean while a small value indicates a close cluster of points about the mean.

Equation (58) can be investigated by looking at the integral function. This term represents the mean squared surface velocity spectrum, where the velocity is equivalent to the quasi-Eulerian velocity discussed earlier in conjunction with the mean scattering. The root mean squared error, $(\overline{\varepsilon^2})^{1/2}$, then represents a mean of the individually unpredictable random variations of the quasi-Eulerian velocity data points about the mean quasi-Eulerian velocity multiplied by the constant n.

The unidirectional non-linear effect on the square of the phase speed can be represented in terms of the mean deviation from linear theory plus the random scattering. Combining the square root of (58) with (55) and then substituting (1) into the combination,

$$c^2 = c_o^2 \{1 + (c/c_o^2)\int_{k_1}\int_{n_1} k_1 n_1 X(k_1,n_1)dk_1dn_1 - (3/2)\frac{\gamma k}{c_o^2}$$
$$\int_{k_1}\int_{n_1} k_1^2 X(k_1,n_1)dk_1dn_1 \pm (c/c_o^2)\left[\int_{k_1}\int_{n_1} n_1^2 X(k_1,n_1)dk_1dn_1\right]^{1/2} \quad (85)$$

Quantitatively, all components of (85) except the last one, $c_o^{-2}(\overline{\varepsilon^2})^{1/2}$ have been determined from the equilibrium spectral values.

In the gravity wave range the integral function in this last component becomes, after using (60) and (65)

$$\beta g^2 \int_{n_1} n_1^{-3} dn_1 \ . \quad (86)$$

Thus, for gravity waves after integrating and noting (1) and (66),

$$c_o^{-2}(\overline{\varepsilon^2})^{1/2} = \pm (c/c_o^2)(\beta/2)^{1/2}(g/n_1)$$

$$= \pm (\beta/2)^{1/2}(n/n_1) \quad . \tag{87}$$

Combining (87) with (67),

$$c^2 = c_0^2[1 + \beta(n/n_1) \pm (\beta/2)^{1/2}(n/n_1)] \quad . \tag{88}$$

Since β is such a small quantity, the square root of β is an order of magnitude greater than β. It is seen from (88), then, that the random scattering in the gravity wave range has a far greater effect on the phase speed than the mean deviation. Physically, this large scattering arises from quasi-Eulerian velocity components which have a small mean but large fluctuations.

In terms of wave number and frequency, (1) and (67) are substituted into (88) to yield

$$n^2 = gk[1 + \beta(n/n_1) \pm (\beta/2)^{1/2}(n/n_1)] \quad . \tag{89}$$

Once again using a truncated binomial series,

$$gk = n^2[1 - \beta(n/n_1) \pm (\beta/2)^{1/2}(n/n_1)] \quad . \tag{90}$$

As in the expression for the phase speed (88), the random scattering has a greater effect than the mean deviation.

In the capillary wave range the integral function in the last component of (80) becomes, after using (62) and (72),

$$\beta\gamma^{2/3} \int_{n_1} n_1^{-1/3} dn_1 \quad . \tag{91}$$

Thus, for capillary waves

$$c_0^{-2}(\overline{\varepsilon^2})^{1/2} = \pm (c/c_0^2)\gamma^{1/3}(3\beta'/2)^{1/2}n_1^{1/3} \quad . \tag{92}$$

Combining (92) with (73),

$$c^2 = c_0^2\{1 - (\beta'/c_0^2)[(3/2\gamma k)\ln n_1 - 3c\gamma^{1/3}n_1^{1/3}]$$

$$\pm (c/c_0^2)(3\beta'/2)^{1/2}\gamma^{1/3}\eta^{1/3}\} \quad . \tag{93}$$

It is seen from (93) that the large random fluctuations of the quasi-Eulerian velocity components cause the random scattering to have a greater effect on the phase speed than the mean deviation for capillary waves as well as for gravity waves.

In terms of wave number and frequency, (1) and (72) are substituted into (93) to yield, after rearranging,

$$\gamma k^3[1 - (3/2)\beta'\ln n_1] + \gamma^{(1/3)}k\{[3\beta' \pm (3\beta'/2)^{1/2}]nn_1^{(1/3)}\}$$

$$- n^2 = 0 \quad . \tag{94}$$

Equation (94) differs from (77) only in the coefficient of $\gamma^{1/3}k$. Following the development of (83), it is readily seen that the cube of the solution of (94) for $\gamma^{1/3}k$ is

$$\gamma k^3 = n^2\{1 + (3\beta'/2)\ln n_1 - (n_1/n)^{1/3}[3\beta' \pm (3\beta'/2)^{1/2}]\} \quad . \tag{95}$$

As in the expression for the phase speed (93), the random scattering has a greater effect than the mean deviation.

The non-linear effects on the phase speed for the gravity and capillary wave range is shown in Figure 6 and Figure 7. The ratio c_0^2/c^2 is

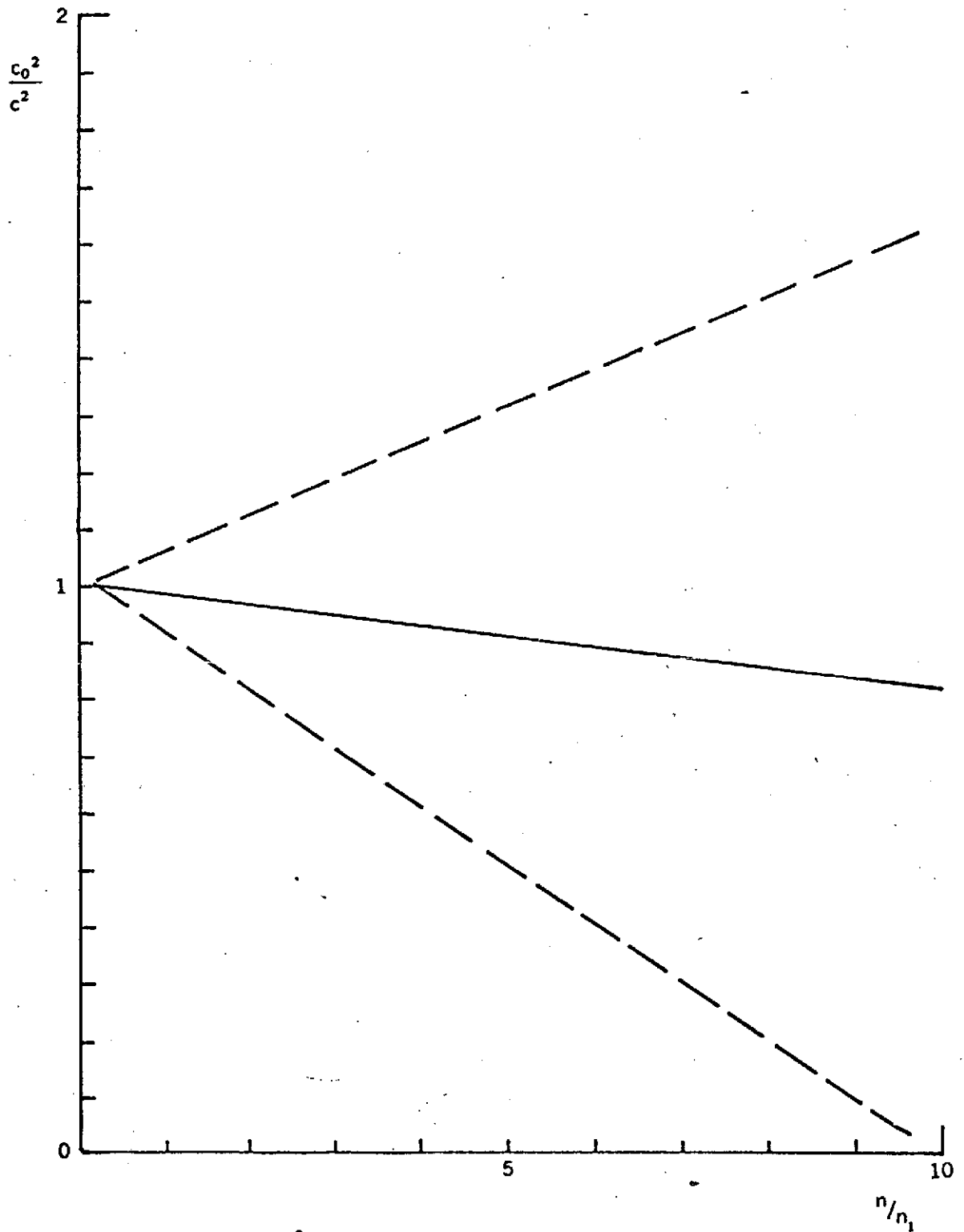

Figure 6. Plot of c_0^2/c^2 vs. n/n_1 for gravity waves showing the mean (———) and random scattering (— —)

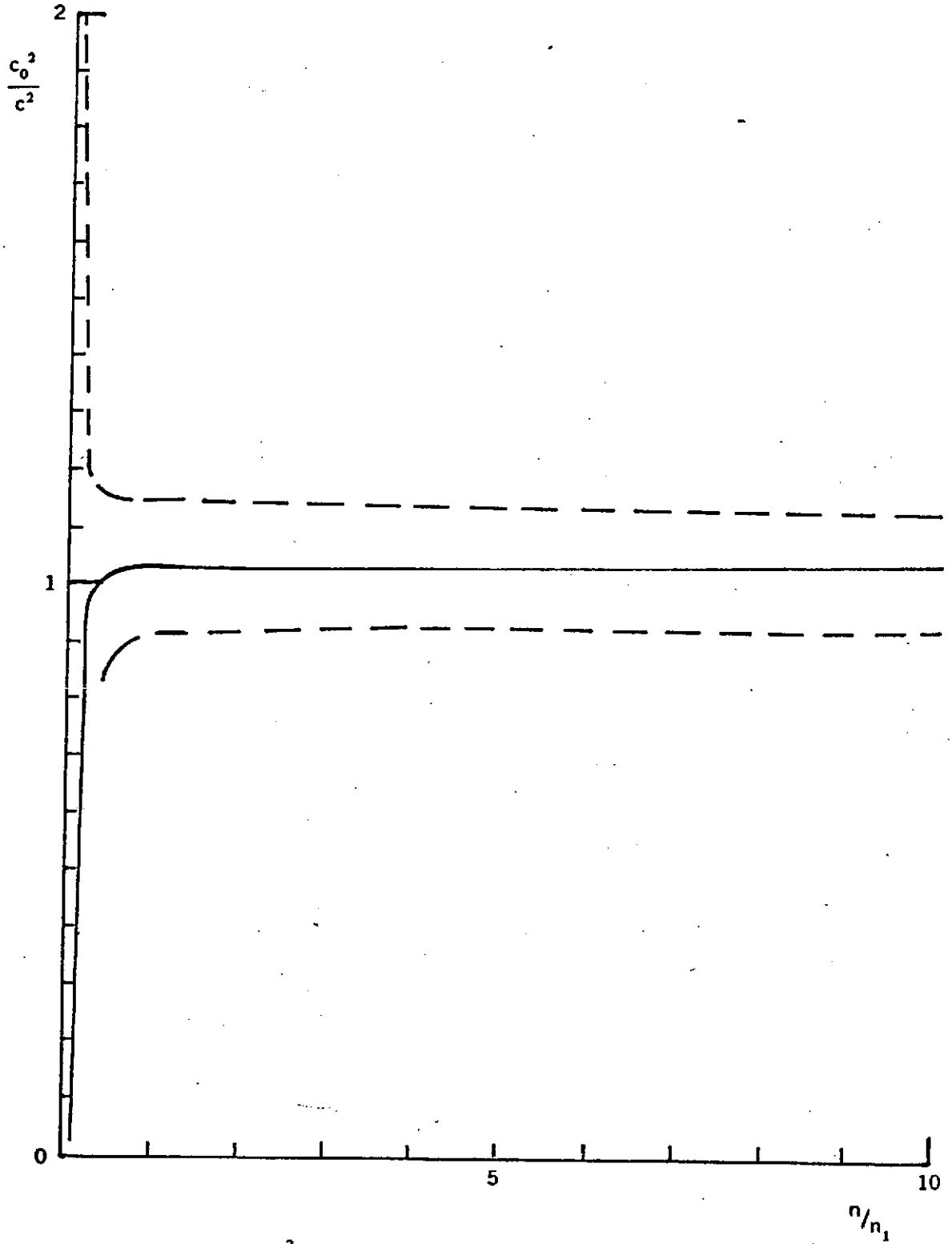

Figure 7. Plot of c_0^2/c^2 vs. n/n_1 for capillary waves showing the mean (———) and random scattering (— — —)

is plotted against n/n_1 for gravity waves in Figure 6 and for capillary waves in Figure 7. From (88), in the gravity wave range

$$c_o^2/c^2 = [1 + \beta(n/n_1) \pm (\beta/2)^{1/2}(n/n_1)]^{-1}$$

$$\simeq 1 - \beta(n/n_1) \pm (\beta/2)^{1/2}(n/n_1) \qquad (96)$$

after using the truncated binomial series. In the capillary wave range, multiplying (76) by k^2 gives

$$\gamma k^3 = c_o^2 k^2 \quad . \qquad (97)$$

Applying (97) and (1) to (95) and rearranging,

$$c_o^2/c^2 = 1 + (3\beta'/2)\ln n_1 - (n_1/n)^{1/3}[3\beta' \pm (3\beta'/2)^{1/2}] \quad . \qquad (98)$$

In terms of the relationship between wave number and frequency, Figure 8 is a gravity wave representation and Figure 9 is a capillary wave representation of n_o^2/n^2 against n/n_1 where n_o^2 is the linear squared frequency. For gravity waves

$$n_o^2 = gk \qquad (99)$$

and for capillary waves

$$n_o^2 = \gamma k^3 \quad . \qquad (100)$$

Figure 8 is determined from (90) and Figure 9 is determined from (95).

The mean deviation as shown in Figure 6 and Figure 8 decreases in the gravity wave range as n/n_1 increases. In the capillary wave range the mean deviation as shown in Figure 7 and Figure 9 increases as n/n_1

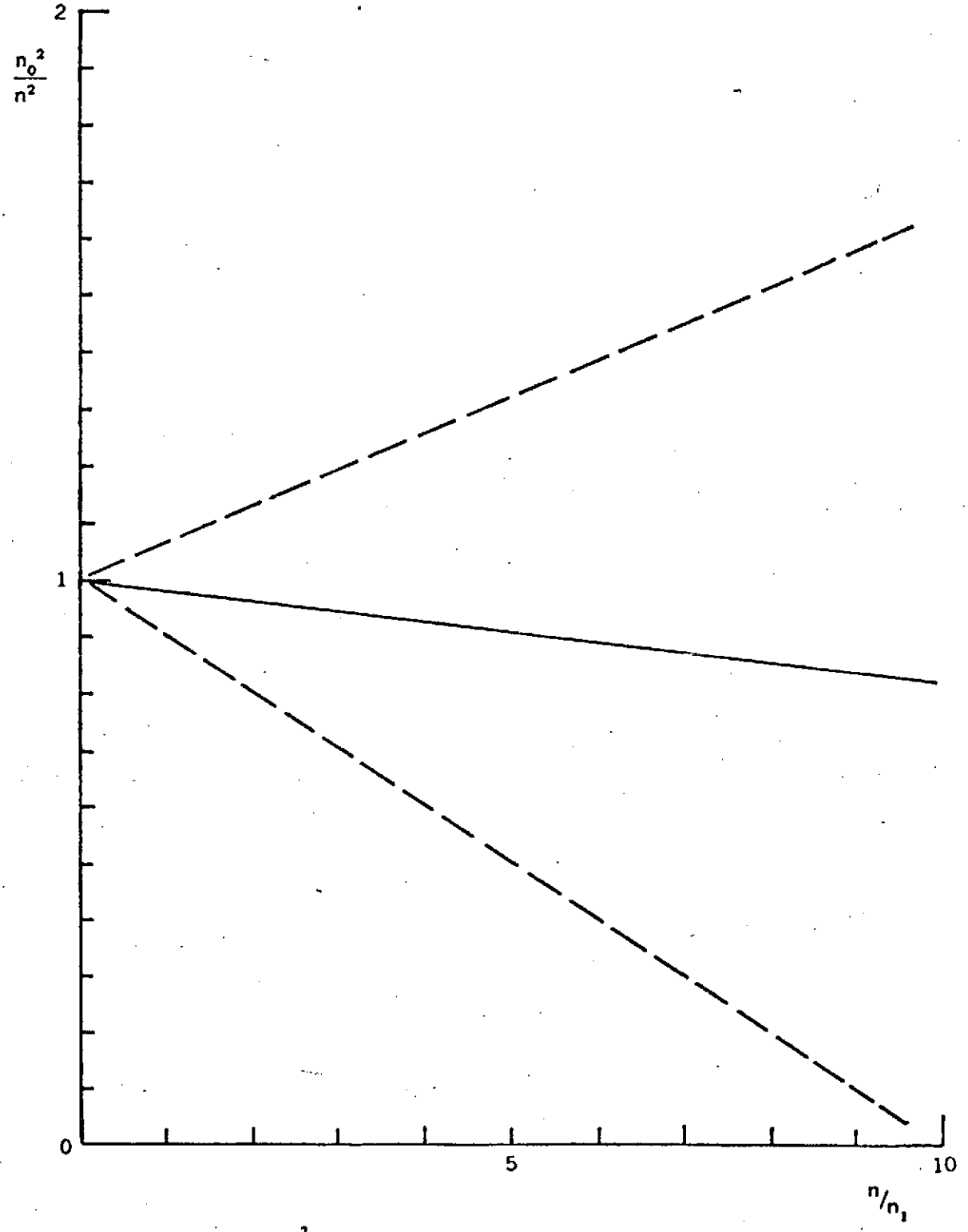

Figure 8. Plot of n_0^2/n^2 vs. n/n_1 for gravity waves showing the mean (———) and random scattering (— — —)

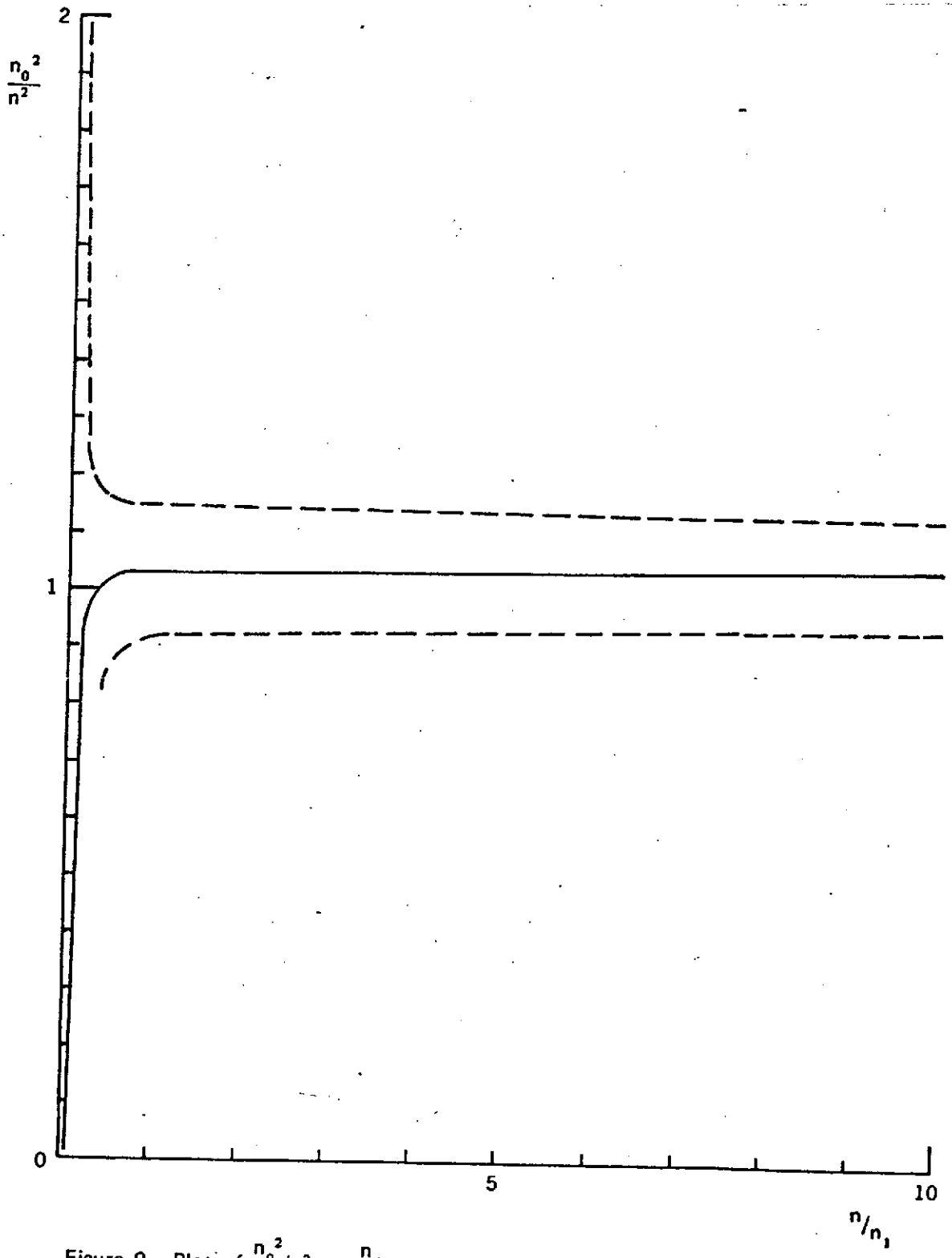

Figure 9. Plot of n_0^2/n^2 vs. n/n_1 for capillary waves showing the mean (———) and random scattering (— — —)

increases. This reversal can be explained by looking at the integrated mean quasi-Eulerian velocity in (59). This term is directly proportional to n and inversely proportional to n_1 in the gravity wave range as shown in (67). For capillary waves, however, this term is directly proportional to both n and $n_1^{1/3}$ as shown in (77). A change in n/n_1 will therefore cause the velocity in the two wave ranges to change in opposite directions.

The random scattering for gravity waves as depicted in Figure 6 and Figure 8 increases as n/n_1 increases. For capillary waves, however, depicted in Figure 7 and Figure 9, the scatter decreases as n/n_1 increases. These results are explained by considering the integrated quasi-Eulerian velocity spectra from which the random errors are derived. In the gravity wave range the spectrum is computed from the square root of the integral function in (58) after using (60). Thus,

$$\left[\int_{k_1}\int_{n_1} n_1^2 X(k_1,n_1)\,dk_1\,dn_1\right]^{1/2} = (\beta/2)^{1/2}(g/n_1) \quad . \tag{101}$$

Equation (101) shows that the velocity increases as n_1 decreases. For a constant n, therefore, the velocity will increase as the ratio n/n_1 increases. This causes the increasing scatter in Figure 6 and Figure 8. For capillary waves, (58) and (62) yield

$$\left[\int_{k_1}\int_{n_1} n_1^2 X(k_1,n_1)\,dk_1\,dn_1\right]^{1/2} = \gamma^{1/3}(3\beta'/2)^{1/2} n_1^{1/3} \tag{102}$$

so that the velocity decreases as n_1 decreases. Thus, for a constant n, the scatter will decrease as n/n_1 increases as reflected in Figure 7 and Figure 9.

LIST OF REFERENCES

Burling, R. W., 1959: The spectrum of waves at short fetches. Deut. Hydrogr. Zeit., 12, 45-64, 96-117.

Carrier, G. F. and A. R. Robinson, 1962: On the theory of the wind-driven ocean circulation. J. Fluid Mech., 12, 49-80.

Cole, J. D., 1968: Perturbation Methods in Applied Mathematics. Waltham, Mass., Blaisdell, 260pp.

Cox, C. S., 1958: Measurements of slopes of high-frequency wind waves. J. Mar. Res., 16, 199-225.

_____ and W. H. Munk, 1956: Slopes of the sea surface deduced from photographs of sun glitter. Bull. Scripps Inst. Oceanogr., 6, 401-488.

Crapper, G. D., 1957: An exact solution for progressive capillary waves of arbitrary amplitude. J. Fluid Mech., 2, 532-540.

Edgeworth, F. Y., 1904: The law of error. Cambridge Phil. Trans., 20, 36-65.

Grose, P. L., 1971: Deep Water Surface Wave Spectra Measured in the Trade Wind Regime. Ph.D. Dissertation, Florida State University. Tallahassee, Florida.

_____, K. L. Warsh and M. Garstang, 1972: Dispersion relations and wave shapes. J. Geophys. Res., 77, 3902-3906.

Huang, N. E., 1971: Derivation of Stokes drift for a deep-water random gravity wave field. Deep-Sea Res., 18, 255-259.

_____, 1972: Non-linear dispersion relation for a random gravity wave field. Presented at the 53rd Annual Meeting, Amer. Geophys. Union, Washington, D. C.

_____, D. T. Chen, C. -C. Tung and J. R. Smith, 1972: Interactions between steady non-uniform currents and gravity waves with applications for current measurements. J. Phys. Oceanogr., in press.

Kendall, M. G., 1952: The Advanced Theory of Statistics, Vol. 1. New York, Hafner, 457pp.

Kinsman, B. 1960: Surface waves at short fetches and low wind speeds--a field study. The Johns Hopkins Univ., Chesapeake Bay Inst., Tech. Rep. no. 19, 581pp.

_____, 1965: Wind Waves: Their Generation and Propagation on the Ocean Surface. Englewood Cliffs, N. J., Prentice-Hall, 676pp.

Longuet-Higgins, M. S., 1963a: The generation of capillary waves by steep gravity waves. J. Fluid Mech., 16, 138-159.

_____, 1963b: The effect of non-linearities on statistical distributions in the theory of sea waves. J. Fluid Mech., 17, 459-480.

_____, D. E. Cartwright and N. D. Smith, 1963: Observations of the directional spectrum of sea waves using the motions of a floating buoy. Ocean Wave Spectra. Englewood Cliffs, N. J., Prentice-Hall, 111-136.

_____ and O. M. Phillips, 1962: Phase velocity effects in tertiary wave interactions. J. Fluid Mech., 12, 333-336.

_____ and R. W. Stewart, 1960: Changes in the form of short gravity waves on long waves and tidal currents. J. Fluid Mech., 8, 565-583.

MacKay, J. H., 1959: On the Gaussian nature of ocean waves. Georgia Inst. Tech., Engrg. Exp. Sta., Project A-366, Internal Tech. Note No. 8, 20pp.

McGoldrick, L. F., 1965. Resonant interactions among capillary-gravity waves. J. Fluid Mech., 21, 305-331.

Phillips, O. M., 1958: The equilibrium range in the spectrum of wind-generated waves. J. Fluid Mech., 4, 426-434.

_____, 1960a: On the dynamics of unsteady gravity waves of finite amplitude, Part 1. J. Fluid Mech., 9, 193-217.

_____, 1960b: The mean horizontal momentum and surface velocity of finite-amplitude random gravity waves. J. Geophys. Res., 65, 3473-3476.

_____, 1961: On the dynamics of unsteady gravity waves of finite-amplitude, Part 2. J. Fluid Mech., 11, 143-155.

_____, 1969: The Dynamics of the Upper Ocean. London, Cambridge University Press, 261pp.

Pierson, W. J., ed., 1960: The directional spectrum of a wind generated sea as determined from data obtained by the Stereo Wave Observation Project. New York University, Coll. Engrg. Meteor. Pap., 2, No. 6, 88pp.

_____ and W. Marks, 1952: The power spectrum analysis of ocean-wave records. Trans. Amer. Geophys. Union, 33, 834-844.

Plate, E. and M. Trawle, 1970: A note on the celerity of wind waves on a water current. J. Geophys. Res., 75, 3537-3544.

Rudnick, P., 1951: Correlograms for Pacific Ocean waves. Proc. of the 2nd Berkeley Symp. on Math. Stat. and Prob. Berkeley, University of Calif. Press, 627-638.

Schooley, A. H., 1955: Curvature distributions of wind-created water waves. Trans. Amer. Geophys. Union, 36, 273-278.

_____, 1963: Simple tools for measuring wind fields above wind-generated water waves. J. Geophys. Res., 68, 5497-5504.

Stokes, G. G., 1847: On the theory of oscillatory waves. Trans. Cambridge Phil. Soc., 8, 441-455.

_____, 1880: Supplement to a paper on the theory of oscillatory waves. Math. and Phys. Pap., Vol. I. London, Cambridge University Press, 314-326.

Whitham, G. B., 1960: A note on group velocity. J. Fluid Mech., 9, 347-352.

_____, 1962: Mass, momentum and energy flux in water waves. J. Fluid Mech., 12, 135-147.

Wu, J., 1972: Sea-surface and equilibrium wind-wave spectra. Phys. Fluids, 15, 741-747.

Yefimov, V. V. and G. N. Khristoforov, 1971: Wave-related and turbulent components of velocity spectrum in the top sea layer. Izv., Atmos. and Oceanic Phys., 7, 200-211.

APPENDICES

Appendix A

Third Order Relationship Between $dA(\underset{\sim}{k},n)$ and $dB(\underset{\sim}{k},n)$

Rewriting (31)

$$\iint_{\underset{\sim}{k}n} -in\,dB(\underset{\sim}{k},n)\exp[i(\underset{\sim}{k}\cdot\underset{\sim}{x} - nt)] = \iint_{\underset{\sim}{k}n} |\underset{\sim}{k}|\,dA(\underset{\sim}{k},n)\exp[|\underset{\sim}{k}|\zeta]\exp[i(\underset{\sim}{k}\cdot\underset{\sim}{x} - nt)]$$

$$+ \iiint_{\underset{\sim}{k}n\underset{\sim}{k}_1 n_1} \int \underset{\sim}{k}\cdot\underset{\sim}{k}_1\, dA(\underset{\sim}{k},n)\,dB(\underset{\sim}{k}_1,n_1)\exp[|\underset{\sim}{k}|\zeta]\exp\{i[(\underset{\sim}{k}+\underset{\sim}{k}_1)\cdot\underset{\sim}{x} - (n+n_1)t]\} \tag{31}$$

Substituting a series expansion for $\exp[|\underset{\sim}{k}|\zeta]$, and using (26),

$$\iint_{\underset{\sim}{k}n} -in\,dB(\underset{\sim}{k},n)\exp[i(\underset{\sim}{k}\cdot\underset{\sim}{x}-nt)] = \iint_{\underset{\sim}{k}n} |\underset{\sim}{k}|\,dA(\underset{\sim}{k},n)[1 + |\underset{\sim}{k}|\zeta + \tfrac{1}{2}|\underset{\sim}{k}|^2\zeta^2]\exp[i(\underset{\sim}{k}\cdot\underset{\sim}{x}-nt)]$$

$$+ \iiint_{\underset{\sim}{k}n\underset{\sim}{k}_1 n_1} \int \underset{\sim}{k}\cdot\underset{\sim}{k}_1\, dA(\underset{\sim}{k},n)\,dB(\underset{\sim}{k}_1,n_1)[1 + |\underset{\sim}{k}|\zeta]\exp$$

$$\{i[(\underset{\sim}{k}+\underset{\sim}{k}_1)\cdot\underset{\sim}{x} - (n+n_1)t]\}$$

$$= \iint_{\underset{\sim}{k}n} |\underset{\sim}{k}|\,dA(\underset{\sim}{k},n)\exp[i(\underset{\sim}{k}\cdot\underset{\sim}{x} - nt)] + \iiint_{\underset{\sim}{k}n\underset{\sim}{k}_1 n_1} \int |\underset{\sim}{k}|^2 dA(\underset{\sim}{k},n)\,dB(\underset{\sim}{k}_1,n_1)$$

$$\exp\{i[(\underset{\sim}{k}+\underset{\sim}{k}_1)\cdot\underset{\sim}{x} - (n+n_1)t] + \tfrac{1}{2}\iiint_{\underset{\sim}{k}n\underset{\sim}{k}_1 n_1}\int\int_{\underset{\sim}{k}_2 n_2} \int |\underset{\sim}{k}|^3 dA(\underset{\sim}{k},n)\,dB(\underset{\sim}{k}_1,n_1)$$

$$dB(\underset{\sim}{k}_2,n_2)\exp\{i[(\underset{\sim}{k}+\underset{\sim}{k}_1+\underset{\sim}{k}_2)\cdot\underset{\sim}{x} - (n+n_1+n_2)t] + \iiint_{\underset{\sim}{k}n\underset{\sim}{k}_1 n_1} \int \underset{\sim}{k}\cdot\underset{\sim}{k}_1$$

$$dA(\underset{\sim}{k},n)\,dB(\underset{\sim}{k}_1,n_1)\exp\{i[(\underset{\sim}{k}+\underset{\sim}{k}_1)\cdot\underset{\sim}{x} - (n+n_1)t]\}$$

$$+ \iiint_{\underset{\sim}{k}n\underset{\sim}{k}_1 n_1}\int\int_{\underset{\sim}{k}_2 n_2} \int |\underset{\sim}{k}|\,\underset{\sim}{k}\cdot\underset{\sim}{k}_1\, dA(\underset{\sim}{k},n)\,dB(\underset{\sim}{k}_1,n_1)\,dB(\underset{\sim}{k}_2,n_2)$$

$$\exp\{i[(\underset{\sim}{k}+\underset{\sim}{k}_1+\underset{\sim}{k}_2)\cdot\underset{\sim}{x} - (n+n_1+n_2)t]\} \tag{A-1}$$

For the first order let

$$\underset{\sim}{k} = \underset{\sim}{k}_o \ , \quad n = n_o \ . \tag{A-2}$$

For the second order let

$$\underset{\sim}{k} + \underset{\sim}{k}_1 = \underset{\sim}{k}_o \ , \quad n + n_1 = n_o \ . \tag{A-3}$$

For the third order let

$$\underset{\sim}{k} + \underset{\sim}{k}_1 + \underset{\sim}{k}_2 = \underset{\sim}{k}_o \ , \quad n + n_1 + n_2 = n_o \ . \tag{A-4}$$

Then, after substituting (A-2), (A-3) and (A-4) into (A-1),

$$\int_{\underset{\sim}{k}_o} \int_{n_o} -in_o dB(\underset{\sim}{k}_o, n_o) \exp[i(\underset{\sim}{k}_o \cdot \underset{\sim}{x} - n_o t)] = \int_{\underset{\sim}{k}_o} \int_{n_o} |\underset{\sim}{k}_o| dA(\underset{\sim}{k}_o, n_o) \exp[i(\underset{\sim}{k}_o \cdot \underset{\sim}{x} - n_o t)]$$

$$+ \int_{\underset{\sim}{k}_o} \int_{n_o} \int_{\underset{\sim}{k}_1} \int_{n_1} |\underset{\sim}{k}_o - \underset{\sim}{k}_1|^2 dA(\underset{\sim}{k}_o - \underset{\sim}{k}_1, n_o - n_1) dB(\underset{\sim}{k}_1, n_1) \exp[i(\underset{\sim}{k}_o \cdot \underset{\sim}{x} - n_o t)]$$

$$+ \frac{1}{2} \int_{\underset{\sim}{k}_o} \int_{n_o} \int_{\underset{\sim}{k}_1} \int_{n_1} \int_{\underset{\sim}{k}_2} \int_{n_2} |\underset{\sim}{k}_o - \underset{\sim}{k}_1 - \underset{\sim}{k}_2|^3 dA(\underset{\sim}{k}_o - \underset{\sim}{k}_1 - \underset{\sim}{k}_2, n_o - n_1 - n_2)$$

$$dB(\underset{\sim}{k}_1, n_1) dB(\underset{\sim}{k}_2, n_2) \exp[i(\underset{\sim}{k}_o \cdot \underset{\sim}{x} - n_o t)] + \int_{\underset{\sim}{k}_o} \int_{n_o} \int_{\underset{\sim}{k}_1} \int_{n_1} (\underset{\sim}{k}_o - \underset{\sim}{k}_1) \cdot \underset{\sim}{k}_1$$

$$dA(\underset{\sim}{k}_o - \underset{\sim}{k}_1, n_o - n_1) dB(\underset{\sim}{k}_1, n_1) \exp[i(\underset{\sim}{k}_o \cdot \underset{\sim}{x} - n_o t)] + \int_{\underset{\sim}{k}_o} \int_{n_o} \int_{\underset{\sim}{k}_1} \int_{n_1} \int_{\underset{\sim}{k}_2} \int_{n_2}$$

$$|\underset{\sim}{k}_o - \underset{\sim}{k}_1 - \underset{\sim}{k}_2| (\underset{\sim}{k}_o - \underset{\sim}{k}_1 - \underset{\sim}{k}_2) \cdot \underset{\sim}{k}_1 dA(\underset{\sim}{k}_o - \underset{\sim}{k}_1 - \underset{\sim}{k}_2, n_o - n_1 - n_2)$$

$$dB(\underset{\sim}{k}_1, n_1) dB(\underset{\sim}{k}_2, n_2) \exp[i(\underset{\sim}{k}_o \cdot \underset{\sim}{x} - n_o t)] \ . \tag{A-5}$$

Since each component of (A-5) is integrated over $(\underset{\sim}{k}_o, n_o)$, only the integrands of the integration over $(\underset{\sim}{k}_o, n_o)$ need to be considered. After dropping the zero subscripts, these integrands in (A-5) can be rearranged so that

$$dA(\underset{\sim}{k},n) = -\frac{in}{|\underset{\sim}{k}|}\,dB(\underset{\sim}{k},n) - \int_{\underset{\sim}{k}_1}\int_{n_1}\left[|\underset{\sim}{k}-\underset{\sim}{k}_1|^2 + \underset{\sim}{k}_1\cdot(\underset{\sim}{k}-\underset{\sim}{k}_1)\right]\frac{1}{|\underset{\sim}{k}|}\,dA(\underset{\sim}{k}-\underset{\sim}{k}_1,n-n_1)$$

$$dB(\underset{\sim}{k}_1,n_1) - \int_{\underset{\sim}{k}_1}\int_{n_1}\int_{\underset{\sim}{k}_2}\int_{n_2}\left[\frac{1}{2}|\underset{\sim}{k}-\underset{\sim}{k}_1-\underset{\sim}{k}_2|^3 + |\underset{\sim}{k}-\underset{\sim}{k}_1-\underset{\sim}{k}_2|\underset{\sim}{k}_1\cdot(\underset{\sim}{k}-\underset{\sim}{k}_1-\underset{\sim}{k}_2)\right.$$

$$\left.\frac{1}{|\underset{\sim}{k}|}\,dA(\underset{\sim}{k}-\underset{\sim}{k}_1-\underset{\sim}{k}_2,n-n_1-n_2)dB(\underset{\sim}{k}_1,n_1)dB(\underset{\sim}{k}_2,n_2)\right. \qquad \text{(A-6)}$$

Using successive approximations, to the first order

$$dA(\underset{\sim}{k},n) = -\frac{in}{|\underset{\sim}{k}|}\,dB(\underset{\sim}{k},n) \qquad \text{(A-7)}$$

To the second order, after substituting (A-7) for $dA(\underset{\sim}{k}-\underset{\sim}{k}_1,n-n_1)$ in (A-6),

$$dA(\underset{\sim}{k},n) = -\frac{in}{|\underset{\sim}{k}|}\,dB(\underset{\sim}{k},n) - \int_{\underset{\sim}{k}_1}\int_{n_1}\left[|\underset{\sim}{k}-\underset{\sim}{k}_1|^2 + \underset{\sim}{k}_1\cdot(\underset{\sim}{k}-\underset{\sim}{k}_1)\right]\frac{1}{|\underset{\sim}{k}|}\left[-\frac{i(n-n_1)}{|\underset{\sim}{k}-\underset{\sim}{k}_1|}\right.$$

$$\left.dB(\underset{\sim}{k}-\underset{\sim}{k}_1,n-n_1)\right]dB(\underset{\sim}{k}_1,n_1)$$

$$= -\frac{in}{|\underset{\sim}{k}|}\,dB(\underset{\sim}{k},n) + i\int_{\underset{\sim}{k}_1}\int_{n_1}\frac{\underset{\sim}{k}\cdot(\underset{\sim}{k}-\underset{\sim}{k}_1)}{|\underset{\sim}{k}||\underset{\sim}{k}-\underset{\sim}{k}_1|}\,(n-n_1)dB(\underset{\sim}{k}-\underset{\sim}{k}_1,n-n_1)$$

$$dB(\underset{\sim}{k}_1,n_1) \qquad \text{(A-8)}$$

Continuing the approximation, substitution of (A-8) into (A-6) yields the third order relationship

$$dA(\underset{\sim}{k},n) = -\frac{in}{|\underset{\sim}{k}|}\,dB(\underset{\sim}{k},n) - \int_{\underset{\sim}{k}_1}\int_{n_1} \frac{\underset{\sim}{k}\cdot(\underset{\sim}{k}-\underset{\sim}{k}_1)}{|\underset{\sim}{k}|}\left[-\frac{i(n-n_1)}{|\underset{\sim}{k}-\underset{\sim}{k}_1|}\,dB(\underset{\sim}{k}-\underset{\sim}{k}_1,n-n_1)\right.$$

$$+ i\int_{\underset{\sim}{k}_2}\int_{n_2}\frac{(\underset{\sim}{k}-\underset{\sim}{k}_1)\cdot(\underset{\sim}{k}-\underset{\sim}{k}_1-\underset{\sim}{k}_2)}{|\underset{\sim}{k}-\underset{\sim}{k}_1||\underset{\sim}{k}-\underset{\sim}{k}_1-\underset{\sim}{k}_2|}\,(n-n_1-n_2)dB(\underset{\sim}{k}-\underset{\sim}{k}_1-\underset{\sim}{k}_2,$$

$$\left.n-n_1-n_2)dB(\underset{\sim}{k}_2,n_2)\right]dB(\underset{\sim}{k}_1,n_1) - \int_{\underset{\sim}{k}_1}\int_{n_1}\int_{\underset{\sim}{k}_2}\int_{n_2}\left[\frac{1}{2}|\underset{\sim}{k}-\underset{\sim}{k}_1-\underset{\sim}{k}_2|^3\right.$$

$$\left. + |\underset{\sim}{k}-\underset{\sim}{k}_1-\underset{\sim}{k}_2|(\underset{\sim}{k}-\underset{\sim}{k}_1-\underset{\sim}{k}_2)\cdot\underset{\sim}{k}_1\right]\frac{1}{|\underset{\sim}{k}|}\left[-\frac{i(n-n_1-n_2)}{|\underset{\sim}{k}-\underset{\sim}{k}_1-\underset{\sim}{k}_2|}\right.$$

$$\left.dB(\underset{\sim}{k}-\underset{\sim}{k}_1-\underset{\sim}{k}_2,n-n_1-n_2)\right]\,dB(\underset{\sim}{k}_1,n_1)dB(\underset{\sim}{k}_2,n_2)\quad . \qquad \text{(A-9)}$$

Rearranging

$$dA(\underset{\sim}{k},n) = -\frac{in}{|\underset{\sim}{k}|}\,dB(\underset{\sim}{k},n) + i\int_{\underset{\sim}{k}_1}\int_{n_1}\frac{\underset{\sim}{k}\cdot(\underset{\sim}{k}-\underset{\sim}{k}_1)}{|\underset{\sim}{k}||\underset{\sim}{k}-\underset{\sim}{k}_1|}(n-n_1)dB(\underset{\sim}{k}-\underset{\sim}{k}_1,n-n_1)$$

$$dB(\underset{\sim}{k}_1,n_1) + i\int_{\underset{\sim}{k}_1}\int_{n_1}\int_{\underset{\sim}{k}_2}\int_{n_2}\frac{(n-n_1-n_2)}{|\underset{\sim}{k}|}\left[\frac{1}{2}\,(\underset{\sim}{k}+\underset{\sim}{k}_1-\underset{\sim}{k}_2)\cdot(\underset{\sim}{k}-\underset{\sim}{k}_1-\underset{\sim}{k}_2)\right.$$

$$\left.-\frac{\underset{\sim}{k}\cdot(\underset{\sim}{k}-\underset{\sim}{k}_1)(\underset{\sim}{k}-\underset{\sim}{k}_1)\cdot(\underset{\sim}{k}-\underset{\sim}{k}_1-\underset{\sim}{k}_2)}{|\underset{\sim}{k}-\underset{\sim}{k}_1||\underset{\sim}{k}-\underset{\sim}{k}_1-\underset{\sim}{k}_2|}\right]\,dB(\underset{\sim}{k}-\underset{\sim}{k}_1-\underset{\sim}{k}_2,n-n_1-n_2)$$

$$dB(\underset{\sim}{k}_1,n_1)dB(\underset{\sim}{k}_2,n_2)\quad . \qquad \text{(A-10)}$$

Appendix B

Third Order Expansion of the Dispersive Relationship

Rewriting (39)

$$g\zeta = -(\partial\phi/\partial t)_\zeta - \tfrac{1}{2}(\nabla\phi)^2_\zeta + \gamma(\nabla_h^2\zeta)[1 + (\nabla_h\zeta)^2]^{-(3/2)} \quad . \quad (39)$$

Expanding the term raised to the -3/2 power in a binomial series,

$$g\zeta = -(\partial\phi/\partial t)_\zeta - \tfrac{1}{2}(\nabla\phi)^2_\zeta + \gamma(\nabla_h^2\zeta)[1 - (3/2)(\nabla_h\zeta)^2] \quad . \quad (B\text{-}1)$$

Using (25) and (26) to substitute for ϕ and ζ,

$$\iint_{\underset{\sim}{k}n} gdB(\underset{\sim}{k},n)\exp[i(\underset{\sim}{k}\cdot\underset{\sim}{x} - nt)] = \iint_{\underset{\sim}{k}n} indA(\underset{\sim}{k},n)\exp[|\underset{\sim}{k}|\zeta]\exp[i(\underset{\sim}{k}\cdot\underset{\sim}{x} - nt)]$$

$$- \tfrac{1}{2}\iiint_{\underset{\sim}{k}n\underset{\sim}{k}_1 n_1}\int (|\underset{\sim}{k}||\underset{\sim}{k}_1| - \underset{\sim}{k}\cdot\underset{\sim}{k}_1)dA(\underset{\sim}{k},n)dA(\underset{\sim}{k}_1,n_1)\exp[(|\underset{\sim}{k}| + |\underset{\sim}{k}_1|)\zeta]$$

$$\exp\{i[(\underset{\sim}{k}+\underset{\sim}{k}_1)\cdot\underset{\sim}{x} - (n+n_1)t]\} - \gamma\iint_{\underset{\sim}{k}n} |\underset{\sim}{k}|^2 dB(\underset{\sim}{k},n)\exp[i(\underset{\sim}{k}\cdot\underset{\sim}{x} - nt)]$$

$$- \gamma(3/2)\iiint_{\underset{\sim}{k}n\underset{\sim}{k}_1 n_1}\int\int\int_{\underset{\sim}{k}_2 n_2} |\underset{\sim}{k}|^2\underset{\sim}{k}_1\cdot\underset{\sim}{k}_2 dB(\underset{\sim}{k},n)dB(\underset{\sim}{k}_1,n_1)dB(\underset{\sim}{k}_2,n_2)$$

$$\exp\{i[(\underset{\sim}{k}+\underset{\sim}{k}_1+\underset{\sim}{k}_2)\cdot\underset{\sim}{x} - (n+n_1+n_2)t]\} \quad . \quad (B\text{-}2)$$

Expanding the surface slope exponential functions into Taylor series around ζ=0,

$$\iint_{\underset{\sim}{k}n} gdB(\underset{\sim}{k},n)\exp[i(\underset{\sim}{k}\cdot x - nt)] = \iint_{\underset{\sim}{k}n} in[1+|\underset{\sim}{k}|\zeta + \tfrac{1}{2}|\underset{\sim}{k}|^2\zeta^2]dA(\underset{\sim}{k},n)$$

$$\exp[i(\underset{\sim}{k}\cdot\underset{\sim}{x} - nt)] - \tfrac{1}{2}\iiint_{\underset{\sim}{k}n\underset{\sim}{k}_1 n_1}\int (|\underset{\sim}{k}||\underset{\sim}{k}_1| - \underset{\sim}{k}\cdot\underset{\sim}{k}_1)[1+(|\underset{\sim}{k}|+|\underset{\sim}{k}_1|)\zeta]$$

$$dA(\underset{\sim}{k},n)dA(\underset{\sim}{k}_1,n_1)\exp\{i[(\underset{\sim}{k}+\underset{\sim}{k}_1)\cdot\underset{\sim}{x} - (n+n_1)t]\}$$

$$- \gamma \int\int_{\underset{\sim}{k}n} |\underset{\sim}{k}|^2 dB(\underset{\sim}{k},n)\exp[i(\underset{\sim}{k}\cdot\underset{\sim}{x}-nt)] - \gamma(3/2) \int\int\int\int_{\underset{\sim}{k}n\underset{\sim}{k}_1 n_1} \int\int_{\underset{\sim}{k}_2 n_2} |\underset{\sim}{k}|^2 \underset{\sim}{k}_1\cdot\underset{\sim}{k}_2$$

$$dB(\underset{\sim}{k},n)dB(\underset{\sim}{k}_1,n_1)dB(\underset{\sim}{k}_2,n_2)\exp\{i[(\underset{\sim}{k}+\underset{\sim}{k}_1+\underset{\sim}{k}_2)\cdot x - (n+n_1+n_2)t]\} \quad .$$

(B-3)

Rearranging,

$$\int\int_{\underset{\sim}{k}n} g dB(\underset{\sim}{k},n)\exp[i(\underset{\sim}{k}\cdot\underset{\sim}{x}-nt)] = \int\int_{\underset{\sim}{k}n} in dA(\underset{\sim}{k},n)\exp[i(\underset{\sim}{k}\cdot\underset{\sim}{x}-nt)] + \int\int\int_{\underset{\sim}{k}n\underset{\sim}{k}_1 n_1}$$

$$in|\underset{\sim}{k}|dA(\underset{\sim}{k},n)dB(\underset{\sim}{k}_1,n_1)\exp\{i[(\underset{\sim}{k}+\underset{\sim}{k}_1)\cdot\underset{\sim}{x} - (n+n_1)t]\} + \frac{1}{2}\int\int\int\int_{\underset{\sim}{k}n\underset{\sim}{k}_1 n_1} \int\int_{\underset{\sim}{k}_2 n_2}$$

$$in|\underset{\sim}{k}|^2 dA(\underset{\sim}{k},n)dB(\underset{\sim}{k}_1,n_1)dB(\underset{\sim}{k}_2,n_2)\exp\{i[(\underset{\sim}{k}+\underset{\sim}{k}_1+\underset{\sim}{k}_2)\cdot x - (n+n_1+n_2)t]\}$$

$$- \frac{1}{2}\int\int\int_{\underset{\sim}{k}n\underset{\sim}{k}_1 n_1} (|\underset{\sim}{k}||\underset{\sim}{k}_1| - \underset{\sim}{k}\cdot\underset{\sim}{k}_1)\, dA(\underset{\sim}{k},n)dA(\underset{\sim}{k}_1,n_1)\exp\{i[(\underset{\sim}{k}+\underset{\sim}{k}_1)\cdot\underset{\sim}{x} - (n+n_1)t]\}$$

$$- \frac{1}{2}\int\int\int_{\underset{\sim}{k}n\underset{\sim}{k}_1 n_1} \int\int_{\underset{\sim}{k}_2 n_2} (|\underset{\sim}{k}||\underset{\sim}{k}_1| - \underset{\sim}{k}\cdot\underset{\sim}{k}_1)(|\underset{\sim}{k}| + |\underset{\sim}{k}_1|)dA(\underset{\sim}{k},n)dA(\underset{\sim}{k}_1,n_1)$$

$$dB(\underset{\sim}{k}_2,n_2)\exp\{i[(\underset{\sim}{k}+\underset{\sim}{k}_1+\underset{\sim}{k}_2)\cdot\underset{\sim}{x} - (n+n_1+n_2)t]\} - \gamma \int\int_{\underset{\sim}{k}n} |\underset{\sim}{k}|^2$$

$$dB(\underset{\sim}{k},n)\exp[i(\underset{\sim}{k}\cdot\underset{\sim}{x}-nt)] - \gamma(3/2)\int\int\int\int_{\underset{\sim}{k}n\underset{\sim}{k}_1 n_1} \int\int_{\underset{\sim}{k}_2 n_2} |\underset{\sim}{k}|^2 \underset{\sim}{k}_1\cdot\underset{\sim}{k}_2 dB(\underset{\sim}{k},n)$$

$$dB(\underset{\sim}{k}_1,n_1)dB(\underset{\sim}{k}_2,n_2)\exp\{i[(\underset{\sim}{k}+\underset{\sim}{k}_1+\underset{\sim}{k}_2)\cdot\underset{\sim}{x} - (n+n_1+n_2)t]\} \quad . \qquad \text{(B-4)}$$

Numbering each term on the right hand side of (B-4) consecutively from I to VII and substituting for $dA(\underset{\sim}{k},n)$ from (36), to third order

$$I = \iint_{\underset{\sim}{k}n} \frac{n^2}{|\underset{\sim}{k}|}\, dB(\underset{\sim}{k},n)\exp[i(\underset{\sim}{k}\cdot\underset{\sim}{x} - nt)] - \iiint_{\underset{\sim}{k}n\underset{\sim}{k}_1 n_1} \frac{\underset{\sim}{k}\cdot(\underset{\sim}{k}-\underset{\sim}{k}_1)}{|\underset{\sim}{k}||\underset{\sim}{k}-\underset{\sim}{k}_1|}\, n(n-n_1)$$

$$dB(\underset{\sim}{k}-\underset{\sim}{k}_1,n-n_1)dB(\underset{\sim}{k}_1,n_1)\exp[i(\underset{\sim}{k}\cdot\underset{\sim}{x} - nt)] - \iiint\iint_{\underset{\sim}{k}n\underset{\sim}{k}_1 n_1\underset{\sim}{k}_2 n_2} \frac{n(n-n_1-n_2)}{|\underset{\sim}{k}|}$$

$$\left[\frac{1}{2}(\underset{\sim}{k}+\underset{\sim}{k}_1-\underset{\sim}{k}_2)\cdot(\underset{\sim}{k}-\underset{\sim}{k}_1-\underset{\sim}{k}_2) - \frac{\underset{\sim}{k}\cdot(\underset{\sim}{k}-\underset{\sim}{k}_1)(\underset{\sim}{k}-\underset{\sim}{k}_1)\cdot(\underset{\sim}{k}-\underset{\sim}{k}_1-\underset{\sim}{k}_2)}{|\underset{\sim}{k}-\underset{\sim}{k}_1||\underset{\sim}{k}-\underset{\sim}{k}_1-\underset{\sim}{k}_2|}\right]$$

$$dB(\underset{\sim}{k}-\underset{\sim}{k}_1-\underset{\sim}{k}_2,n-n_1-n_2)dB(\underset{\sim}{k}_1,n_1)dB(\underset{\sim}{k}_2,n_2)\exp[i(\underset{\sim}{k}\cdot\underset{\sim}{x} - nt)] \quad . \quad \text{(B-5)}$$

For second order let

$$\underset{\sim}{k} - \underset{\sim}{k}_1 = \underset{\sim}{k}', \quad n - n_1 = n' \quad . \qquad \text{(B-6)}$$

For third order let

$$\underset{\sim}{k} - \underset{\sim}{k}_1 - \underset{\sim}{k}_2 = \underset{\sim}{k}', \quad n - n_1 - n_2 = n' \quad . \qquad \text{(B-7)}$$

Then, after substituting (B-6) and (B-7) into (B-5) and dropping the primes,

$$I = \iint_{\underset{\sim}{k}n} \frac{n^2}{|\underset{\sim}{k}|}\, dB(\underset{\sim}{k},n)\exp[i(\underset{\sim}{k}\cdot\underset{\sim}{x} - nt)] - \iiint_{\underset{\sim}{k}n\underset{\sim}{k}_1 n_1} \frac{\underset{\sim}{k}\cdot(\underset{\sim}{k}+\underset{\sim}{k}_1)}{|\underset{\sim}{k}||\underset{\sim}{k}+\underset{\sim}{k}_1|}\, n(n+n_1)$$

$$dB(\underset{\sim}{k},n)dB(\underset{\sim}{k}_1,n_1)\exp\{i[(\underset{\sim}{k}+\underset{\sim}{k}_1)\cdot\underset{\sim}{x} - (n+n_1)t]\}$$

$$- \iiint\iint_{\underset{\sim}{k}n\underset{\sim}{k}_1 n_1\underset{\sim}{k}_2 n_2} \frac{(n+n_1+n_2)n}{|\underset{\sim}{k}+\underset{\sim}{k}_1+\underset{\sim}{k}_2|}\left[\frac{1}{2}(\underset{\sim}{k}+2\underset{\sim}{k}_1)\cdot\underset{\sim}{k} - \frac{(\underset{\sim}{k}+\underset{\sim}{k}_1+\underset{\sim}{k}_2)\cdot(\underset{\sim}{k}+\underset{\sim}{k}_2)}{|\underset{\sim}{k}+\underset{\sim}{k}_2||\underset{\sim}{k}|}\right.$$

$$(\underset{\sim}{k}+\underset{\sim}{k}_2)\cdot\underset{\sim}{k}]dB(\underset{\sim}{k},n)dB(\underset{\sim}{k}_1,n_1)dB(\underset{\sim}{k}_2,n_2)\exp\{i[(\underset{\sim}{k}+\underset{\sim}{k}_1+\underset{\sim}{k}_2)\cdot\underset{\sim}{x} - (n+n_1+n_2)t]\}$$

(B-8)

Looking at the second term on the right hand side of (B-4), after using (36)

$$II = \iiint_{\underset{\sim}{k}n\underset{\sim}{k}_1n_1} \int n^2 dB(\underset{\sim}{k},n)dB(\underset{\sim}{k}_1,n_1)\exp\{i[(\underset{\sim}{k}+\underset{\sim}{k}_1)\cdot\underset{\sim}{x} - (n+n_1)t]\}$$

$$- \iiint_{\underset{\sim}{k}n\underset{\sim}{k}_1n_1} \int\int\int_{\underset{\sim}{k}_2n_2} \frac{\underset{\sim}{k}\cdot(\underset{\sim}{k}-\underset{\sim}{k}_1)}{|\underset{\sim}{k}-\underset{\sim}{k}_1|}\, n(n-n_1)dB(\underset{\sim}{k}-\underset{\sim}{k}_1,n-n_1)dB(\underset{\sim}{k}_1,n_1)$$

$$dB(\underset{\sim}{k}_2,n_2)\exp\{i[(\underset{\sim}{k}+\underset{\sim}{k}_2)\cdot x - (n+n_2)t]\} \quad . \qquad \text{(B-9)}$$

For the third order let

$$\underset{\sim}{k} - \underset{\sim}{k}_1 = \underset{\sim}{k}' \quad , \; n - n_1 = n' \quad . \qquad \text{(B-10)}$$

Then, after substituting (B-10) into (B-9) and dropping the primes,

$$II = \iiint_{\underset{\sim}{k}n\underset{\sim}{k}_1n_1} \int n^2 dB(\underset{\sim}{k},n)dB(\underset{\sim}{k}_1,n_1)\exp\{i[(\underset{\sim}{k}+\underset{\sim}{k}_1)\cdot\underset{\sim}{x} - (n+n_1)t]\}$$

$$- \iiint_{\underset{\sim}{k}n\underset{\sim}{k}_1n_1} \int\int\int_{\underset{\sim}{k}_2n_2} \frac{(\underset{\sim}{k}+\underset{\sim}{k}_1)\cdot\underset{\sim}{k}}{|\underset{\sim}{k}|}\, n(n+n_1)dB(\underset{\sim}{k},n)dB(\underset{\sim}{k}_1,n_1)dB(\underset{\sim}{k}_2,n_2)$$

$$\exp\{i[(\underset{\sim}{k}+\underset{\sim}{k}_1+\underset{\sim}{k}_2)\cdot\underset{\sim}{x} - (n+n_1+n_2)t]\} \quad . \qquad \text{(B-11)}$$

Using (36), the third term on the right hand side of (B-4) becomes

$$III = \frac{1}{2} \iiint\int\int\int_{\underset{\sim}{k}n\underset{\sim}{k}_1 n_1 \underset{\sim}{k}_2 n_2} n^2 |\underset{\sim}{k}| dB(\underset{\sim}{k},n) dB(\underset{\sim}{k}_1,n_1) dB(\underset{\sim}{k}_2,n_2) \exp\{i[(\underset{\sim}{k}+\underset{\sim}{k}_1+\underset{\sim}{k}_2)\cdot\underset{\sim}{x}$$

$$- (n+n_1+n_2)t]\} \qquad (B\text{-}12)$$

and the fourth term becomes

$$IV = -\frac{1}{2} \iiint\int_{\underset{\sim}{k}n\underset{\sim}{k}_1 n_1} [|\underset{\sim}{k}_1||\underset{\sim}{k}| - \underset{\sim}{k}\cdot\underset{\sim}{k}_1] \left\{ -\frac{in}{|\underset{\sim}{k}|} dB(\underset{\sim}{k},n) + i \int\int_{\underset{\sim}{k}_2 n_2} \frac{\underset{\sim}{k}\cdot(\underset{\sim}{k}-\underset{\sim}{k}_2)}{|\underset{\sim}{k}||\underset{\sim}{k}-\underset{\sim}{k}_2|} \right.$$

$$\left. (n-n_2) dB(\underset{\sim}{k}-\underset{\sim}{k}_2, n-n_2) dB(\underset{\sim}{k}_2,n_2) \right\} \left\{ -\frac{in_1}{|\underset{\sim}{k}_1|} dB(\underset{\sim}{k}_1,n_1) \right.$$

$$\left. + i \int\int_{\underset{\sim}{k}_2 n_2} \frac{\underset{\sim}{k}_1\cdot(\underset{\sim}{k}_1-\underset{\sim}{k}_2)}{|\underset{\sim}{k}_1||\underset{\sim}{k}_1-\underset{\sim}{k}_2|} (n_1-n_2) dB(\underset{\sim}{k}_1-\underset{\sim}{k}_2, n_1-n_2) dB(\underset{\sim}{k}_2,n_2) \right\}$$

$$\exp\{i[(\underset{\sim}{k}+\underset{\sim}{k}_1)\cdot\underset{\sim}{x} - (n+n_1)t]\} \ . \qquad (B\text{-}13)$$

Rearranging,

$$IV = \frac{1}{2} \iiint\int_{\underset{\sim}{k}n\underset{\sim}{k}_1 n_1} \left[1 - \frac{\underset{\sim}{k}\cdot\underset{\sim}{k}_1}{|\underset{\sim}{k}||\underset{\sim}{k}_1|}\right] nn_1 dB(\underset{\sim}{k},n) dB(\underset{\sim}{k}_1,n_1) \exp\{i[(\underset{\sim}{k}+\underset{\sim}{k}_1)\cdot\underset{\sim}{x}$$

$$- (n+n_1)t]\} - \frac{1}{2} \iiint\int\int\int_{\underset{\sim}{k}n\underset{\sim}{k}_1 n_1 \underset{\sim}{k}_2 n_2} \left[1 - \frac{\underset{\sim}{k}\cdot\underset{\sim}{k}_1}{|\underset{\sim}{k}||\underset{\sim}{k}_1|}\right] \frac{\underset{\sim}{k}_1\cdot(\underset{\sim}{k}_1-\underset{\sim}{k}_2)}{|\underset{\sim}{k}_1-\underset{\sim}{k}_2|}$$

$$n(n_1-n_2) dB(\underset{\sim}{k},n) dB(\underset{\sim}{k}_1-\underset{\sim}{k}_2, n_1-n_2) dB(\underset{\sim}{k}_2,n_2) \exp\{i[(\underset{\sim}{k}+\underset{\sim}{k}_1)\cdot x$$

$$-(n+n_1)t] - \frac{1}{2} \iiint\int\int\int_{\underset{\sim}{k}n\underset{\sim}{k}_1 n_1 \underset{\sim}{k}_2 n_2} \left[1 - \frac{\underset{\sim}{k}\cdot\underset{\sim}{k}_1}{|\underset{\sim}{k}||\underset{\sim}{k}_1|}\right] \frac{\underset{\sim}{k}\cdot(\underset{\sim}{k}-\underset{\sim}{k}_2)}{|\underset{\sim}{k}-\underset{\sim}{k}_2|} n_1(n-n_2)$$

$$dB(\underset{\sim}{k}-\underset{\sim}{k}_2,n-n_2)dB(\underset{\sim}{k}_1,n_1)dB(\underset{\sim}{k}_2,n_2)\exp\{i[(\underset{\sim}{k}+\underset{\sim}{k}_1)\cdot x - (n+n_1)t]\}$$

(B-14)

In the third term on the right side of (B-14), let

$$\underset{\sim}{k} - \underset{\sim}{k}_2 = \underset{\sim}{k}', \quad n - n_2 = n' \quad . \tag{B-15}$$

Then, after substituting (B-15) into (B-14) and dropping the primes,

$$IV = \frac{1}{2} \int\int\int_{\underset{\sim}{k}n} \int_{\underset{\sim}{k}_1 n_1} \left[1 - \frac{\underset{\sim}{k}\cdot\underset{\sim}{k}_1}{|\underset{\sim}{k}||\underset{\sim}{k}_1|}\right] nn_1 dB(\underset{\sim}{k},n)dB(\underset{\sim}{k}_1,n_1)\exp\{i[(\underset{\sim}{k}+\underset{\sim}{k}_1)\cdot\underset{\sim}{x}$$

$$- (n+n_1)t] - \frac{1}{2} \int\int\int_{\underset{\sim}{k}n} \int_{\underset{\sim}{k}_1 n_1} \int_{\underset{\sim}{k}_2 n_2} \left[1 - \frac{\underset{\sim}{k}\cdot\underset{\sim}{k}_1}{|\underset{\sim}{k}||\underset{\sim}{k}_1|}\right] \frac{\underset{\sim}{k}_1\cdot(\underset{\sim}{k}_1-\underset{\sim}{k}_2)}{|\underset{\sim}{k}_1-\underset{\sim}{k}_2|}$$

$$n(n_1-n_2)dB(\underset{\sim}{k},n)dB(\underset{\sim}{k}_1-\underset{\sim}{k}_2,n_1-n_2)dB(\underset{\sim}{k}_2,n_2)\exp\{i[(\underset{\sim}{k}+\underset{\sim}{k}_1)\cdot\underset{\sim}{x}$$

$$- (n+n_1)t]\} - \frac{1}{2} \int\int\int_{\underset{\sim}{k}n} \int_{\underset{\sim}{k}_1 n_1} \int_{\underset{\sim}{k}_2 n_2} \left[1 - \frac{(\underset{\sim}{k}+\underset{\sim}{k}_2)\cdot\underset{\sim}{k}_1}{|\underset{\sim}{k}+\underset{\sim}{k}_2||\underset{\sim}{k}_1|}\right] \frac{(\underset{\sim}{k}+\underset{\sim}{k}_2)\cdot\underset{\sim}{k}}{|\underset{\sim}{k}|}$$

$$(nn_1)dB(\underset{\sim}{k},n)dB(\underset{\sim}{k}_1,n_1)dB(\underset{\sim}{k}_2,n_2)\exp\{i[(\underset{\sim}{k}+\underset{\sim}{k}_1+\underset{\sim}{k}_2)\cdot\underset{\sim}{x}$$

$$- (n+n_1+n_2)t]\} \quad . \tag{B-16}$$

Substituting (36) into the fifth term on the right hand side of (B-4) and rearranging,

$$V = - \frac{1}{2} \int\int\int_{\underset{\sim}{k}n} \int_{\underset{\sim}{k}_1 n_1} \int_{\underset{\sim}{k}_2 n_2} [|\underset{\sim}{k}||\underset{\sim}{k}_1| - \underset{\sim}{k}\cdot\underset{\sim}{k}_1](|\underset{\sim}{k}|+|\underset{\sim}{k}_1|)\left\{-\frac{in}{|\underset{\sim}{k}|} dB(\underset{\sim}{k},n)\right\}$$

$$\left\{-\frac{in_1}{|\underset{\sim}{k}_1|} dB(\underset{\sim}{k}_1,n_1)\right\} dB(\underset{\sim}{k}_2,n_2)\exp\{i[(\underset{\sim}{k}+\underset{\sim}{k}_1+\underset{\sim}{k}_2)\cdot\underset{\sim}{x} - (n+n_1+n_2)t]\}$$

$$= \frac{1}{2} \int\int\int\int_{\underset{\sim}{k}n\underset{\sim}{k}_1 n_1 \underset{\sim}{k}_2 n_2} \left[1 - \frac{\underset{\sim}{k}\cdot\underset{\sim}{k}_1}{|\underset{\sim}{k}||\underset{\sim}{k}_1|}\right](|\underset{\sim}{k}| + |\underset{\sim}{k}_1|)nn_1 dB(\underset{\sim}{k},n)dB(\underset{\sim}{k}_1,n_1)$$

$$dB(\underset{\sim}{k}_2,n_2)\exp\{i[(\underset{\sim}{k}+\underset{\sim}{k}_1+\underset{\sim}{k}_2)\cdot\underset{\sim}{x} - (n+n_1+n_2)t]\} \quad . \qquad \text{(B-17)}$$

The dynamic boundary condition is now specified in terms of $dB(\underset{\sim}{k},n)$ so that

$$\int\int_{\underset{\sim}{k}n} gdB(\underset{\sim}{k},n)\exp[i(\underset{\sim}{k}\cdot\underset{\sim}{x}-nt)] = I + II + III + IV + V + VI + VII \ . \qquad \text{(B-18)}$$

Equation (B-18) can be rearranged and then rewritten as

$$\int\int_{\underset{\sim}{k}n} F(\underset{\sim}{k},n;\ \underset{\sim}{k}_1,n_1;\ \underset{\sim}{k}_2,n_2)dB(\underset{\sim}{k},n)\exp[i(\underset{\sim}{k}\cdot\underset{\sim}{x} - nt)] = 0 \qquad \text{(B-19)}$$

where

$$F(\underset{\sim}{k},n;\underset{\sim}{k}_1,n_1;\ \underset{\sim}{k}_2,n_2) = -g - \gamma|\underset{\sim}{k}|^2 + \frac{n^2}{|\underset{\sim}{k}|} + \int_{\underset{\sim}{k}_1 n_1}\int [n^2 - \frac{\underset{\sim}{k}\cdot(\underset{\sim}{k}+\underset{\sim}{k}_1)}{|\underset{\sim}{k}||\underset{\sim}{k}+\underset{\sim}{k}_1|} n(n+n_1) + \frac{1}{2}$$

$$(1 - \frac{\underset{\sim}{k}\cdot\underset{\sim}{k}_1}{|\underset{\sim}{k}||\underset{\sim}{k}_1|})nn_1]dB(\underset{\sim}{k}_1,n_1)\exp[i(\underset{\sim}{k}_1\cdot\underset{\sim}{x}-n_1 t)] - \int_{\underset{\sim}{k}_1 n_1}\int_{\underset{\sim}{k}_2 n_2}\int\int \left\{\frac{n(n+n_1+n_2)}{|\underset{\sim}{k}+\underset{\sim}{k}_1+\underset{\sim}{k}_2|}\right.$$

$$\left[\frac{1}{2}(\underset{\sim}{k}+2\underset{\sim}{k}_1)\cdot\underset{\sim}{k} - \frac{(\underset{\sim}{k}+\underset{\sim}{k}_1+\underset{\sim}{k}_2)\cdot(\underset{\sim}{k}+\underset{\sim}{k}_2)(\underset{\sim}{k}+\underset{\sim}{k}_2)\cdot\underset{\sim}{k}}{|\underset{\sim}{k}+\underset{\sim}{k}_2||\underset{\sim}{k}|}\right]$$

$$+ \frac{(\underset{\sim}{k}+\underset{\sim}{k}_1)\cdot\underset{\sim}{k}}{|\underset{\sim}{k}|} n(n+n_1) - \frac{1}{2}n^2|\underset{\sim}{k}| - \frac{1}{2}\left[1 - \frac{\underset{\sim}{k}\cdot\underset{\sim}{k}_1}{|\underset{\sim}{k}||\underset{\sim}{k}_1|}\right](|\underset{\sim}{k}| + |\underset{\sim}{k}_1|)nn_1$$

$$\left. + \frac{1}{2}\left[1 - \frac{(\underset{\sim}{k}+\underset{\sim}{k}_2)\cdot\underset{\sim}{k}_1}{|\underset{\sim}{k}+\underset{\sim}{k}_2||\underset{\sim}{k}_1|}\right]\frac{(\underset{\sim}{k}+\underset{\sim}{k}_2)\cdot\underset{\sim}{k}}{|\underset{\sim}{k}|} nn_1 + (3/2)\gamma|\underset{\sim}{k}|^2\underset{\sim}{k}_1\cdot\underset{\sim}{k}_2\right\}$$

$$dB(\underset{\sim}{k}_1,n_1)dB(\underset{\sim}{k}_2,n_2)\exp\{i[(\underset{\sim}{k}_1+\underset{\sim}{k}_2)\cdot\underset{\sim}{x} - (n_1+n_2)t]\}$$

$$-\frac{1}{2}\int_{\underset{\sim}{k}_1}\int_{n_1}\int_{\underset{\sim}{k}_2}\int_{n_2}\left[1-\frac{\underset{\sim}{k}\cdot\underset{\sim}{k}_1}{|\underset{\sim}{k}||\underset{\sim}{k}_1|}\right]\frac{\underset{\sim}{k}_1\cdot(\underset{\sim}{k}_1-\underset{\sim}{k}_2)}{|\underset{\sim}{k}_1-\underset{\sim}{k}_2|}\,n(n_1-n_2)dB(\underset{\sim}{k}_1-\underset{\sim}{k}_2,\ n_1-n_2)$$

$$dB(\underset{\sim}{k}_2,n_2)\exp[i(\underset{\sim}{k}_1\cdot\underset{\sim}{x} - n_1t)] \quad . \tag{B-20}$$

Since $dB(\underset{\sim}{k},n)$ can be any function,

$$F(\underset{\sim}{k},n;\ \underset{\sim}{k}_1,n_1;\ \underset{\sim}{k}_2,n_2) = 0 \tag{B-21}$$

Thus, after setting (B-20) to zero and rearranging terms, the third order dispersive relationship can be written in the following form:

$$g + \gamma|\underset{\sim}{k}|^2 - \frac{n^2}{|\underset{\sim}{k}|} = \int_{\underset{\sim}{k}_1}\int_{n_1}\left[n^2 - \frac{\underset{\sim}{k}\cdot(\underset{\sim}{k}+\underset{\sim}{k}_1)}{|\underset{\sim}{k}||\underset{\sim}{k}+\underset{\sim}{k}_1|}\,n(n+n_1) + \frac{1}{2}\left(1-\frac{\underset{\sim}{k}\cdot\underset{\sim}{k}_1}{|\underset{\sim}{k}||\underset{\sim}{k}_1|}\right)nn_1\right]$$

$$dB(\underset{\sim}{k}_1,n_1)\exp[i(\underset{\sim}{k}_1\cdot\underset{\sim}{x} - n_1t)] - \int_{\underset{\sim}{k}_1}\int_{n_1}\int_{\underset{\sim}{k}_2}\int_{n_2}\left\{\frac{n(n+n_1+n_2)}{|\underset{\sim}{k}+\underset{\sim}{k}_1+\underset{\sim}{k}_2|}\right.$$

$$\left[\frac{1}{2}(\underset{\sim}{k}+2\underset{\sim}{k}_1)\cdot\underset{\sim}{k} - \frac{(\underset{\sim}{k}+\underset{\sim}{k}_1+\underset{\sim}{k}_2)\cdot(\underset{\sim}{k}+\underset{\sim}{k}_2)(\underset{\sim}{k}+\underset{\sim}{k}_2)\cdot\underset{\sim}{k}}{|\underset{\sim}{k}+\underset{\sim}{k}_2||\underset{\sim}{k}|}\right]$$

$$+\frac{(\underset{\sim}{k}+\underset{\sim}{k}_1)\cdot\underset{\sim}{k}}{|\underset{\sim}{k}|}\,n(n+n_1) - \frac{1}{2}n^2|\underset{\sim}{k}| - \frac{1}{2}\left[1-\frac{\underset{\sim}{k}\cdot\underset{\sim}{k}_1}{|\underset{\sim}{k}||\underset{\sim}{k}_1|}\right](|\underset{\sim}{k}|+|\underset{\sim}{k}_1|)nn_1$$

$$\left.+\frac{1}{2}\left[1-\frac{(\underset{\sim}{k}+\underset{\sim}{k}_2)\cdot\underset{\sim}{k}_1}{|\underset{\sim}{k}+\underset{\sim}{k}_2||\underset{\sim}{k}_1|}\right]\frac{(\underset{\sim}{k}+\underset{\sim}{k}_2)\cdot\underset{\sim}{k}}{|\underset{\sim}{k}|}\,nn_1 + \frac{3}{2}\gamma|\underset{\sim}{k}|^2\,\underset{\sim}{k}_1\cdot\underset{\sim}{k}_2\right\}$$

$$dB(\underset{\sim}{k}_1,n_1)dB(\underset{\sim}{k}_2,n_2)\exp\{i[(\underset{\sim}{k}_1+\underset{\sim}{k}_2)\cdot\underset{\sim}{x} - (n_1+n_2)t]\}$$

$$- \frac{1}{2} \int_{\underset{\sim}{k}_1} \int_{n_1} \int_{\underset{\sim}{k}_2} \int_{n_2} \left[1 - \frac{\underset{\sim}{k} \cdot \underset{\sim}{k}_1}{|\underset{\sim}{k}||\underset{\sim}{k}_1|} \right] \frac{\underset{\sim}{k}_1 \cdot (\underset{\sim}{k}_1 - \underset{\sim}{k}_2)}{|\underset{\sim}{k}_1 - \underset{\sim}{k}_2|} \, n(n_1 - n_2) dB(\underset{\sim}{k}_1 - \underset{\sim}{k}_2, \, n_1 - n_2)$$

$$dB(\underset{\sim}{k}_2, n_2) \exp[i(\underset{\sim}{k}_1 \cdot \underset{\sim}{x} - n_1 t)] \quad . \qquad \text{(B-22)}$$

2. Statistical properties of surface waves under non-uniform currents.

2.1 Introduction

Previous studies (Longuet-Higgins and Stewart, 1961; Huang et al, 1972; Phillips, 1966) have shown that when waves encounter current, wave characteristics undergo changes due to interactions between the waves and the current.

In order to utilize the phenomenon of wave-current interactions as a means of measuring current, it is desirable to first conduct a comprehensive study of the effects of current on relevant statistical properties of waves. This includes those of wave elevation, wave amplitude (peak), zero crossing rate, number of maxima, velocity of zeros and specular points, and other related quantities for both the one-dimensional and two-dimensional wave systems. Those quantities that are most sensitive to wave-current interactions and particularly suited for current measurement by remote sensing devices will then be identified.

Work to date has been devoted to one dimensional wave systems only. The effects of current on wave elevation, wave amplitude, zero crossing rate, number of wave maxima, and velocity of zeros have been studied and reported in the following.

2.2 Distribution of Wave Elevation

Both theoretical and field studies show that the surface elevation of a random wave field is approximately Gaussian. That is, the probability density function $p(\xi)$ of surface elevation ξ, measured from mean sea level is

$$p(\xi) = \frac{1}{\sqrt{2\pi}\sigma} \exp[-\frac{1}{2}\frac{\xi^2}{\sigma^2}] \qquad (2.1)$$

in which σ is the standard deviation of ξ which can be obtained from the spectrum of surface elevation.

It was shown previously (Huang et al, 1972) that under the influence of a steady non-uniform current, the frequency spectrum of a random gravity wave field is given by

$$\phi(n) = \frac{4\phi^*(n)}{[1 + (1 + \frac{4Un}{g})^{1/2}]\ [(1 + \frac{4Un}{g})^{1/2} + (1 + \frac{4Un}{g})]} \tag{2.2}$$

in which n is total frequency, U is current speed, g is gravitational acceleration and $\phi^*(n)$ is wave frequency spectrum without the influence of current. In this study, the Kitaigorodskii-Pierson-Moskowitz spectrum is used. That is,

$$\phi^*(n) = \frac{\beta g^2}{n^5} \exp[-\alpha(\frac{n_o}{n})^4] \tag{2.3}$$

in which α and β are non-dimensional constants equal to 0.74 and 8.1×10^{-3} respectively, and $n_o = g/W$, W being mean wind speed.

The standard deviation σ that appears in equation (2.1) is given by

$$\sigma = \int_0^{n_c} \phi(n) dn \tag{2.4}$$

in which n_c is the cut-off frequency of the wave spectrum taken as that of a wave 30 cm in length.

The probability density functions as given by equation (2.1) are plotted in figures 2.1, 2.2, and 2.3 for different current and wind speeds. It is seen that for a given wind, positive current reduces the probability of large wave elevations while negative current increases the same. It is also noted that the larger the wind speed, the smaller is the effect of current on wave elevation.

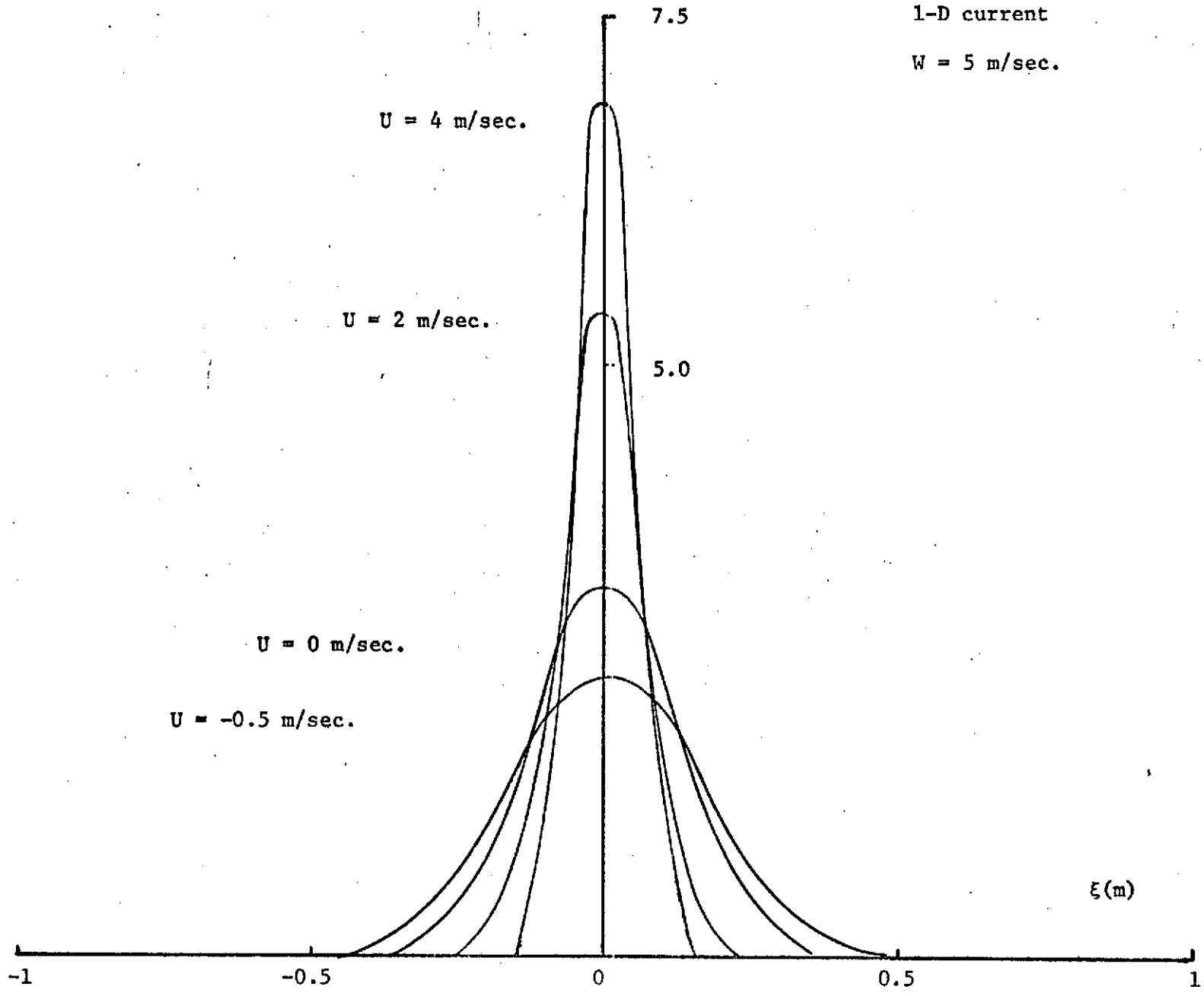

Figure 2.1 Probability density function of wave surface elevation under current for wind speed at 5 m/sec.

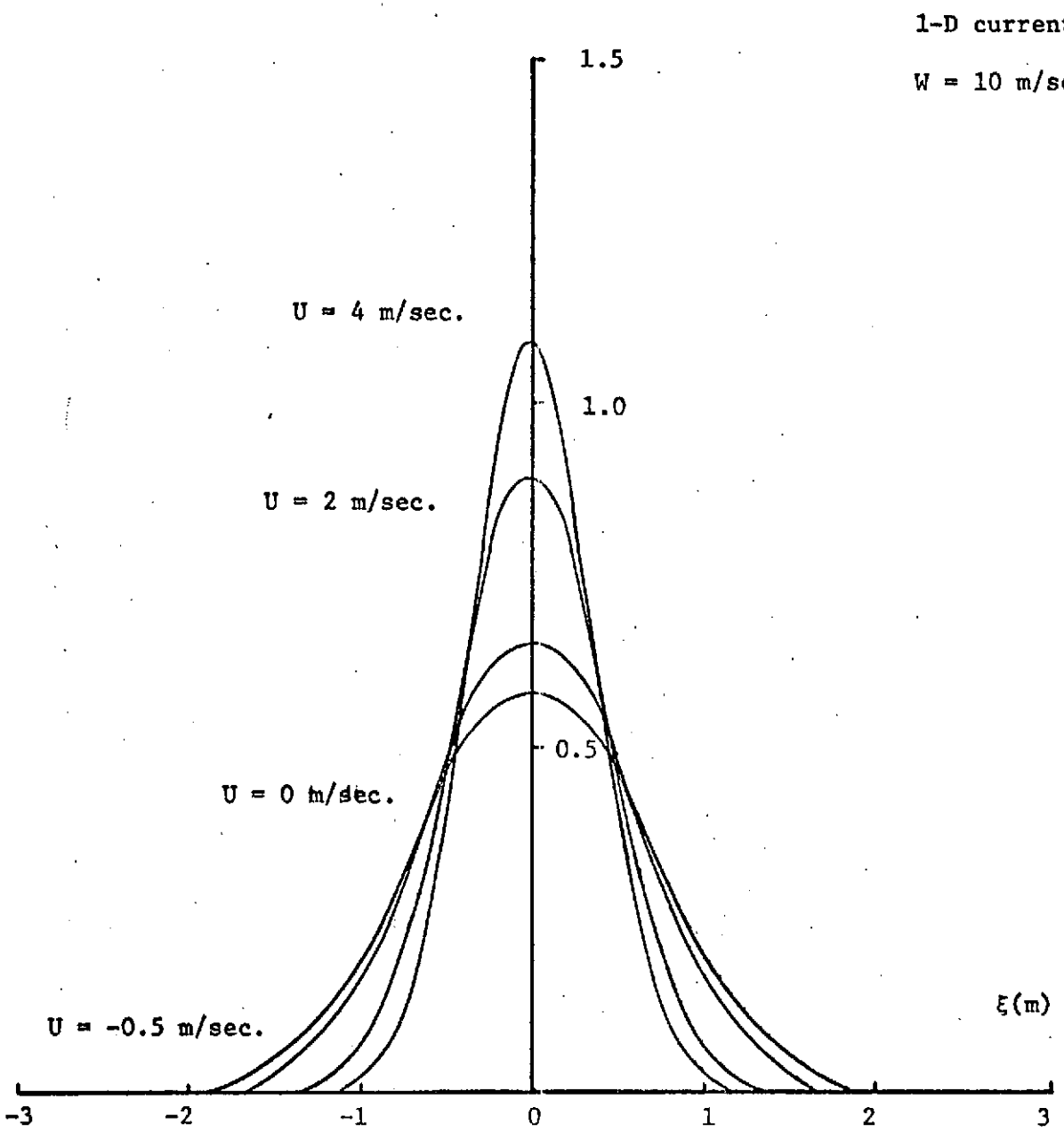

Figure 2.2 Probability density function of wave surface elevation under current for wind speed at 10 m/sec.

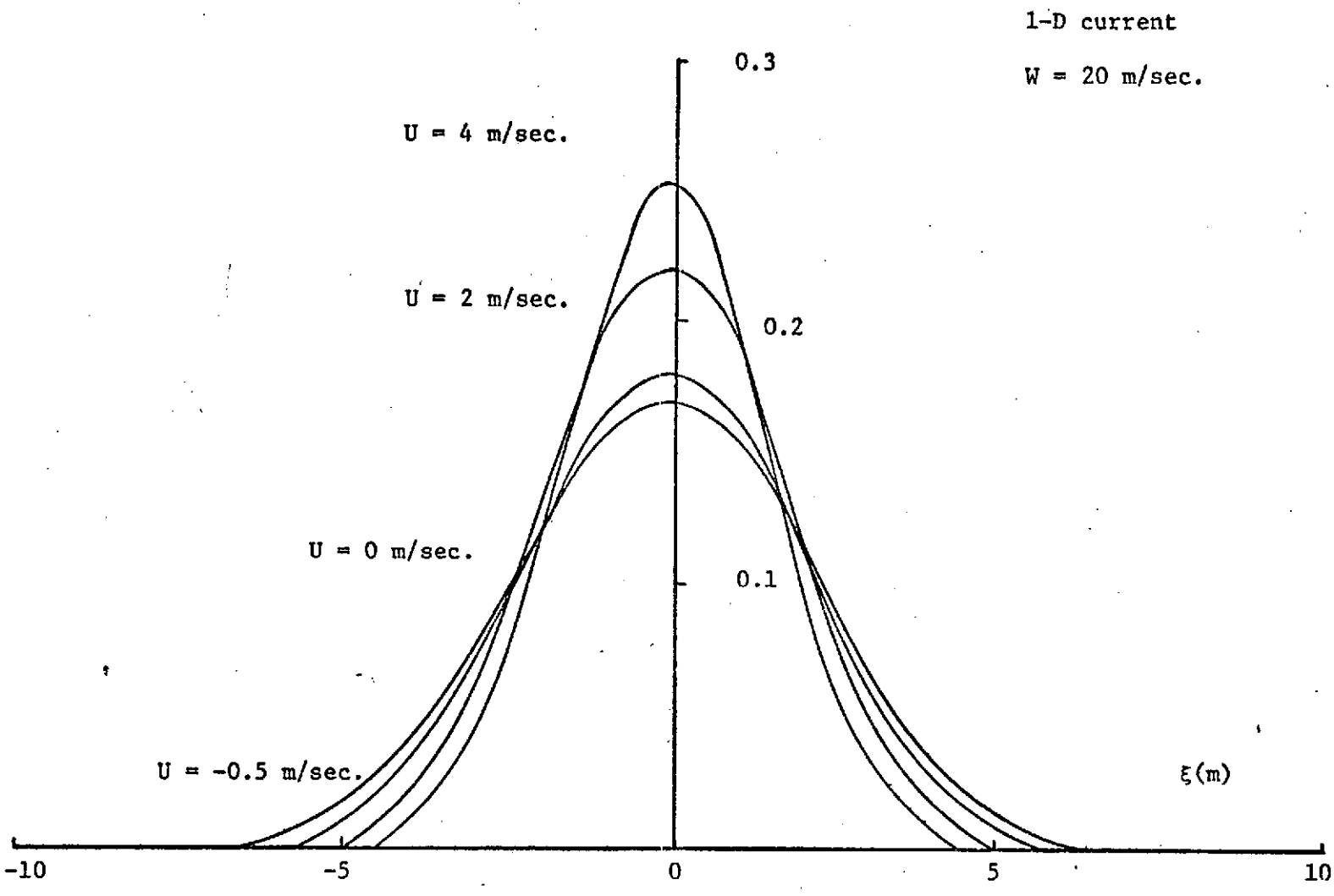

Figure 2.3 Probability density function of wave surface elevation under current for wind speed at 20 m/sec.

2.3 Distribution of Wave Amplitude

For a Gaussian, zero mean, stationary sea, the probability density function $p(\eta)$ of the amplitudes η (peak) of the waves is given by (Longuet-Higgins, 1956).

$$p(\eta) = \frac{1}{\sqrt{2\pi m_o}} \left[\varepsilon \exp\left(-\frac{1}{2}\frac{\eta^2}{m_o \varepsilon^2}\right) + \sqrt{\frac{1-\varepsilon^2}{m_o}}\,\eta \exp\left(-\frac{1}{2}\frac{\eta^2}{m_o}\right) \int_{-\infty}^{\frac{\eta}{\varepsilon}\sqrt{\frac{1-\varepsilon^2}{m_o}}} \exp\left(-\frac{1}{2}x^2\right) dx \right] \tag{2.5}$$

in which

$$\varepsilon^2 = 1 - \frac{m_2^2}{m_o m_4} \tag{2.6}$$

a parameter measuring the r.m.s. width of the spectrum and, in the case when the waves are considered a function of time t,

$$\begin{aligned} m_o &= \int_n \phi(n)\,dn \\ m_2 &= \int_n n^2 \phi(n)\,dn \\ m_4 &= \int_n n^4 \phi(n)\,dn \end{aligned} \tag{2.7}$$

If the waves are considered as a function of space n, $\phi(n)$ is to be replaced by $\psi(k)$, the wave-number spectrum and n is replaced by k, the wave number. In either case the integrations in equation (2.7) are to be extended over the entire gravity wave range.

Other statistical properties of wave amplitudes such as the mean υ_1', variance υ_2, and coefficient of skewness B, can be readily derived from the expression of probability density function $p(\eta)$ of wave peaks in equation (2.5). These are

$$\upsilon_1' = \sqrt{\frac{\pi}{2} m_o (1-\epsilon^2)}, \tag{2.8}$$

$$\upsilon_2 = m_o [1-(\frac{\pi}{2} -1)(1-\epsilon^2)], \tag{2.9}$$

$$B = \sqrt{\frac{\pi}{2}} (\pi-3) (\frac{m_o(1-\epsilon^2)}{\upsilon_2})^{3/2} . \tag{2.10}$$

Another quantity of interest is the proportion of negative peaks (peaks of negative magnitude) out of the total number of peaks of the waves, denoted by γ, and is given by

$$\gamma = \frac{1}{2} [1-(1-\epsilon^2)^{1/2}] \tag{2.11}$$

Effects of current on the statistical quantities mentioned above are computed for the case when the waves are treated as functions of time and presented in graphical forms. In figure 2.4 the ratio of mean wave amplitude υ_1' with and without the influence of current is plotted against current speed U with mean wind speed W as a parameter. It is seen that positive current reduces mean wave amplitude while, due to energy pile up, negative current increases the same and the effects of current are more pronounced at lower mean wind speed.

Figure 2.5 gives the ratio of variance of wave amplitudes υ_2 with and without current. The same trend that is observed in figure 2.4 is noted here.

Presented in figure 2.6 is the ratio of coefficient of skewness B with and without current considered. It is seen that positive (negative) current gives rise to an increase (decrease) in skewness of wave amplitude distribution. This is because under the influence of a positive current the waves become smoother and therefore of narrower band giving rise to more positive peaks than negative peaks resulting in a more skewed

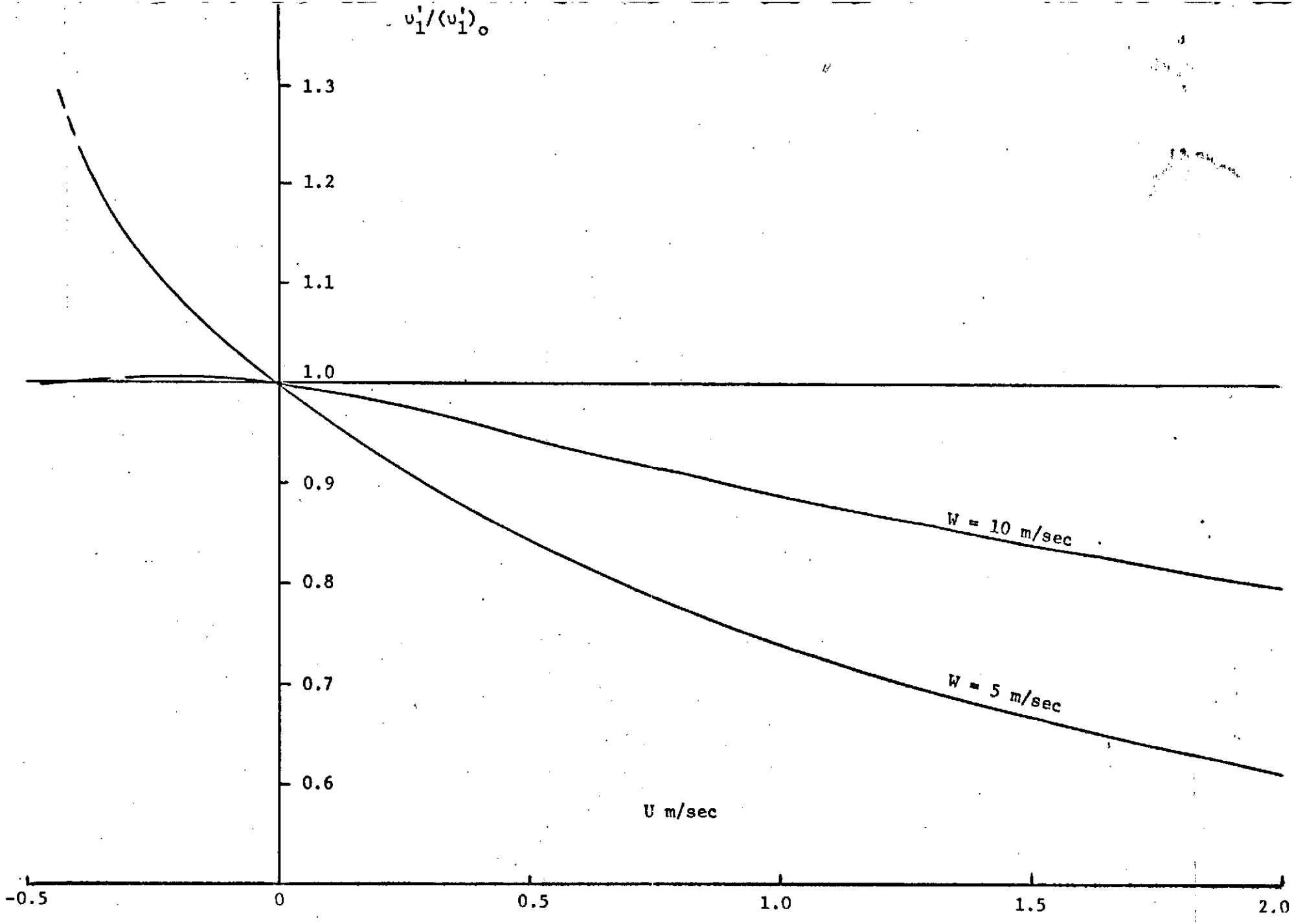

Figure 2.4 Change of mean wave amplitude under current.

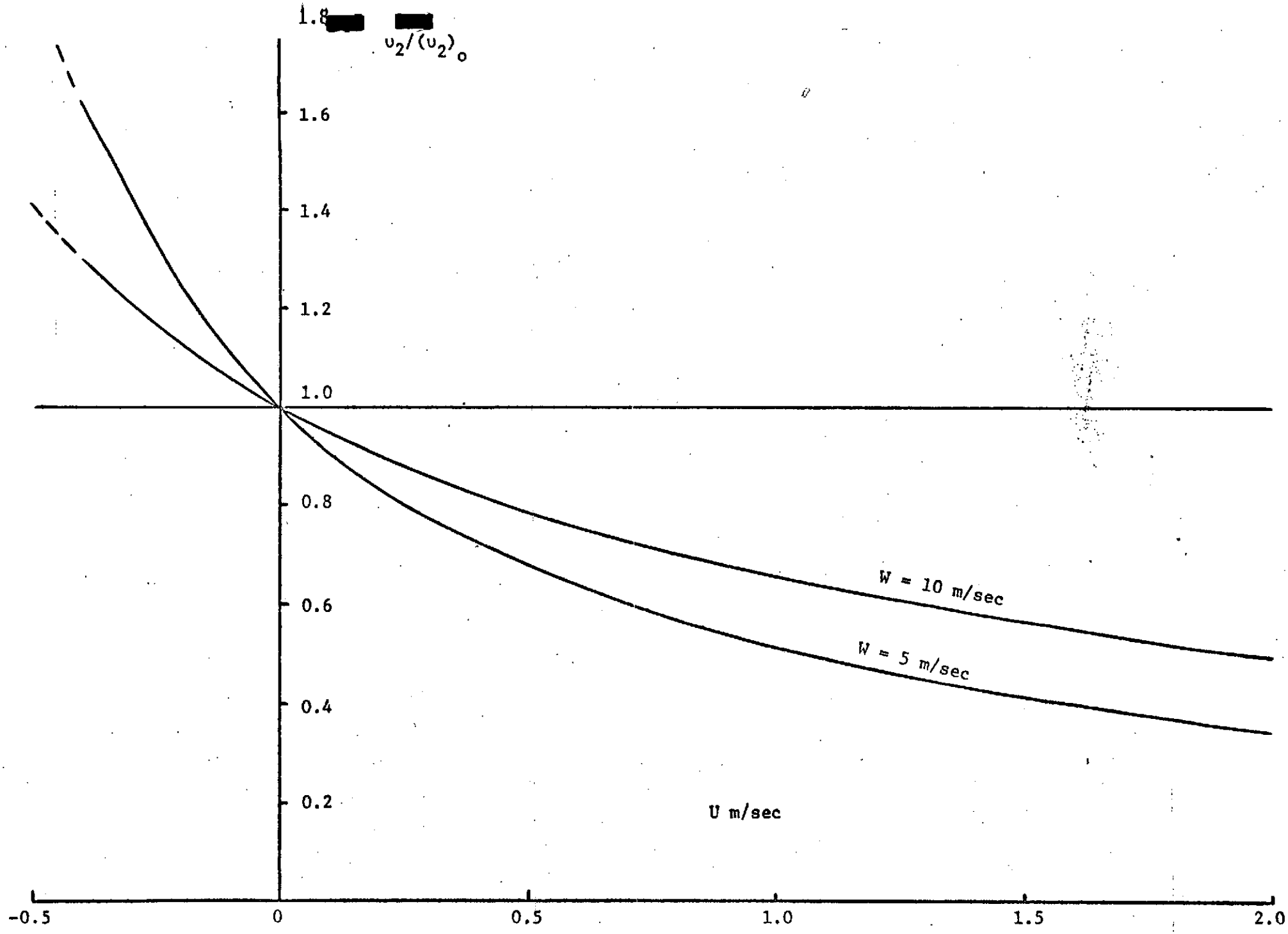

Figure 2.5 Change of variance of wave amplitude under current.

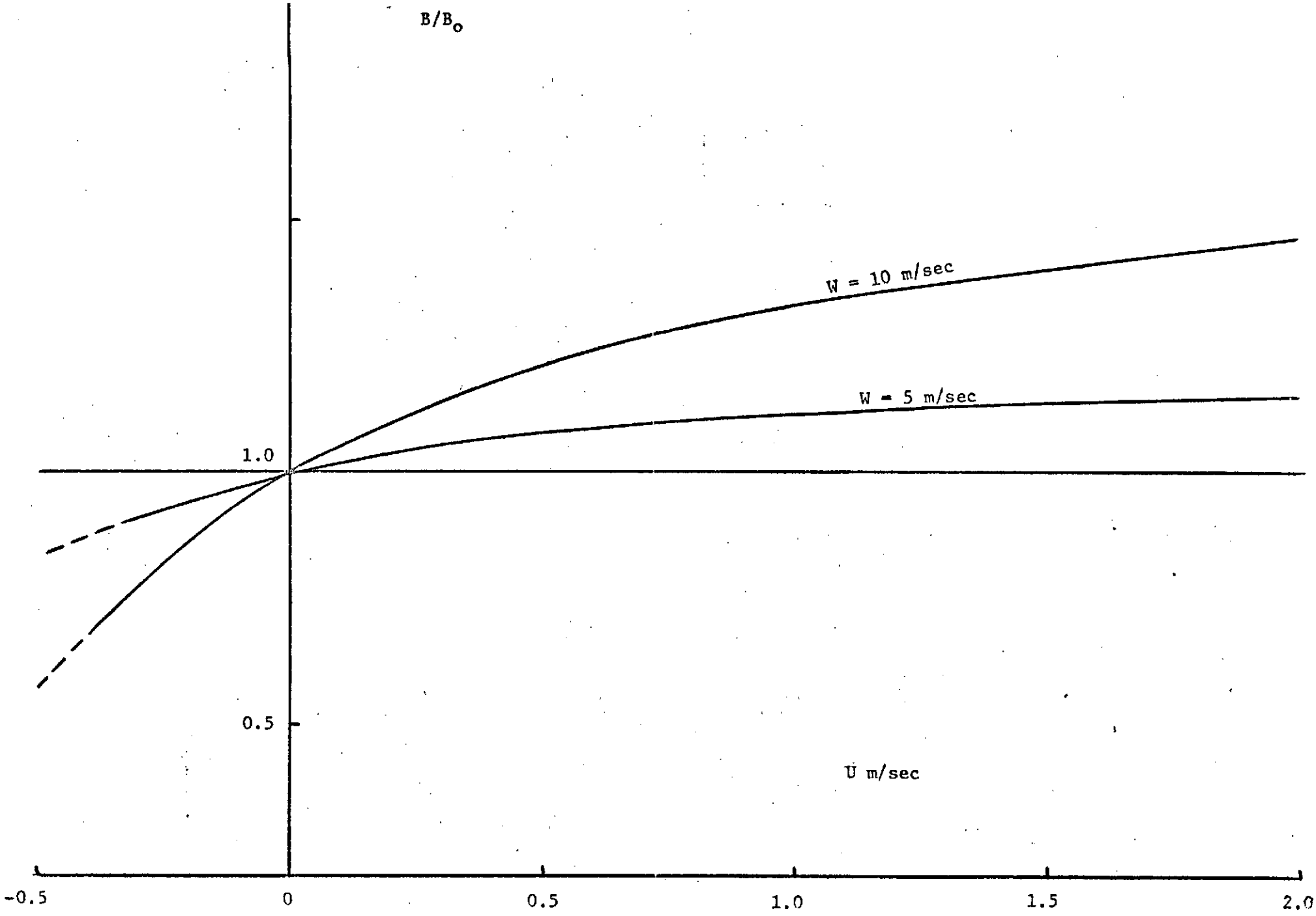

Figure 2.6 Change of skewness of amplitude distribution under current.

amplitude distribution. Conversely, negative current feeds energy into the wave system. The waves become more choppy and therefore of wider band giving rise to a less skewed wave amplitude distribution.

Figure 2.7 presents the ratio of γ with and without current included. That there are less negative peaks in the presence of a positive current than when the current speed is negative is clearly noted. The physical mechanism underlying the behavior of the curves in figure 2.6 also governs that of the curves shown in figure 2.7.

With the statistical moments of wave amplitudes discussed, the characteristics of the probability density function of wave amplitudes as given by equation (2.5) and presented in figure 2.8 can be readily understood. In figure 2.8 the probability density functions $p(\eta)$ of wave amplitudes are given for wind speed W=10 m/s and current speed U=2, 0, and -0.4 m/s. That positive current gives rise to smaller values of mean and spread of wave amplitudes than negative current does is clearly seen. The curves also show that the amplitude distribution is more skewed under positive current than in the case of negative current.

2.4 Expected Number of Zero Crossings and Maxima

In addition to amplitude distribution, the statistics of number of threshold crossings and extrema of random functions and, in this case, sea waves are often used. While it is difficult to obtain the distributions of these quantities, their expected values are easy to compute both theoretically and from field observations.

According to Longuet-Higgins (1962), the expected rate of zero crossings, denoted N_o, is given by

$$N_o = \frac{1}{\pi} \left(\frac{m_2}{m_o}\right)^{1/2} \tag{2.12}$$

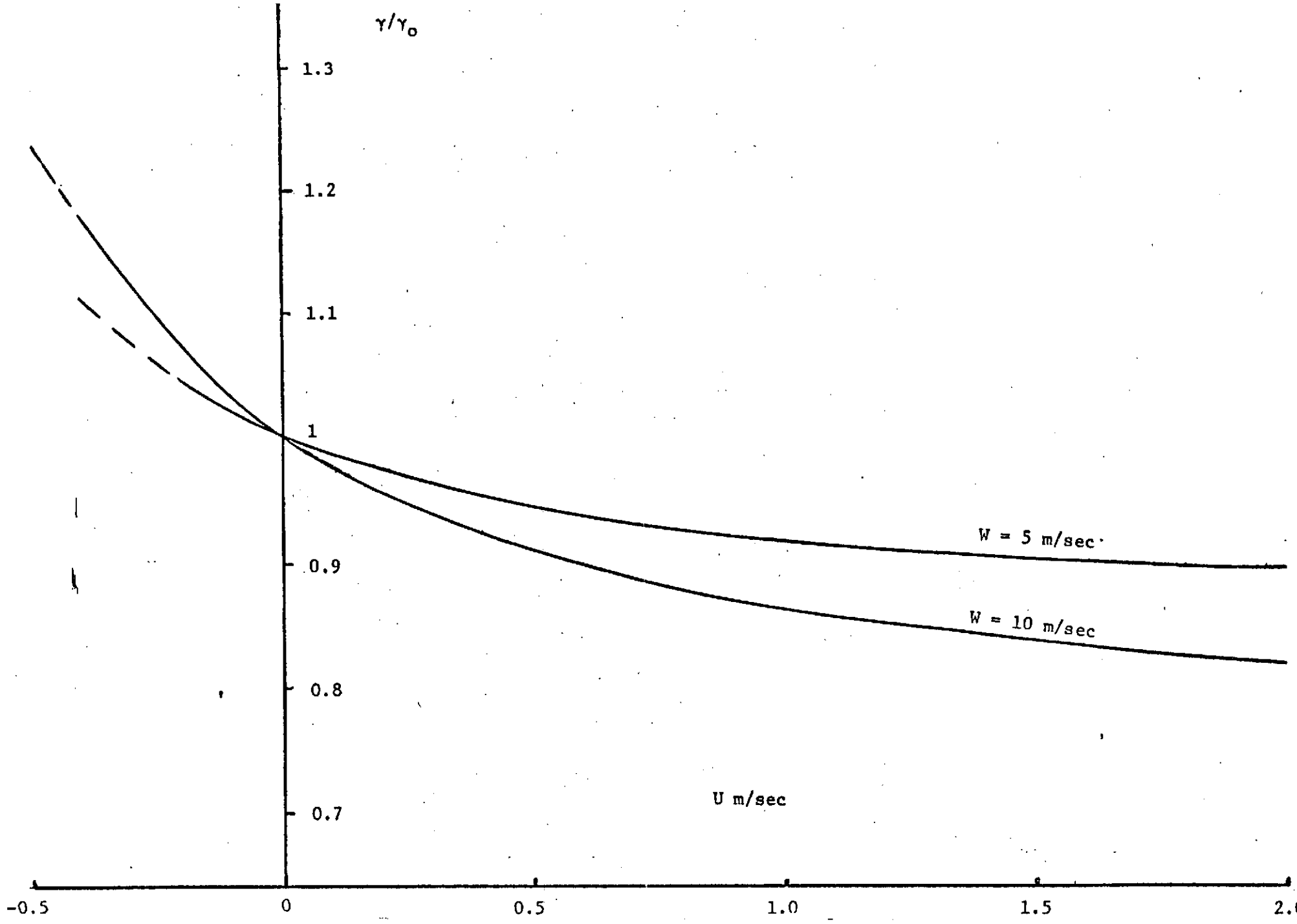

Figure 2.7 Change of number of negative peaks under current.

and the expected number of extrema per unit time is

$$N_e = \frac{1}{\pi} \left(\frac{m_4}{m_2}\right)^{1/2} \quad (2.13)$$

When the waves are considered as a function of time, the m's are obtained from equation (2.7). When the waves are treated as a function of space, $\psi(k)$ and k should be used in place of $\phi(n)dn$ in equation (2.7). In this study, only the former case is considered.

In figure 2.9 the ratio of N_e with and without the influence of current is presented. In the presence of positive (negative) current, waves are of a narrower (broader) band resulting in a decrease (increase) in expected number of extrema, per unit time.

In figure 2.10 the ratio of N_o with and without the influence of current is also presented. It is seen that the same trend observed in figure 2.9 is noted.

2.5 Velocity of Zero

The quantities examined above all refer to waves either treated as a function of time t for a fixed point in space or as a function of space x, for a given instant of time. Moving waves are, however, functions of both space and time. It is, therefore, of interest to investigate some statistical properties of moving wave forms. Presented in the following is velocity of zero.

Consider a one-dimensional random wave f(x,t), the velocity of the zero, denoted ζ, is given by (Longuet-Higgins, 1956, 1957)

$$\zeta = -\frac{\partial f/\partial t}{\partial f/\partial x} \quad (2.14)$$

The distribution of ζ, it was shown (Longuet-Higgins, 1956, 1957), depends on $\psi(k)$, the wave-number spectrum. Under the influence of current,

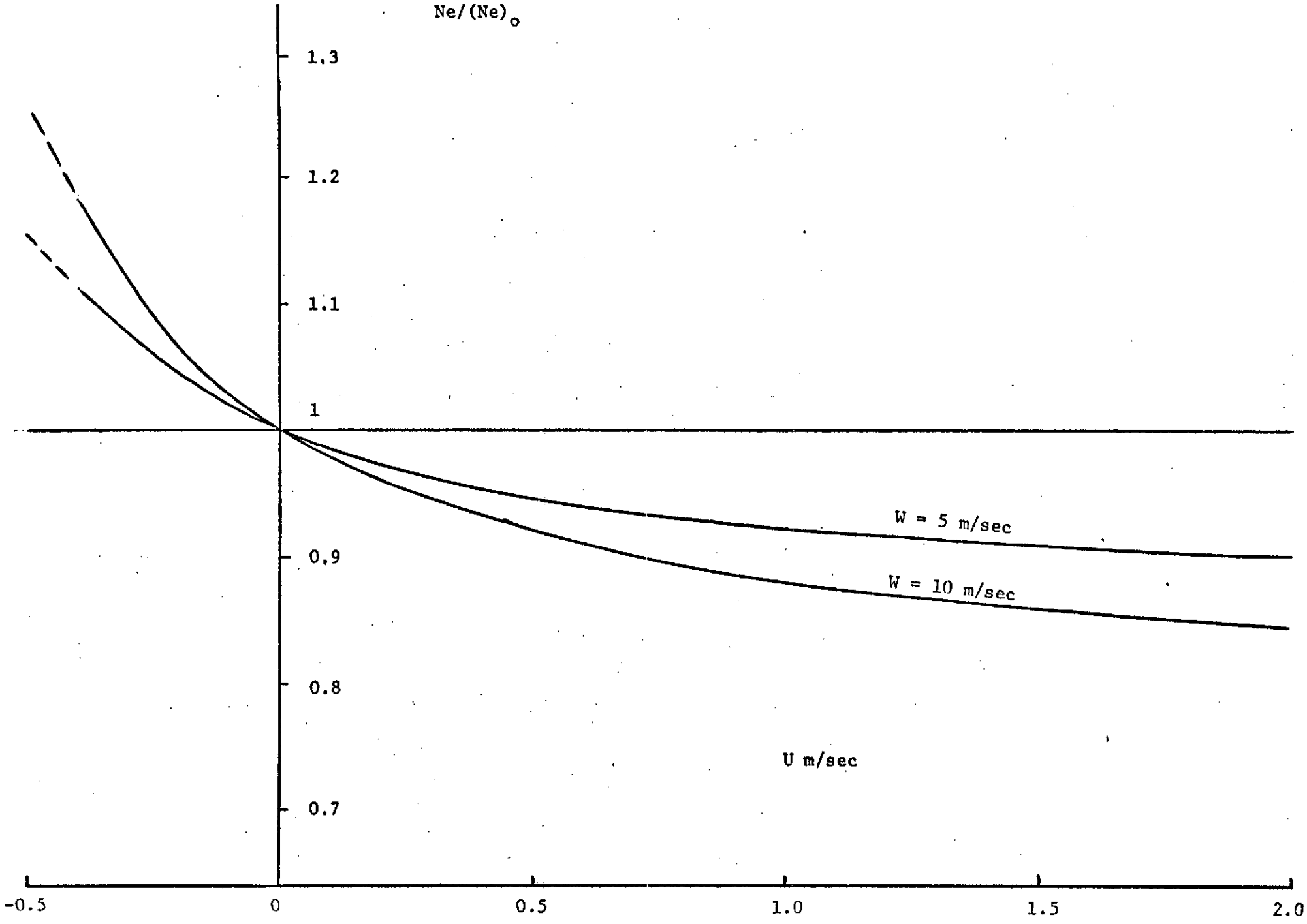

Figure 2.9 Change of number of extrema under current.

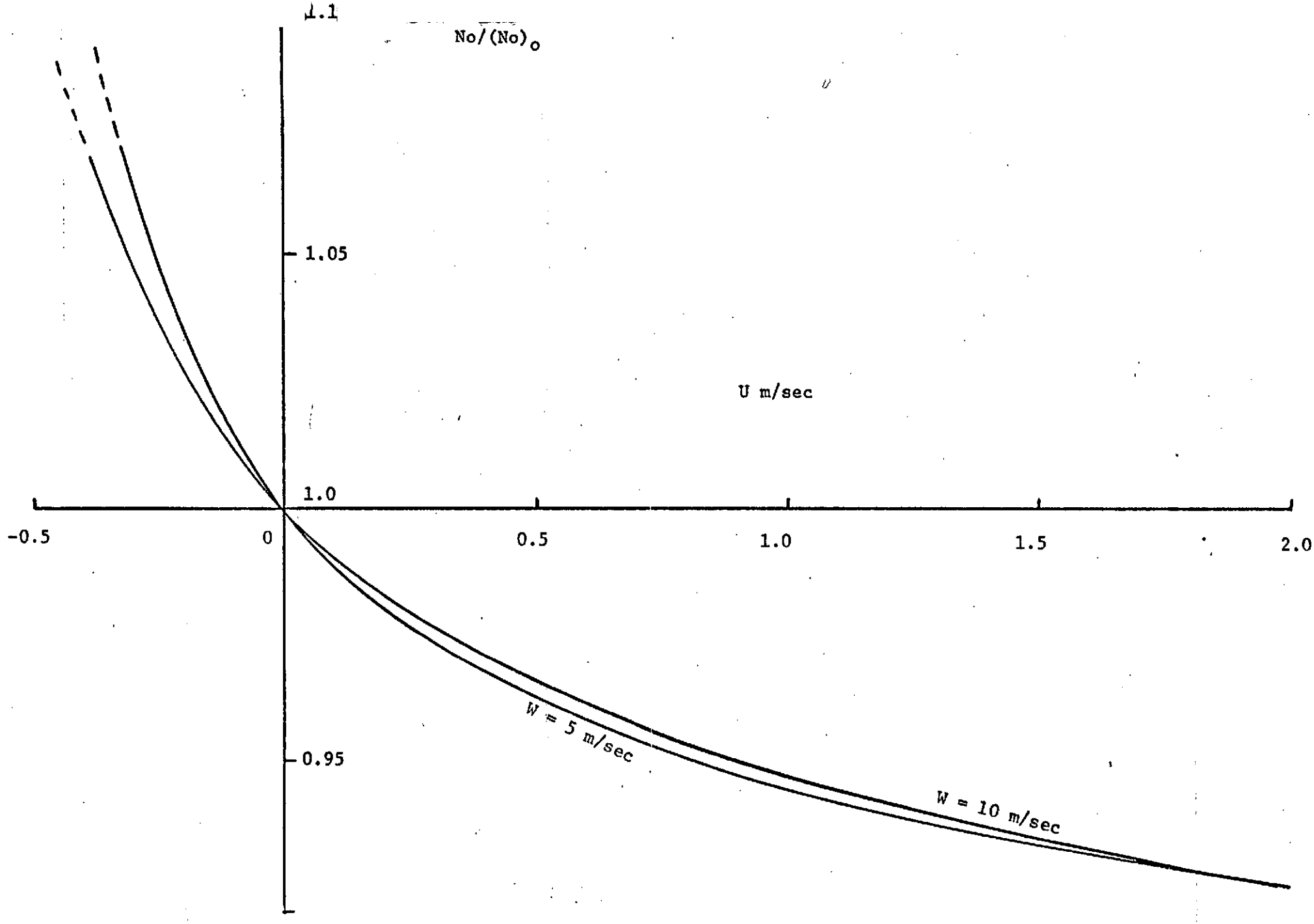

Figure 2.10 Change of number of zero crossing under current.

$\psi(k)$ is given by (Huang, et al, 1972)

$$\psi(k) = \frac{\beta}{2(1+\frac{U}{c})^7} \frac{1}{k^3} \exp[-\alpha(\frac{n_o}{k(U+c)})^4] \tag{2.15}$$

in which $c = (g/k)^{1/2}$, the phase speed. The above expression for $\psi(k)$ is derived based on the assumption that when there is no current the wave frequency spectrum is given by equation (2.2). Defining the following moments of $\psi(k)$ as

$$\begin{aligned} m_2 &= \int_k k^2\psi(k)dk \\ m_1' &= \int_k kn\psi(k)dk \\ m_o'' &= \int_k n^2\psi(k)dk \end{aligned} \tag{2.16}$$

in which under the influence of current the relationship between frequency n and wave-number k is given by (Huang et al, 1972)

$$gk = \frac{n^2}{[\frac{1}{2}+\frac{1}{2}(1+\frac{4Un}{g})^{1/2}]^2}, \tag{2.17}$$

the probability density function $p(\zeta)$ of velocity of the zero ζ is (Longuet-Higgins, 1957)

$$p(\zeta) = \frac{1}{2} \frac{\Delta_o/m_2^2}{[(\zeta-\bar{\zeta})^2 + \Delta_o/m_2^2]^{3/2}} \tag{2.18}$$

in which $\Delta_o = m_2\, m_o'' - m_1'^2$ and $\bar{\zeta} = -m_1'/m_2$, the mean of ζ. The interquartile range ω, a measure of the spread of ζ, is $\omega = 2\sqrt{3}\Delta_o/m_2$.

Plotted in figure 2.11 is the ratio of $\bar{\zeta}$ with and without current. It is seen that the mean of ζ increases (decreases) with increasing positive (negative) current. It is also noted that the larger the wind speed, the

less is the effect of current on the quantity considered. It is worth noting that comparison of figure 2.11 with figures 2.4 to 2.10 indicates that the effect of current is more pronounced on velocity of the zero than on any of the other quantities examined in this report, suggesting that velocity of zero may well be a quantity to be used for current measurement by remote sensing devices.

In figure 2.12 the interquartile range ω with and without current is studied. The curves exhibit the same characteristics as those of the curves in figure 2.11.

Finally, the probability density function $p(\zeta)$ of ζ is shown in figure 2.13 for W = 10 m/s and U = 2 m/s, 0, and -0.4 m/s. The influence of current on the mean and spread of velocity of zero shown in figures 2.11 and 2.12 is clearly reflected in figure 2.13.

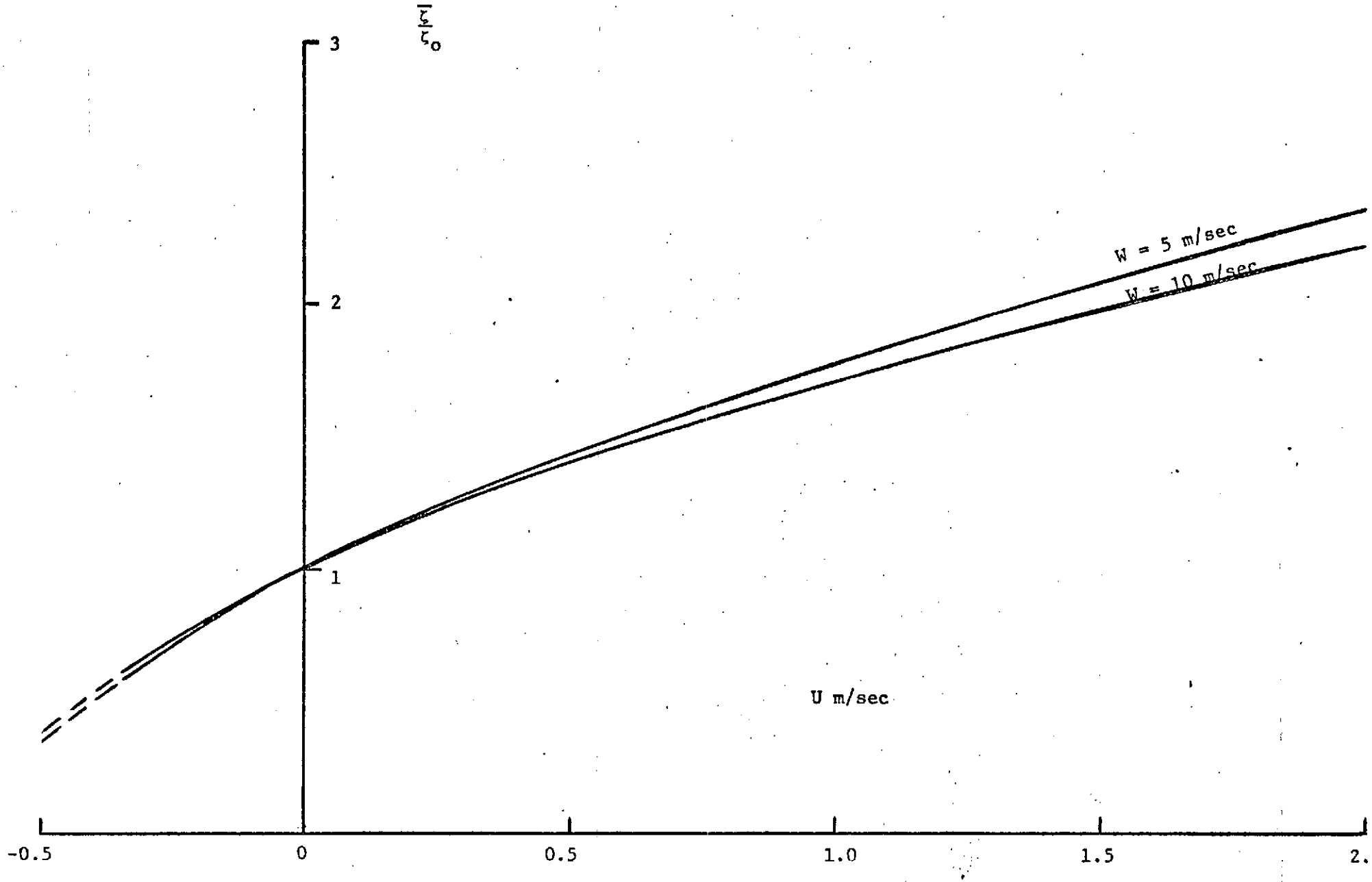

Figure 2.11 Change of phase velocity at zero crossing points.

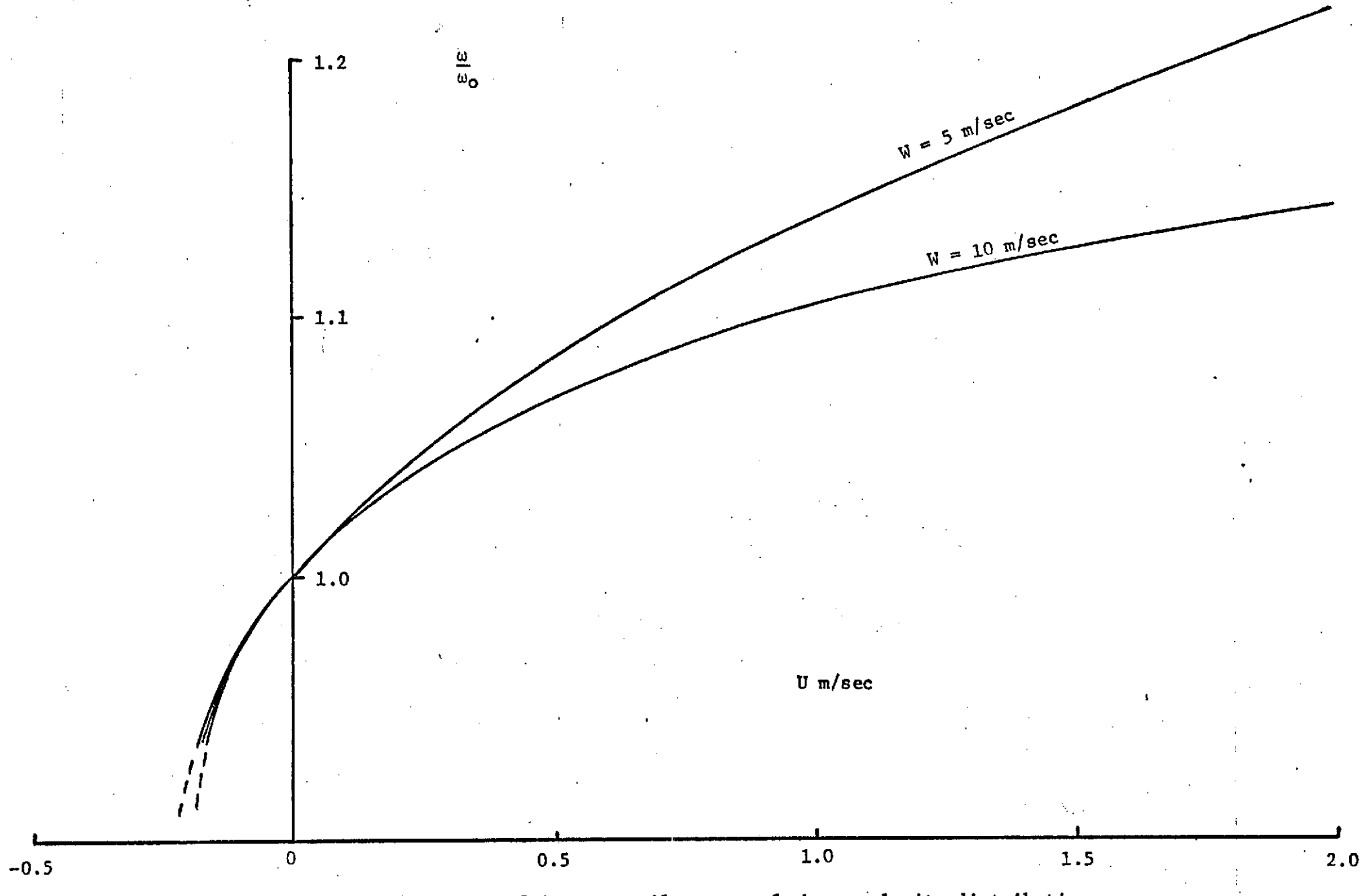

Figure 2.12 Change of interquartile range of phase velocity distribution.

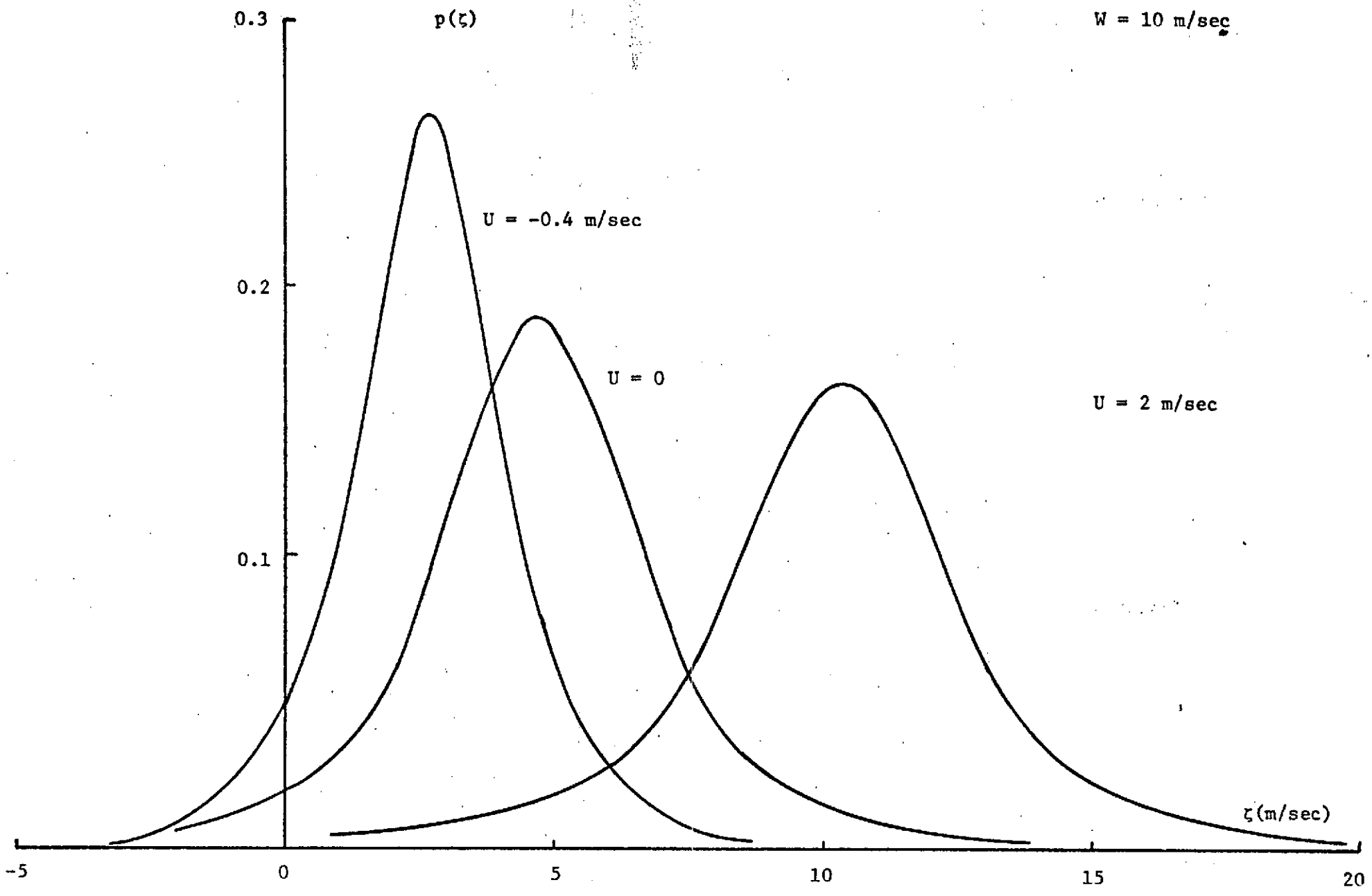

Figure 2.13 Probability density function of phase speed.

2.6 Conclusion

The results of the theoretical studies indicate that the statistical properties of the sea surface are sensitive to whatever causes changes in the wave energy distribution; i.e., the spectral functions. This is true even with higher order expensions such as in the Gram-Charlier series for wave height probability density function. In the open ocean, mechanisms that will change energy distribution substantially are, of course, winds and major currents. However, before more detailed knowledge of generation of waves by wind is available, it is impossible to utilize these properties as a means to measure surface wind over the ocean. On the other hand, current-wave interaction is more definite and the effect is of the first order. Furthermore, since the change depends on relative values of currents, it is less susceptible to the error in establishing an absolute relationship as required in wind wave generation studies. Under normal conditions a wind system will cover an area substantially larger than the wave scales and thus provide a homogeneous field for wave actions. Take an inlet or a river mouth for example, the local flow will generate a non-uniform velocity field over a homogeneous wave field. Consequently, the waves will interact and change characteristics depending on the flow conditions. Such changes can be detected easily from the probability density function.

Another example is the Gulf Stream. The width of the system is about 100km with strong shear zones on its sides. Though the decay scale of a wave 30cm in length is only 1700m, it is not unusual to find substantial current velocity changes across such a distance as reported by Stommel (1966). When waves encounter such current systems, their characteristics will change accordingly. Although the analyses in this report did not

include shear current cases where as in the Gulf Stream the shear will be important, a qualitative prediction on the wave height probability density function can be made with the available results as a guide. To facilitate the discussion, a schematic diagram is given in figure 4.1 in which a typical velocity cross section of the Gulf Stream measured by Worthington (1954) is shown. The total flow region is further divided into four different sub-zones numbered one through four, with A and B indicating the local extreme of velocity. If wind generated waves are propagating from the open ocean of zone 4 across the Gulf Stream to zone 1 toward the land, they will first encounter counter current in zone 3. The probability density function of wave elevation will become increasingly flat until it reaches point B. From there on the relative change of the current is increasing in the direction of the waves; therefore, the flatness of the density function will become less and less until point A is reached. After waves pass point A, relative change of the current is in the opposing direction of the wave again, and the flatness will increase accordingly. Granted that no single wave will last the whole current system under moderate or light wind conditions, but as long as the locally generated waves can experience different current conditions, the changes in probability curves will still show the effects. Such changes are easily detected by means of remote sensing devices, and thus it offers a new way of measuring the major ocean current systems.

Although this seems to solve the problem in principle, there are related problems that will have to be solved before the final result can be used to set up a routine in practice. One of the problems is that the results in the theoretical analysis are based on one-dimensional currents

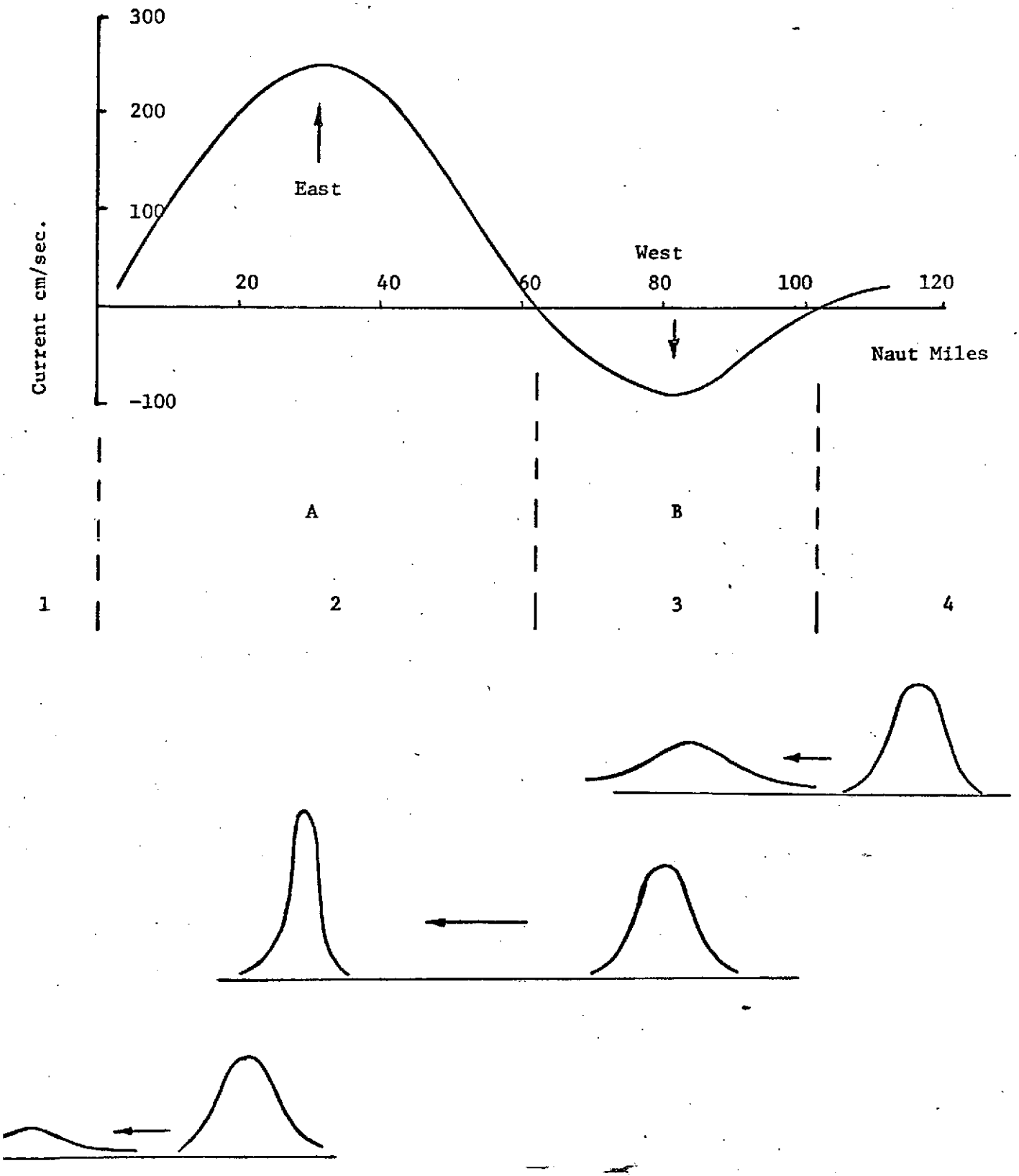

Figure 2.14 Schematic diagram on change of wave elevation distribution across the Gulf Stream.

and waves, which is not realistic compared to all the ocean situation; therefore, an extension into the two-dimensional model is necessary.

Secondly, we have to transform all the analyses into wave number space. For the one-dimensional model, a frequency spectrum is sufficient, while frequency spectra are easily available from data collected by the conventional methods in the form of time series, the remote sensing method is more effective in collecting data at any instance covering a large area. Such data in spatial variables will give us more complete information in the form of wave number spectra; therefore, the results presented in this report will have to be converted into parameters reflecting spatial distributions.

Thirdly, we need a definite relationship between wave number and frequency in a random wave field. This is critical especially in this developing stage when checks between remote sensing and in situ results are indispensable in calibration and improvement of the system. In such processes, it is necessary to transform information from frequency space (obtained by in situ methods) into wave number space (obtained by remote sensing methods) and vice versa. In the past a rough relationship based on a single train of linear small amplitude waves has been used. The deficiency of this approximation is tolerated for lack of alternatives. A new method of establishing a more accurate relationship is being developed during this study.

References

Huang, N. E., D. T. Chen, C. C. Tung, and J. R. Smith, 1972. Interactions between steady non-uniform currents and gravity waves with applications for current measurements. J. Physical Oceanography, 2, 420-431.

Longuet-Higgins, M. S. and R. W. Stewart, 1961. The changes in amplitude of short gravity waves on steady non-uniform currents. J. Fluid Mech., 10, 529-549.

Longuet-Higgins, M. S., 1956. The statistical distribution of the maxima of a random function. Proc. Roy. Soc. London, A-237, 212-232.

Longuet-Higgins, M. S., 1962. The statistical geometry of random surfaces. Proc. Symp. in Appl. Math., 13, 105-143.

Longuet-Higgins, M. S., 1956. Statistical properties of a moving wave-form. Proc. Camb. Phil. Soc., 52, 234-245.

Longuet-Higgins, M. S., 1957. On the velocities of the maxima in a moving wave form. Proc. Camb. Phil. Soc., 53, 230-233.

Phillips, O. M., 1960. The Dynamics of the Upper Ocean, Camb. Univ. Press.

3. Interaction of Capillary-Gravity Waves with Non-Uniform Current

One of the problems of a laboratory study of wave interactions has been the difficulty of generating waves in the laboratory which correspond with the type of waves involved in the existing mathematical descriptions of the interaction process. One such description is that of Huang et al (1973) which rigorously develops the interaction of pure capillary waves with current in the one-dimensional case. However, the single wave trains generated under laboratory conditions are almost never pure capillary waves, but are rather capillary-gravity waves, described by the equation

$$\sigma^2 = \gamma k^3 + gk, \tag{3.1}$$

where σ is the wave frequency in radians, γ is the surface tension constant, g is the gravitational acceleration constant, and k is the wave number, equal to $2\pi/\lambda$, where λ is the wavelength. Waves generated with a frequency of 30 cy/sec still consist of approximately 34% from gravity wave contributions, represented by gk in (3.1) above. At 40 cy/sec, these gravity wave contributions are still approximately 23%; thus increasing the frequency results in the generation of waves which approach the pure capillary case. Unfortunately though, one phenomena limits the development of a single train of pure capillary waves--cross waves generated at the wave maker perpendicular to the direction of propagation desired. Between 30 and 40 cy/sec, these cross waves appear and increase in intensity until at about 40 cy/sec almost all energy goes into these cross waves. At this point, no single wave train is possible. Thus in reality, the single wave trains generated in the laboratory are basically capillary-gravity waves at the shorter wavelengths, and conversely, gravity-capillary waves at the longer wavelengths. Therefore, what must be described mathematically is a more complex wave made up of both capillary and gravity type terms. In general, phase speed c and wavelength λ are related as shown in Figure 3.1. To the left of the minimum phase speed, at λ = 1.76 cm, are the values corresponding to capillary-gravity waves, and to the right, gravity-capillary waves. Moving further to the right or left results in a more "pure" wave. Note that for any c other than the minimum value, the relation between c and λ is double-valued. Because of this, only the capillary-gravity region will be treated here. The method to be used is the perturbation method, with the perturbation ϵ being such so that $\epsilon < 1$.

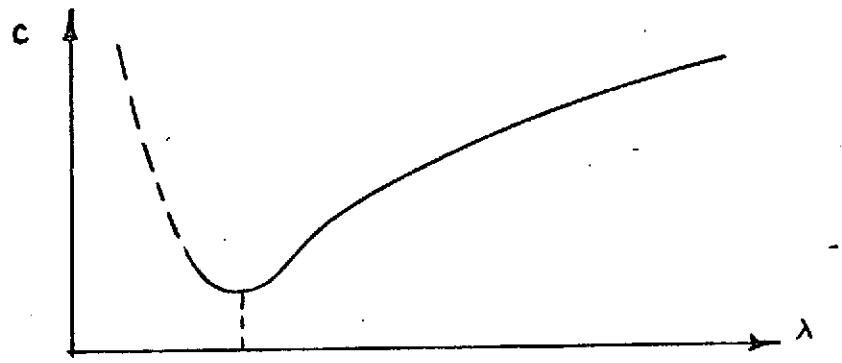

Figure 3.1. The relationship between phase speed c and wavelength λ

In this approach, we use the energy conservation equation as used by Phillips (1966) which states that

$$\frac{\partial E}{\partial t} + \frac{\partial}{\partial x_\alpha}\{E[U_\alpha + c_{g\alpha}]\} + S_{\alpha\beta}\frac{\partial U_\beta}{\partial x_\alpha} = \delta, \tag{3.2}$$

where

$\alpha, \beta = 1, 2$, corresponding to $x_1 = x$, $x_2 = y$

$c_{g\alpha}$ = group velocity

U_α = current velocity

E = wave energy

$S_{\alpha\beta}$ = excess momentum tensor, or Reynolds stress

δ = dissipation.

For the one-dimensional case under steady state conditions, and no dissipation, (3.2) can be written as

$$\frac{\partial}{\partial x}\{E[U + c_g]\} + S_{xx}\frac{\partial U}{\partial x} = 0. \tag{3.3}$$

Thus expansions in powers of ϵ are needed to substitute into (3.3). We begin by rewriting (3.1) as

$$\sigma^2 = \gamma k^3\left(1 + \frac{g}{\gamma k^2}\right). \tag{3.4}$$

To develop an expression for c_g, we take $\frac{\partial}{\partial k}$ of (3.4) to get

$$2\sigma\frac{\partial\sigma}{\partial k} = 3\gamma k^2\left(1 + \frac{g}{\gamma k^2}\right) + \gamma k^3\left(-\frac{2g}{\gamma k^3}\right)$$

or

$$\frac{\partial\sigma}{\partial k} = c_g = \frac{3\gamma k^2\left(1 + \frac{g}{\gamma k^2}\right) - 2g}{2\sqrt{\gamma k^3}\left(1 + \frac{g}{\gamma k^2}\right)^{1/2}} . \tag{3.5}$$

Define now

$$K = \frac{k}{\hat{k}} , \quad \varepsilon = \frac{g}{\gamma\hat{k}^2} ,$$

where the hat values denote constant values at the points where U = 0. Thus using these definitions, (3.5) can be rewritten as

$$c_g = \frac{3}{2}\hat{c}_o\left[K^{1/2}\left(1 + \frac{\varepsilon}{K^2}\right)^{1/2} - \frac{2\varepsilon}{3K^{3/2}\left(1 + \frac{\varepsilon}{K^2}\right)^{1/2}}\right], \tag{3.6}$$

where $\hat{c}_o = \sqrt{\gamma\hat{k}}$, the phase velocity of a pure capillary wave at the location where U = 0, thus a constant value. Expanding (3.6) and grouping by orders of ε results in

$$c_g = \frac{3}{2}\hat{c}_o\left[K^{1/2} - \left(\frac{1}{6K^{3/2}}\right)\varepsilon + \left(\frac{5}{24K^{7/2}}\right)\varepsilon^2 + \cdots\right] . \tag{3.7}$$

Now, to develop an expression for U, we start with the kinematic conservation equation, as used by Phillips (1966):

$$\frac{\partial\underset{\sim}{k}}{\partial t} + \nabla n = 0.$$

Assuming steady state conditions, this becomes

$$\nabla(\sigma + \underset{\sim}{k}\cdot\underset{\sim}{U}) = 0.$$

For the one-dimensional case along x, this is just

$$\frac{\partial}{\partial x}(kU + kc) = 0,$$

C-2

since $\sigma = kc$. This means that

$$kU + kc = \text{constant}.$$

The constant will be chosen where $U = 0$, $k = \hat{k}$, $c = \hat{c}$, thus

$$kU + kc = \hat{k}\hat{c}$$

or

$$\frac{U}{\hat{c}} + \frac{c}{\hat{c}} = \frac{\hat{k}}{k} = \frac{1}{K} . \tag{3.8}$$

Since $\frac{\sigma^2}{k^2} = c^2 = \gamma k + \frac{g}{k}$, using (3.1) it follows that

$$\frac{c^2}{\hat{c}^2} = \frac{\gamma k(1 + \frac{g}{\gamma k^2})}{\gamma\hat{k}(1 + \frac{g}{\gamma\hat{k}^2})} = \frac{\gamma\hat{k}K(1 + \frac{\epsilon}{K^2})}{\gamma\hat{k}(1 + \epsilon)} ,$$

or

$$\frac{c}{\hat{c}} = \frac{K^{1/2}(1 + \frac{\epsilon}{K^2})^{1/2}}{(1 + \epsilon)^{1/2}} .$$

Using this result in (3.8) leads to

$$U = \left[\frac{1}{K} - \frac{K^{1/2}(1 + \frac{\epsilon}{K^2})^{1/2}}{(1 + \epsilon)^{1/2}}\right]\hat{c} .$$

Expanding, using $\hat{c} = \hat{c}_o(1 + \frac{1}{2}\epsilon - \frac{1}{8}\epsilon^2 + \cdots)$, and grouping in terms of ϵ orders gives

$$U = \left[(\frac{1}{K} - K^{1/2})\hat{c}_o + \frac{1}{2}\hat{c}_o(\frac{1}{K} - \frac{1}{K^{3/2}})\epsilon - \frac{1}{8}\hat{c}_o(\frac{1}{K^{7/2}} + \frac{1}{K})\epsilon^2 \cdots\right] . \tag{3.9}$$

It thus follows that

$$\frac{\partial U}{\partial x} = \left[(-\frac{1}{K^2} - \frac{1}{2K^{1/2}})\hat{c}_o + \frac{1}{2}\hat{c}_o(\frac{3}{2K^{5/2}} - \frac{1}{K^2})\epsilon + \frac{1}{8}\hat{c}_o(\frac{7}{2K^{9/2}} + \frac{1}{K^2})\epsilon^2 + \cdots\right]\frac{\partial K}{\partial x} . \tag{3.10}$$

Expanding the energy E now as

$$E = E_o + \varepsilon E_1 + \varepsilon^2 E_2 + \cdots \tag{3.11}$$

and the Reynolds stress term as

$$S_{xx} = \frac{3+\varepsilon}{2+2\varepsilon}E = (3+\varepsilon)(\frac{1}{2} - \frac{1}{2}\varepsilon + \frac{1}{2}\varepsilon^2 \cdots)[E_o + \varepsilon E_1 + \varepsilon^2 E_2 + \cdots]$$

or

$$S_{xx} = \frac{3}{2}E_o + (\frac{3}{2}E_1 - E_o)\varepsilon + (\frac{3}{2}E_2 - E_1 + E_o)\varepsilon^2 + \cdots , \tag{3.12}$$

when grouped in orders of ε.

By substituting (3.7), (3.9), (3.10), (3.11), and (3.12) into (3.3), carrying out the multiplications and grouping by orders of ε, the energy equation (3.3) becomes, to order ε^o,

$$\frac{\partial}{\partial x}\left\{E_o\left[(\frac{1}{K} - K^{1/2})\hat{c}_o + \frac{3}{2}K^{1/2}\hat{c}_o\right]\right\} + \frac{3}{2}E_o\hat{c}_o(-\frac{1}{K^2} - \frac{1}{2K^{1/2}})\frac{\partial K}{\partial x} = 0. \tag{3.13}$$

Multiplying (3.13) by $\frac{1}{K^{3/2}}$ results in a perfect partial derivative of a quotient, so that (3.13) can be written as

$$\frac{\partial}{\partial x}\frac{E_o\hat{c}_o[\frac{1}{K} + \frac{1}{2}K^{1/2}]}{K^{3/2}} = 0. \tag{3.14}$$

Thus

$$\frac{E_o\hat{c}_o[\frac{1}{K} + \frac{1}{2}K^{1/2}]}{K^{3/2}} = \text{constant}. \tag{3.15}$$

Again we choose the constant at the locations where U = 0, for there $E_o = \hat{E}_o$, $K = \hat{K} = 1$. This results in a constant of

$$\frac{\hat{E}_o\hat{c}_o[1 + \frac{1}{2}]}{1} = \text{constant} = \frac{3}{2}\hat{E}_o\hat{c}_o .$$

Equation (3.15) now becomes

$$\frac{E_o \hat{c}_o [\frac{1}{K} + \frac{1}{2}K^{1/2}]}{K^{3/2}} = \frac{3}{2}\hat{E}_o \hat{c}_o ,$$

or

$$\frac{E_o}{\hat{E}_o} = \frac{\frac{3}{2}K^{3/2}}{\frac{1}{K} + \frac{1}{2}K^{1/2}} . \tag{3.16}$$

Equation (3.16), where the order is ε^o, corresponds to the pure capillary wave case. This result is the same as that obtained by Crapper (1972), Huang et al (1973), and Holliday (1973). Using (3.9) and (3.10a), (3.16) may be rewritten in the form

$$\frac{E_o}{\hat{E}_o} = \frac{\frac{3}{2}(\frac{c}{\hat{c}_o})^3}{\frac{U}{\hat{c}_o} + \frac{3}{2}(\frac{c}{\hat{c}_o})} \tag{3.17}$$

Writing the energy equation (3.3) in its expanded form to order ε^1, we obtain

$$\frac{\partial}{\partial x} E_o \hat{c}_o (\frac{1}{2K} - \frac{3}{4K^{3/2}}) + E_o \hat{c}_o (\frac{9}{8K^{5/2}} + \frac{1}{4K^2} + \frac{1}{2K^{1/2}}) \frac{\partial K}{\partial x}$$

$$+ \frac{\partial}{\partial x} E_1 \hat{c}_o (\frac{1}{K} + \frac{1}{2}K^{1/2}) - E_1 \hat{c}_o (\frac{3}{2K^2} + \frac{3}{4K^{1/2}}) \frac{\partial K}{\partial x} = 0. \tag{3.18}$$

Note that the E_1 terms of (3.18) are of the same form as the order ε^o case. Thus (3.18) can be simplified immediately by multiplying through with $\frac{1}{K^{3/2}}$, resulting in

$$\frac{1}{K^{3/2}} \frac{\partial}{\partial x} \left\{ E_o \hat{c}_o (\frac{1}{2K} - \frac{3}{4K^{3/2}}) \right\} + E_o \hat{c}_o (\frac{9}{8K^4} + \frac{1}{4K^{7/2}} + \frac{1}{2K^2}) \frac{\partial K}{\partial x}$$

$$+ \frac{\partial}{\partial x} \left\{ \frac{E_1 \hat{c}_o (\frac{1}{K} + \frac{1}{2}K^{1/2})}{K^{3/2}} \right\} = 0. \tag{3.19}$$

By adding and subtracting identical terms, thus adding a well chosen zero to (3.19), its form can be changed to

$$\frac{\partial}{\partial x}\left[\frac{E_o\hat{c}_o\left(\frac{1}{2K}-\frac{3}{4K^{3/2}}\right)}{K^{3/2}}+E_o\hat{c}_o\left(\frac{1}{K^{7/2}}+\frac{1}{2K^2}\right)\frac{\partial K}{\partial x}+\frac{\partial}{\partial x}\left\{\frac{E_1\hat{c}_o\left(\frac{1}{K}+\frac{1}{2}K^{1/2}\right)}{K^{3/2}}\right\}\right]=0. \quad (3.20)$$

Using (3.17), we may substitute for E_o in (3.20) and determine the integral of the middle term, obtaining

$$\frac{3}{2}\hat{E}_o\hat{c}_o \ln K. \quad (3.21)$$

By thus using (3.21), (3.20) can now be written as

$$\frac{\partial}{\partial x}\left[\frac{3}{2}\hat{E}_o\hat{c}_o\left(\frac{2K^{1/2}-3}{4K^{1/2}+2K^2}\right)+E_1\hat{c}_o\left(\frac{1}{K^{5/2}}+\frac{1}{2K}\right)+\frac{3}{2}\hat{E}_o\hat{c}_o \ln K\right]=0. \quad (3.22)$$

Thus

$$\frac{3}{2}\hat{E}_o\hat{c}_o\left(\frac{2K^{1/2}-3}{4K^{1/2}+2K^2}\right)+E_1\hat{c}_o\left(\frac{1}{K^{5/2}}+\frac{1}{2K}\right)+\frac{3}{2}\hat{E}_o\hat{c}_o \ln K=\text{constant}, \quad (3.23)$$

follows from (3.22). Again we choose to develop this constant at the locations where $U = 0$, $K = \hat{K} = 1$, $E_1 = \hat{E}_1$. Thus we obtain

$$\text{constant} = \frac{3}{2}\hat{E}_o\hat{c}_o\left(-\frac{1}{6}\right)+\hat{E}_1\hat{c}_o\left(\frac{3}{2}\right)+\hat{E}_o\hat{c}_o(o)$$

or

$$\text{constant} = \frac{3}{2}\left\{\hat{E}_1\hat{c}_o-\frac{1}{6}\hat{E}_o\hat{c}_o\right\}. \quad (3.24)$$

Notice the $\hat{E}_1$ appearing in (3.24), something we have no expression for. It is thus at present an unknown constant. To determine $\hat{E}_1$, we have to look at the equation of total energy for a capillary-gravity wave, given by

$$E = E_{\text{capillary}} + E_{\text{gravity}}$$

or

$$E = \frac{1}{2}\rho\gamma a^2k^2 + \frac{1}{2}\rho g a^2 = \frac{1}{2}\rho\gamma a^2k^2\left(1 + \frac{g}{\gamma k^2}\right) . \tag{3.25}$$

Then, where $U = 0$, $E = \hat{E}$, $k = \hat{k}$, $a = \hat{a}$, so that

$$\hat{E} = \frac{1}{2}\rho\gamma\hat{a}^2\hat{k}^2\left(1 + \frac{g}{\gamma\hat{k}^2}\right) . \tag{3.26}$$

But this is just

$$\hat{E} = \hat{E}_o(1 + \epsilon) = \hat{E}_o + \epsilon\hat{E}_1 + \epsilon^2\hat{E}_2 + \cdots . \tag{3.27}$$

Thus (3.27) results in the general condition that

$$\hat{E}_i = 0, \; i \geq 2. \tag{3.28}$$

From (3.27), we have now that

$$\hat{E}_1 = \hat{E}_o, \tag{3.29}$$

and (3.24) can be written as

$$\text{constant} = \frac{3}{2}\{\hat{E}_o\hat{c}_o - \frac{1}{6}\hat{E}_o\hat{c}_o\} = \frac{5}{4}\hat{E}_o\hat{c}_o . \tag{3.30}$$

Combining (3.23) and (3.30), our result is now

$$\frac{3}{2}\hat{E}_o\hat{c}_o\left[\frac{2K^{1/2} - 3}{4K^{1/2} + 2K^2} + \ln K\right] + E_1\hat{c}_o\left(\frac{1}{K^{5/2}} + \frac{1}{2K}\right) = \frac{5}{4}\hat{E}_o\hat{c}_o, \tag{3.31}$$

or

$$\frac{E_1}{\hat{E}_o} = \frac{\frac{5}{2}K^{5/2} - 3K^{5/2}\ln K - 3K^{5/2}\left(\frac{2K^{1/2} - 3}{4K^{1/2} + 2K^2}\right)}{K^{3/2} + 2} . \tag{3.32}$$

Equation (3.32) is thus an equation for order ϵ^1 in energy for a capillary-gravity wave meeting a current U.

To obtain the result to order ε^2, we now write the expansion of the energy equation (3.3) in order ε^2, thus

$$\frac{\partial}{\partial x}\{E_o\hat{c}_o(\frac{3}{16K^{7/2}}-\frac{1}{8K})\}+E_o\hat{c}_o(\frac{21}{32K^{9/2}}-\frac{5}{16K^2}-\frac{3}{4K^{5/2}}-\frac{1}{2K^{1/2}})\frac{\partial K}{\partial x}$$

$$+\frac{\partial}{\partial x}\{E_1\hat{c}_o(\frac{1}{2K}-\frac{3}{4K^{3/2}})\}+E_1\hat{c}_o(\frac{9}{8K^{5/2}}+\frac{1}{4K^2}+\frac{1}{2K^{1/2}})\frac{\partial K}{\partial x}$$

$$+\frac{\partial}{\partial x}\{E_2\hat{c}_o(\frac{1}{K}+\frac{1}{2}K^{1/2})\}+E_2\hat{c}_o(-\frac{3}{2K^2}-\frac{3}{4K^{1/2}})\frac{\partial K}{\partial x}=0. \qquad (3.33)$$

Note that the E_2 terms have the same form as the order ε^o case; the E_1 terms the same form as the order ε^o case. Equations (3.16) and (3.32) specify what E_o and E_1 are, thus a similar approach may be used here starting as before by multiplying through by $\frac{1}{K^{3/2}}$, thus making possible the combination of the last two terms in (3.33). This results finally in

$$\frac{E_2}{\hat{E}_o}=\frac{\frac{3}{2}K^{3/2}}{(\frac{1}{K}+\frac{1}{2}K^2)}\left\{\frac{-291}{96}-\left[\frac{3\,\overline{\Phi}\,2K^{5/2}}{16K^{5/2}+8K^4}\right]\right.$$

$$-\left[\frac{2K^{3/2}-3K}{6+3K^{3/2}}\right]\left[\frac{5}{4}-\frac{3}{2}\ln K-\frac{3}{2}(\frac{2K^{1/2}-3}{4K^{1/2}+2K^2})\right]+\frac{3}{8K^{5/2}}$$

$$-\frac{15}{32K}+\frac{3}{K^{1/2}}+\frac{1}{6}\ln K+\frac{1}{2}(\ln K)^2$$

$$+\frac{5\cdot 2^{1/3}}{64}\ln\left[\frac{\left(\frac{1+2^{1/3}}{K^{1/2}+2^{1/3}}\right)^2}{\frac{1-2^{1/3}+2^{2/3}}{K-2^{1/3}K^{1/2}+2^{2/3}}}\right]-$$

$$\left.+\frac{15\cdot 2^{1/3}}{32\sqrt{3}}\left[\arctan\left(\frac{\sqrt{3}}{2^{4/3}-1}\right)-\arctan\left(\frac{K^{1/2}\sqrt{3}}{2^{4/3}-K^{1/2}}\right)\right]\right\}. \qquad (3.34)$$

Thus equations have been determined for E_o (3.16), E_1 (3.32), and E_2 (3.34), and hence we may write the energy to order ϵ^2 as

$$E = E_o + \epsilon E_1 + \epsilon^2 E_2, \tag{3.35}$$

knowing only the dimensionless parameter K. Thus rewriting (3.8) as

$$\frac{k}{\hat{k}}\left(\frac{U}{\hat{c}} + \frac{c}{\hat{c}}\right) = 1$$

or

$$K\left(\frac{U}{\hat{c}} + \frac{c}{\hat{c}}\right) = 1, \tag{3.36}$$

we can define $\bar{U} = \frac{U}{\hat{c}}$, $\bar{c} = \frac{c}{\hat{c}}$, and substitute into (3.36), rearrange, and get

$$K = \frac{1}{\bar{U} + \bar{c}} . \tag{3.37}$$

One possible solution scheme then, is to numerically solve for K for various values of $\bar{U}$ and $\bar{c}$, and then use (3.16), (3.32), (3.34), and (3.35) to obtain the energy value for each particular value of U and c chosen. This is easily done by computer. Note in (3.37) that singularities exist at values where $\bar{U} + \bar{c}$ approach zero. For these singularities, K values become infinite.

Computer analysis can now easily be done and checked with laboratory results.

References

Crapper, G. D., 1972. Non-linear gravity waves on steady non-uniform currents. J. Fluid Mech., 52, 713.

Holliday, D., 1973. Non-linear gravity-capillary surface waves in a slowly varying current. J. Fluid Mech., 57, 797.

Huang, N. E., F. Y. Sorrell, and C. C. Tung, 1973. Engineering studies related to geodetic and oceanographic remote sensing using short pulse techniques. Final engineering report for Task D; prepared under NASA contract NAS6-2135.

Phillips, O. M., 1966. The Dynamics of the Upper Ocean. Cambridge University Press.

PART II

EXPERIMENTAL STUDIES

In this part of the report, the wave measurement system was first discussed. The system was used to study wave decay and capillary-gravity interactions. Some preliminary results of wind waves are also included.

1. INTRODUCTION

This section deals with experiments on Gravity and Capillary waves relative to improving the understanding of how these wave motions are influences by surface currents. It is known that active microwave backscatter results primarily from the capillary waves via the mechanism of resonant or Bragg scattering. The relation between the ocean waves that are the primary contributors to the radar cross section and the incident radar frequency is shown in Figure 1.1. This figures was developed for a radar depression angle (NADIR) of 45°. It is evident that short wavelength or capillary waves contribute the most to the radar cross section. Moreover Huang (1972) has also shown that the shorter waves are more strongly influenced by currents. Therefore, there should be a strong correlation between radar cross section and ocean surface currents.

The dependence of radar cross section on surface current can be expected from this simple argument. However, these has been considerable difficulty in making measurements of the short or capillary waves, and thus difficulty in relating the effect of currents via the change in capillary wave spectrum to radar cross section. Indeed, until recently and with the exception of microwave measurements of the ocean wave spectrum, the only method of making capillary wave measurements was with small wave height probes. McGoldrick (1971) has developed a capacitative wave height probe, specifically designed for capillary wave measurements. Although the system has been used for capillary waves, there has remained some question as to the validity of using a probe for the measurement of short wavelength waves. This is primarily because any probe will have a meniscus on it due to surface tension and because capillary waves are also driven by surface tension. Therefore it was not clear that any effect due to the meniscus could be removed without

altering the wave under consideration. Because of this, various optical systems have been proposed to measure capillary waves or to verify the accuracy of the wave height probe. Recently Tober, et.al.(1973) and Sturm and Sorrell (1973) reported optical wave measurement systems. The data of Tober, et.al.(1973) reveals higher frequency components than measured with a wave height probe for the same conditions. Moreover, Sturm and Sorrell (1973) made a careful comparison of the response of their optical system with a capacitative wave probe of the kind developed by McGoldrick (1971). These results show a gradual roll off of the probe sensitivity with increasing wave frequency or decreasing wave length. Based on these results, the practical limit of the wave height probe is for wave lengths greater than 2-3 cm. This is a longer wave length than much of the wave spectrum of concern here, and thus the use of an optical wave measurement system is required.

The system employed by Sturm and Sorrell (1973) used a one dimensional position sensitive diode. While this diode is commercially available, it restricts the system to measurement of one dimensional wave trains. Most of the data of interest involves 2 dimensions or random wave fields, and thus a different diode array or matrix is needed. Part 2 of this report describes the 2 dimensional diode matrix that is used and the necessary electronics developed for data acquisition with this system.

The following parts of the report deal with capillary wave experiments. An important question is how long the capillary waves live after generation. While this is well understood when no surface current or possibly when a constant current is present, there have been no data for variable currents where wave-current interaction is expected. In addition the presence of

any surface film can alter the capillary wave damping. Because of this an investigation of capillary wave decay on constant and variable currents as well as an investigation of surface films was undertaken. Part 3 reports the results of these experiments.

It is well documented that microwave backscatter occurs by the mechanism of resonant or Bragg scattering from the capillary waves. The presence of the longer waves or the ocean swell is not negligible, however, and there has been considerable work including this in computations of radar cross sections. The more successfull attempts have been with the so-called "composite model" where the swell is considered to simply tilt or alter the orientation of the surface containing the capillary waves. This model requires a knowledge of the wave height spectrum for the capillary waves and an important question is the influence of the ocean swell on the distribution and amplitude of the capillary waves. In simplest form this is the question of any interaction of a long or gravity wave with a capillary wave. To investigate this an experimental study of the interaction of gravity and capillary waves was undertaken. The results of these experiments are given in part 4 of this report.

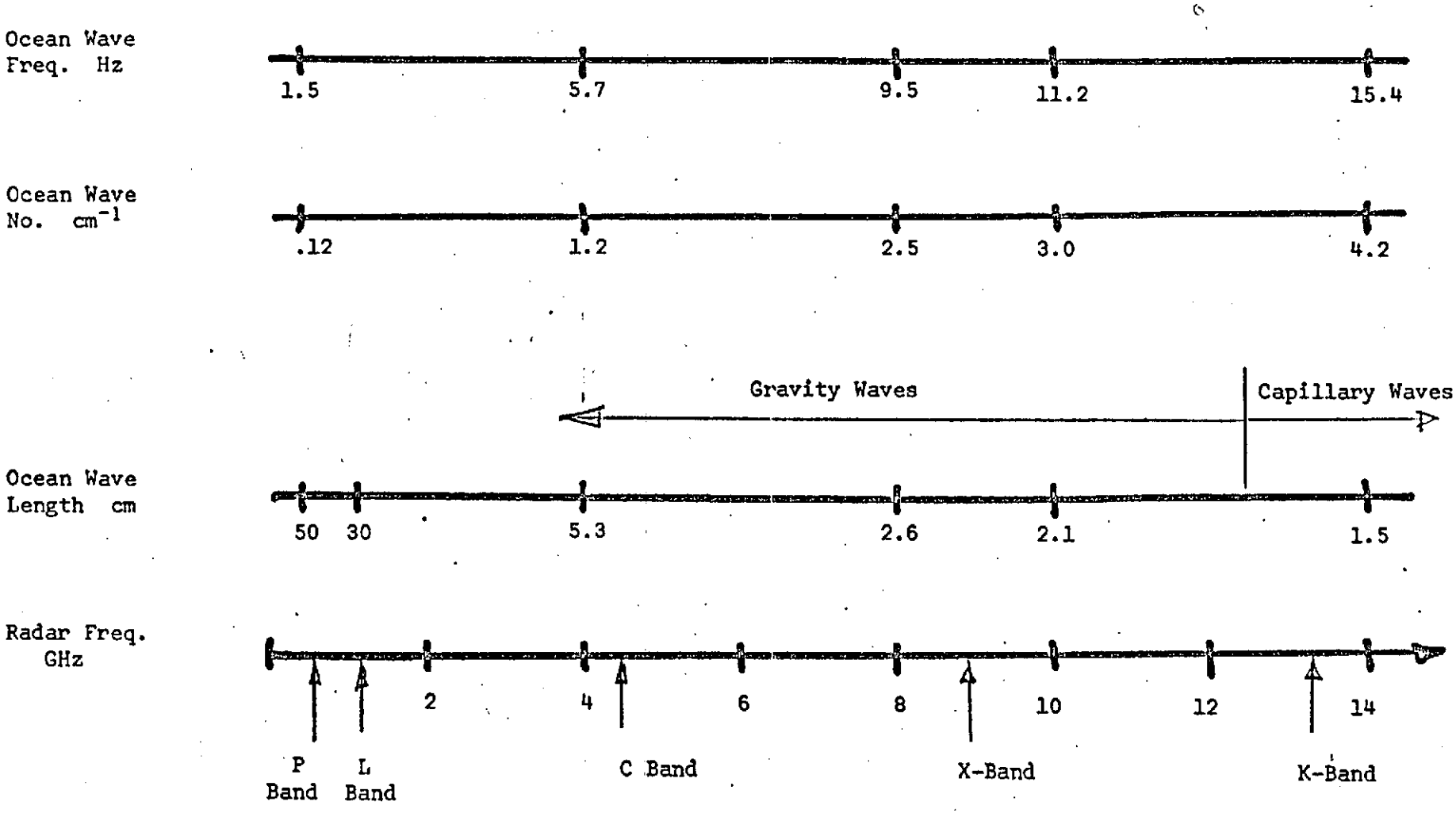

Figure 1.1 Relation between radar frequency and scattering ocean waves.

2. Wave Measurement System

2.1 Introduction

The overriding objective of this work is to aid in the development of remote sensing techniques to the point where the wave characteristics, in particular wave energy or slope spectra, can be used to infer ocean currents. This requires work in two areas (1) development of remote sensing techniques to measure the ocean wave characteristics and (2) relating these wave characteristics to the mean current. Most of the work reported here is devoted to advancement of knowledge relative to problem (2), which is relating the wave characteristics or spectra to the mean current that is present. However this cannot be accomplished without some knowledge of remote sensing techniques.

Most of the presently conceived remote sensing methods employ the reflection of some form of radiation from the ocean surface. This reflection appears to be related to ocean surface roughness or to the slope distribution of the ocean surface, rather than to the height distribution of the surface. However most of the presently employed oceanographic instruments measure wave height and not wave slope. For a single wave there is a direct relation between wave height and wave slope, however for a random wave field there is no such relation, although there are empirical equations that are sometimes used. It is for this reason it is considered desirable to develop instrumentation to measure wave slope and to try to relate this measured wave slope spectra to mean water current. Such instrumentation has two uses in the remote sensing program. (1) It can be used to check or verify the data obtained by various remote sensing techniques. For this purpose the instrument should be able to measure ocean wave slope spectra. (2) It can be used to obtain laboratory data which

are used to relate measured wave slope spectra to known mean water currents. For this purpose the instrument must have a high accuracy.

Since our program is primarily an investigation of the relation of wave characteristics to the current, the development of an instrument to make laboratory measurements has been our major purpose. However, when possible we have also kept the requirements of objective (1) in mind and tried to develop a system that can be modified for ocean measurements.

It should also be noted that much of the ocean's surface roughness is due to the capillary waves and that the longer gravity waves which contain most of the energy only weakly affect the surface roughness. Therefore the most useful information is a relation between capillary wave characteristics and water currents. Any wave measurement technique that requires the imersion of a probe through the water surface will have a meniscus formed on the probe due to the surface tension of the water. Since this surface tension is also the driving force for capillary waves there has been considerable discussion by many people as to the accuracy of any probe technique for measuring capillary waves. Recently Sturm and Sorrell (1973) have shown experimentally that the meniscus does cause significant error when measuring the wave height of short capillary waves with a probe. Therefore it is desirable that the measurement of wave slope be made without a probe being immersed through the surface. Finally, since the capillary waves have very short wave lengths, good spatial resolution is required. Thus the requirements for the wave measurement system are that it (1) measures more slope to a resonable accuracy ($\pm$ 2%) (2) that the spatial resolution be at least 0.5 mm and that the frequency response be at least 100 Hertz. (3) that no probe sticking through the surface be required. (4) If practical, a system that can be adopted to ocean surface measurements be employed.

The system developed to meet these requirements is an optical wave slope measuring system, and at present has met all criteria mentioned except (4). Moreover, at this time there do not appear to be an insurmountable problems in meeting criteria (4).

2.2 Principle of Operation

Because of the inherent disadvantage with the probe system, there have been many optical techniques suggested for the measurement of wave slope. A brief review of some of the most applicable techniques is given with a description of the present system. Early techniques that were considered by Hulburt (1934), Cox and Munk (1954), and Schooley (1954), used the reflection of light to infer ocean surface roughness. While these techniques or modifications of them have been considered as possible remote sensing systems, they are not suited for accurate laboratory measurements. Moreover, they are not generally considered desirable for remote sensing because of the inherent difficulties in data reduction.

The use of the refraction of light at the air-water interface is a more accurate technique. In this method a thin beam of light is usually directed vertically through the surface and the angle that the light beam is refracted from the vertical is measured. This system was first proposed by Cox (1958), and he measured the refraction angle by intensity variation. He experienced some errors due to intensity variation due to factors other than refraction angle and also due to water level changes. Later Prettyman (1969) used refraction and recorded the refraction angle with a high speed movie camera. While this technique is accurate, data reduction is tedious for simple wave systems, and impractical for a random wave field. Recently Tober (1973) reported a refraction system in which an optical arrangement removed the effect

of changes in water elevation. However the refraction angle is measured by a variable density transmission filter, which converts the refraction angle to a change in intensity. Thus any phenomena which results in intensity changes (spray, water impurities, etc.) will cause errors. This system is accurate for water level changes up to $\pm$ 6 cm.

The present system measures refraction angle directly and thus changes in light intensity do not affect the data. The major requirement is that the distance of the detector from the mean water level must be large compared to changes in mean water level.

In order to illustrate this the principle of operation of the system is described. Fig. 2.1 illustrates an idealization of a one-dimensional wave as traversed by the incident light beam.

The light beam enters vertically from below and intercepts the surface which has the instantaneous slope $d\zeta/dx = \tan\theta_1$ at the angle θ_1 with respect to the surface normal. As a result of refraction the beam enters the air at angle θ_2 with respect to the same normal. Angles θ_1, θ_2 and indices of refraction, n_1 and n_2, are related by Snell's law of refraction, $n_1 \sin\theta_1 = n_2 \sin\theta_2$. Since θ_1 and θ_2 are measured from the surface normal, the difference angle $\alpha = \theta_2 - \theta_1$ or simply the angular deviation from the vertical is measure experimentally. The difference angle α can be related to the angle θ_1 through Snell's law to give

$$\cot(\theta_1) = (n_1/n_2) \csc\alpha - \cot\alpha. \qquad (2.1)$$

The surface slope $d\zeta/dx = \tan\theta_1$ is simply the reciprocal of equation (2.1). Hence, by a measurement of α one can obtain the instantaneous surface slope at the point traversed by the light beam. Equation (2.1) is valid for any wave slope as long as θ_1 is less than the critical angle θ_c where total

internal reflection occurs. In order to measure the difference angle α, one relates the offset distance d of the refracted beam from the vertical to the distance ℓ of the distrubed surface to the photodetector as simply $\alpha = \tan^{-1}(d/\ell)$. When $\ell >> a$, where a is the total vertical surface displacement, ℓ may be considered constant. The present system requires that ℓ be constant, and thus for the method in its present form to be used for finite amplitude waves, the detector must be sufficiently far away that $\ell >> a$. This is the only restriction in wave amplitude that is inherent in the system. Previous results using this technique which were reported by Sturm and Sorrell (1973) employed a United Detector model PIN-LSC-9 photodiode which has an active area of 2.5 mm by 225 mm. Because of the narrow width of the diode only one-dimensional waves could be measured. If there is any cross motion the beam refracts perpendicular to the diode axis and does not fall on the active part of the diode. In addition the length of the diode puts an upper limit on the maximum slope and amplitude that can be measured. The requirement that $\ell >> a$ determines a minimum distance, ℓ_{min}, between the diode and the mean water level. However for a fixed vertical refraction angle, α, and diode length, there is a maximum length, ℓ_{max}, for which the light remains on the active part of the diode. Thus ℓ_{max} is determined by the diode length/maximum slope to be measured and ℓ_{min} is determined by the requirement that $\ell >> a$. Therefore there is a restriction on both the minimum and maximum distance of the diode from the mean water level. While this arrangement permits laboratory experiments under some useful conditions (see for example Sturm and Sorrell (1973)) it basically restricts its use to low amplitude one-dimensional wave trains. It is clear that modifications of the system are necessary if it is to be used in studies relative to remote sensing applications. The required modification are in the diode matrix used to measure the refraction angle.

2.3 The Diode Matrix

A new diode matrix was devised to greatly increase the active area of the diode system. A large area position sensitive diode is not presently available, and even if it were it would be prohibitively expensive. The present approach has been to use an array of diodes, in which each diode gives a signal that depends only on the fact that light is incident on the diode. The diodes are arranged in an array or matrix to give the size active area desired, and suitable electronics employed to give a signal whose voltage is proportional to the position of the diode upon which the light is incident.

The diodes utilized are Vactec S-150-LB diodes which have an active area of 15cm X 6.5 cm. A schematic of the diode arrangement is shown in Fig. 2.2. Two diodes are placed end to end giving the matrix a width of 30 cm and 18 diodes units are placed parallel to each to produce a length of 40 cm to 100 cm, depending on the diode spacing. In order to measure slope in 2 dimensions the refracted light beam is divided by a beam splitter and directed onto 2 diode matrices, one which measures position in the x-direction and one which measures position in the y-direction. This arrangement is also shown in Fig. 2.2. The accuracy of the measured slope depends only on the number of diodes employed. For 18 diodes the accuracy is $\frac{1}{18}$ = 5.5% if all diodes are used. The spacing between diodes can be changed to produce an active area that is as long as desired, and thus the system only requires that the array be the minimum distance, ℓ_{min}, from the mean water level.

These diodes are purchased "off the shelf" from Vartec electronics and are quite reasonable ($1.00 - $2.00/each). Thus the diode array presents no particular problem. However the associated electronics to convert the signal from the diode to a voltage proportional to its position in the diode array is quite involved. This has been a major development item for the present investigation and is thus described in detail.

2.4 Electronics for the Diode Matrix

The desired behavior of the diode matrix electronic circuit is to convert the signal output of a single diode to a voltage that is related to that diode's position in the matrix. The conversion of many similar outputs to a single coded signal is best handled with digital logic, therefore the approach has been to amplify the diode output to a voltage compatable with a digital logic system. By using digital logic elements the signal can be easily converted into/to a binary code indicating the diodes position. The resulting binary code can be converted to an analog signal, if desired, by a digital to analog (D/A) converter. The circuit for each step is now described in more detail.

The basic circuit for the diode output is shown in Fig. 2.3, the diode amplifier circuit. The diode (indicated by PC) output goes to the first stage of a dual operational amplifier package, IC1. The first amplifier is used to amplify the current out of the diode. That is, this amplifier is set up for current amplification. The amplified current goes to R2 which is of variable resistance to adjust the voltage input to the second stage of the dual system. The current output for a fixed incident light intensity is not exactly the same for each diode and R2 is used to compensate for this such that the voltage into the 2nd stage is the same for each of the 18 inputs. This voltage goes into one side of the 2nd amplifier, which is wired to operate as a comparator. If the voltage is above the reference voltage, R, the output rises until it is clamped at 4.0 volts by D1, a Zener diode. If the output is less than R the voltage out of the 2nd stage is less than 0.5 volts. R3 is simply a current limiting resistor. These voltage levels are TTL compatible and thus TTL elements can be used for the rest of the circuit elements.

A reference level is employed to allow the diode matrix to be used with high background light levels. That is each diode has some current output when

there is background light and there is an additional output from the diode when the refracted light is incident upon the diode. Thus it was considered desirable to have a reference signal level, such that there is no signal output until the refracted light is incident upon the diode. Because the background light level is highly variable, it was desirable to have the reference level controlled by the diodes themselves. Fig. 2.4 shows the reference voltage circuit which is driven by 2 separate diodes at the top and bottom of the diode matrix. This circuit follows the background light level and supplies a reference output for IC1, the diode comparators. This circuit has variable feedback through R24 so the amplification of the background light can be controlled. The circuit is designed to have a very low output impedance to prevent switching of the comparators to alter the reference voltage level. This circuit appears to work quite well and has successfully removed the background from direct florescent light which oscillates at 120 Hertz.

The output from IC1 has a slow rise time relative to that normal for conventional digital logic elements. When these logic elements experience a slowly rising voltage they exhibit instability and oscillate while the voltage is between the 2 logic levels. For this reason the output of IC1 is directed through a current limiting resistor into a Schmitt trigger, IC2. The Schmitt trigger shapes the output into a fast rising signal. This signal is then run in to an 18 input to 5 bit binary converter made up of NAND gates and NOR gates. This circuit, including Schmitt triggers is shown in Fig. 2.5, as the 18 input to 5 bit binary converter. The 5 bit binary output is indicated as outputs A through E. The choice of 18 inputs is arbitrary as up to 31 diode input channels can be employed with the 5 bit binary system (1 channel must remain at zero).

The 18 input to 5 bit binary converter works for any signal input from the 18 diodes, however anytime the signal is removed the output would be 5 bit binary zero. It is desirable to have the output remain at the last diode position or logic level until the next diode is turned on by the incident light beam. This is accomplished by IC6, which is a Quadruple Bistable Latch. The Latch is triggered by any input and holds the signal input until a signal from another diode is received. The circuit is shown in Fig. 2.6, the 5 bit binary to analog converter. IC5 is a Hex Inverter which inverts the signal 4 times and is used only to add sufficient delay for the Latch to operate. The result is that any diode output is held by the Latch until an output from a different diode occurs. This produces a signal which does not drop to zero when the light beam is between adjacent diodes.

The 5 bit binary output from the Latches goes directly into a D/A converter, IC7, if an analog output is desired. If binary output is desired it can be taken directly out of the Latch. IC8 amplifies the analog output to the desired voltage level.

In most cases only an AC signal is desired. That is any DC offset because the unrefracted light beam is not incident on the center of the matrix is not wanted. Therefore a separate AC coupling amplifier is used. The circuit is shown in Fig. 2.7, the output amplifier. The arrangement provides a direct DC signal and also an AC coupled signal. The operational amplifier, IC12, is used to provide a high inpedance source so AC coupling down to 0.1 Hertz is obtained.

The output from either the AC or DC jack is made of a series of small steps. This is shown in Fig. 2.9, which is a record of the signal out for a single wave train. The steped output, which is due to the position of the individual diodes, could probably cause errors in spectral analysis of the signal.

For this reason an analog smoothing circuit is also included in the output amplifier. This is also shown in the circuit (Fig. 2.7). It is simply another operational amplifier used to smooth the output. Fig. 2.9 shows the DC output and the smoothed output for a single wave. The input impedance R16 and feedback capacitance C4 are variable to produce the desired amount of smoothing. For the data given in Fig. 2.9 R16 was 100K and C4 = .002 μf.

In addition to smoothing, in some cases it is desirable to integrate the wave slope to obtain wave height. While there are some scaling problems associated with obtaining wave height in this manner, see for example Sturm and Sorrell (1973), many situations arise when it is desirable to be able to see wave height versus time, even with the height axis unscaled. This can be accomplished by changing the input inpedance R16 and feedback capacitance C4 to values which make the smoothing amplifier and integrator. Fig. 2.10 shows the integrated wave slope measured by the optical system and the wave height as measured by a capacitance probe. In this application R16 is 39K and C4 is 0.5 μf.

All circuits were made on printed circuit board which was etched from photographic templates that are made in our Laboratory. The 18 input to 5 bit binary circuit with Latch and D/A conversion was the most difficult circuit to wire. A copy of the template used to make the printed circuit board for this part of the circuit is shown in Fig. 2.8. A list of all parts used in the circuit is given in Table 2.1.

2.5 Summary

An optical system to measure random wave slope has been developed and operated in the laboratory. The system has spatial resolution less than 0.5 mm, frequency response greater than 100 Hertz and does not distrub the surface in any way. Output from the system has been used to measure wave slope and wave

height for single wave trains, as reported by Sturm and Sorrell (1973).

The system is presently being used to measure the interaction of capillary waves and gravity waves and to study the interaction of capillary waves with mean water currents. The only meaningful data for real wave-current interaction is to measure the wave slope spectra for a random wave field with current. The system has been designed to do this specifically and such spectra are presently being obtained.

Table 2.1 - Parts List

Integrated Circuits

Part	Number	Function
IC1	µA747	Operational Amplifier
IC2	SN7413	Schmitt Trigger
IC3,IC9	SN7430	8 input NAND gate
IC4,IC10	SN7402	NOR gate
IC5	SN7404	Hex Inverter
IC6	SN7475	Quadruple Bistable Latch
IC7	MC1406	D/A Converter
IC8	µA741	Operational Amplifier
IC12,IC13,IC14		

Active Components

Q1	40409	NPN power transistor
Q2	40410	PNP power transistor
D1	1N747A	3.9 Volt Zener Diode
PC	S 150 LB	Vactec Selenium photovoltaic cell

Capacitors - All Capacitors 50 WVDC ceramic unless otherwise specified

Capacitors	Value
C1	100 pf
C2	1 µf
C3,C5	0.1 µf
C4	
Integration	0.5 µf
Smoothing	0.002 µf
C6,C7	10 µf 25 WVDC electrolytic

Table 2.1 (cont.)

Resistors - All resistors 1/4 watt unless otherwise specified.

Resistor	
R1,R3,R5	1K
R2,R14,R23,R30	10K Trimpot
R4	1K Trimpot
R6	4.7K
R7	6.8 meg.
R8	2 meg. Trimpot
R9,R17	2.2 meg.
R10,R11,R19,R20	10K
R12,R13,R21,R22	1.5K
R15,R25,R26	100 Ω
R16	
Integration	39K
Smoothing	100K
R18	100K
R24	1K Linear Taper Pot
R27,R28	1K - 1 watt
R29	270 Ω - 1 watt

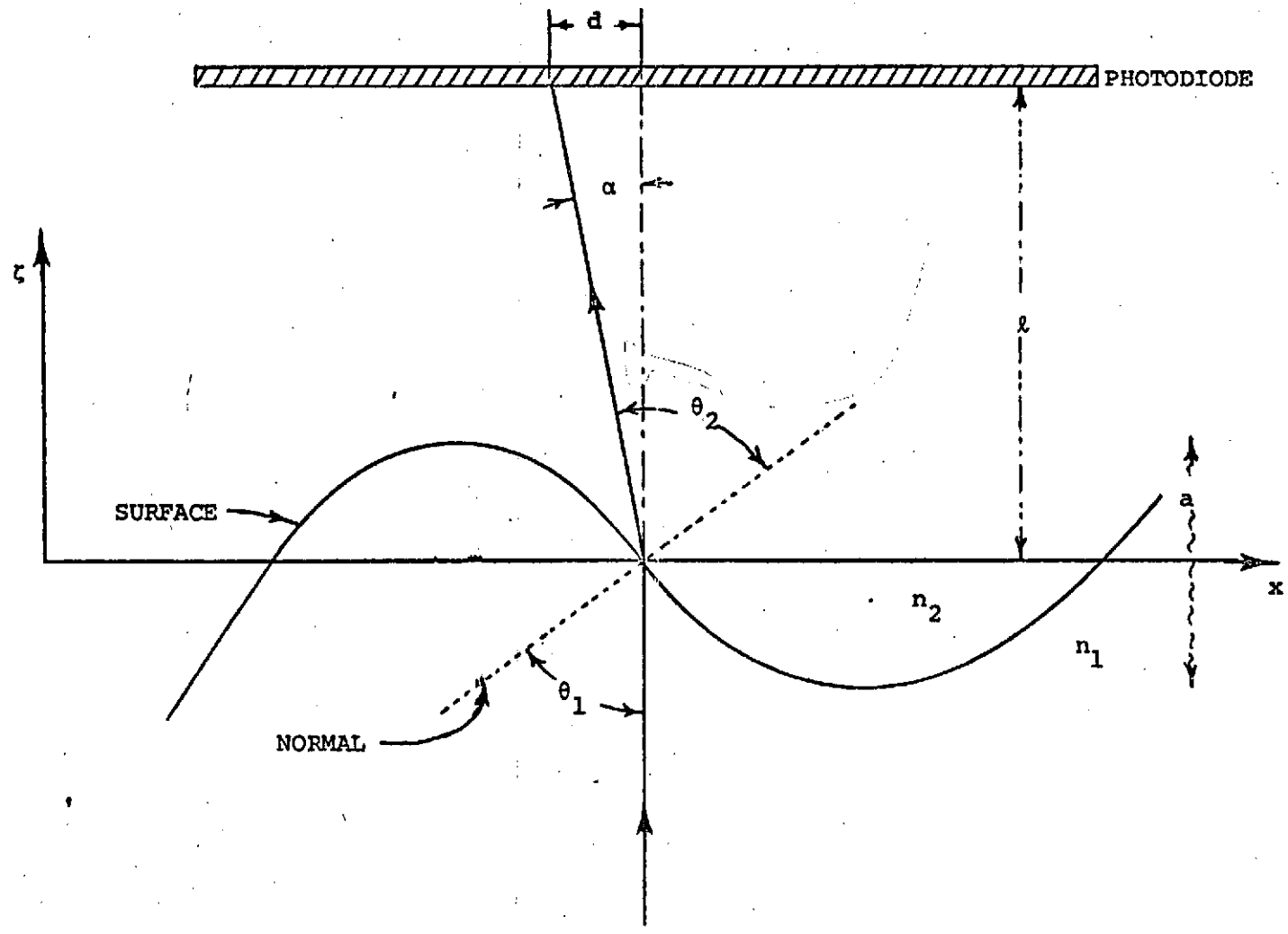

Figure 2.1 Optical path and refraction angles for a one-dimensional wave

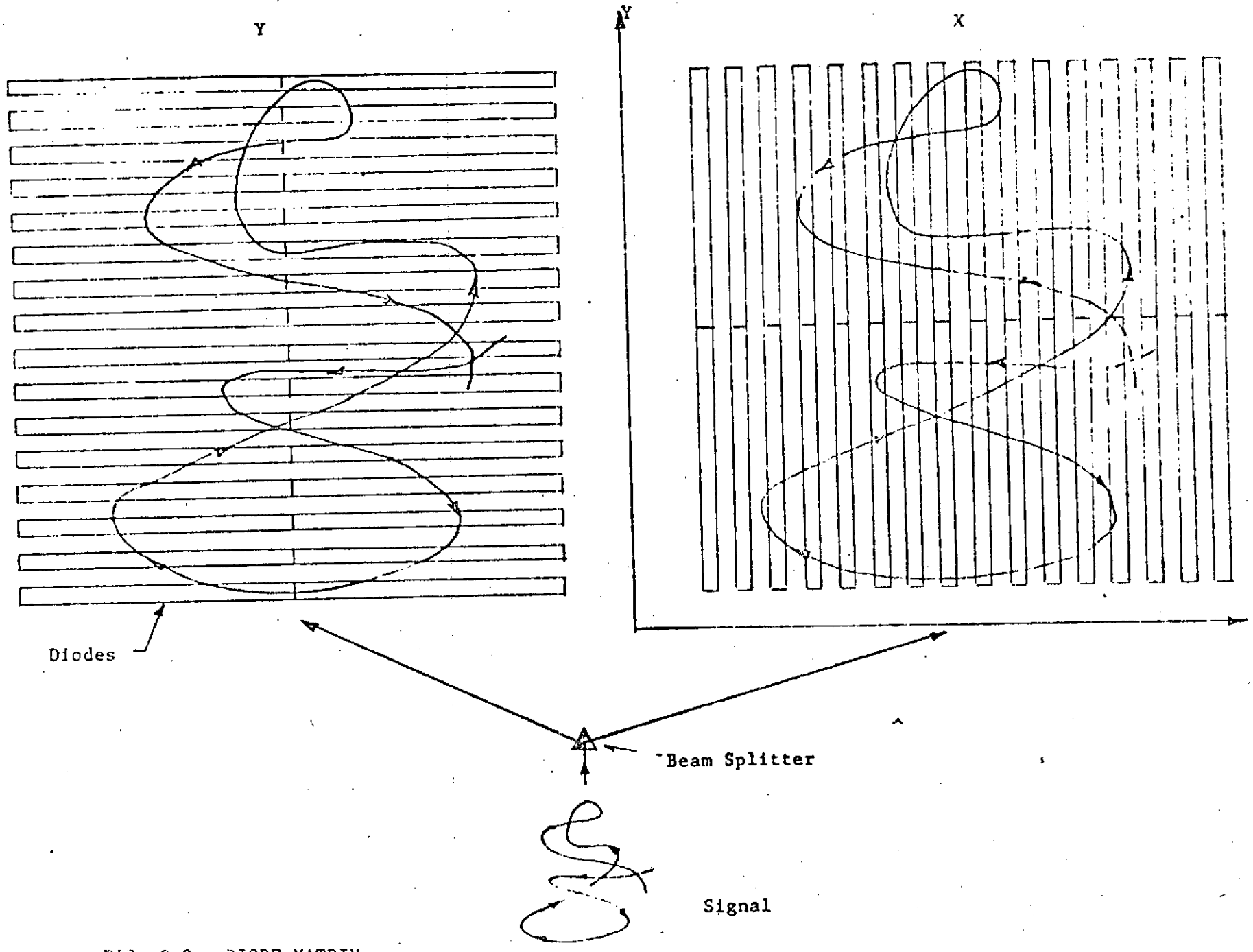

FIG. 2.2 DIODE MATRIX

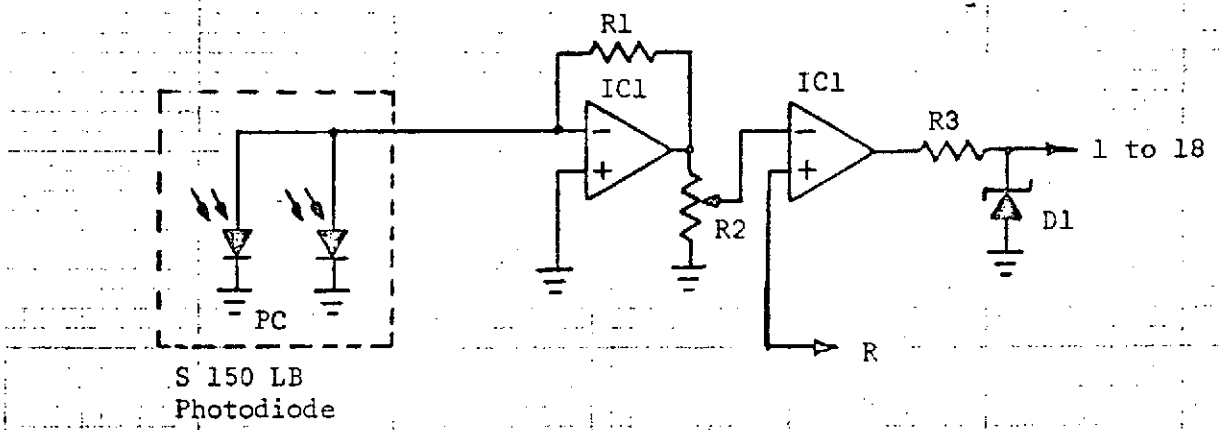

FIG. 2.3 DIODE AMPLIFIER

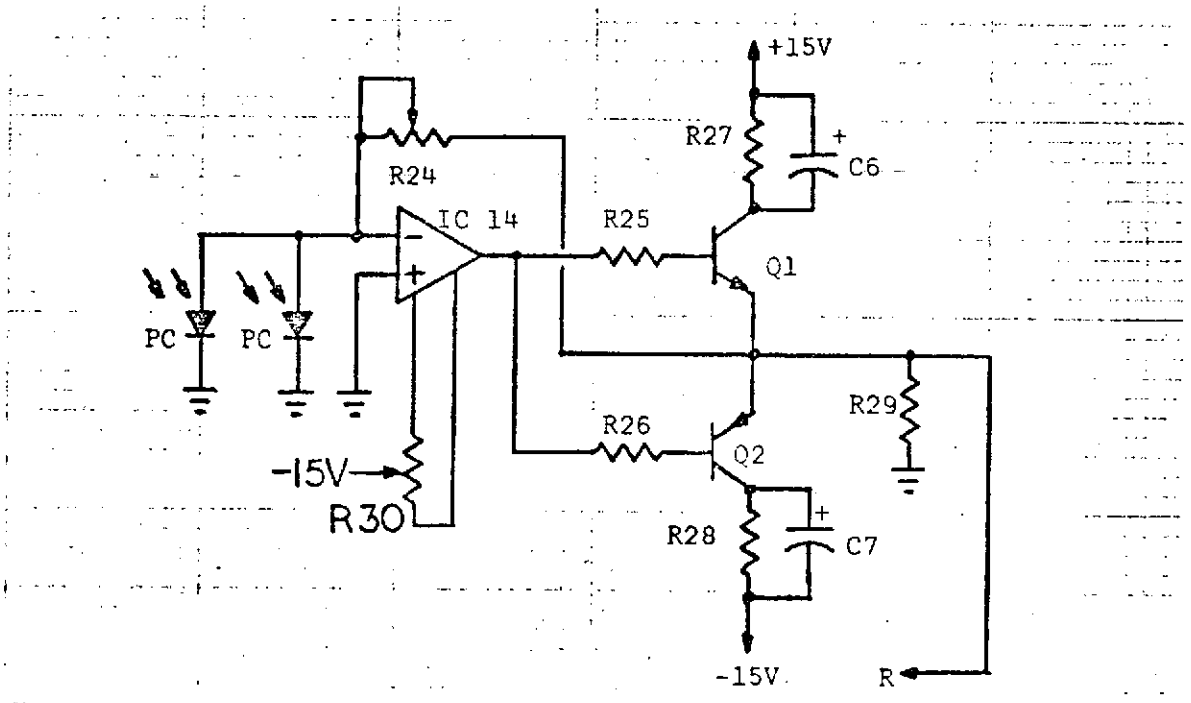

FIG. 2.4 REFERENCE VOLTAGE CIRCUIT

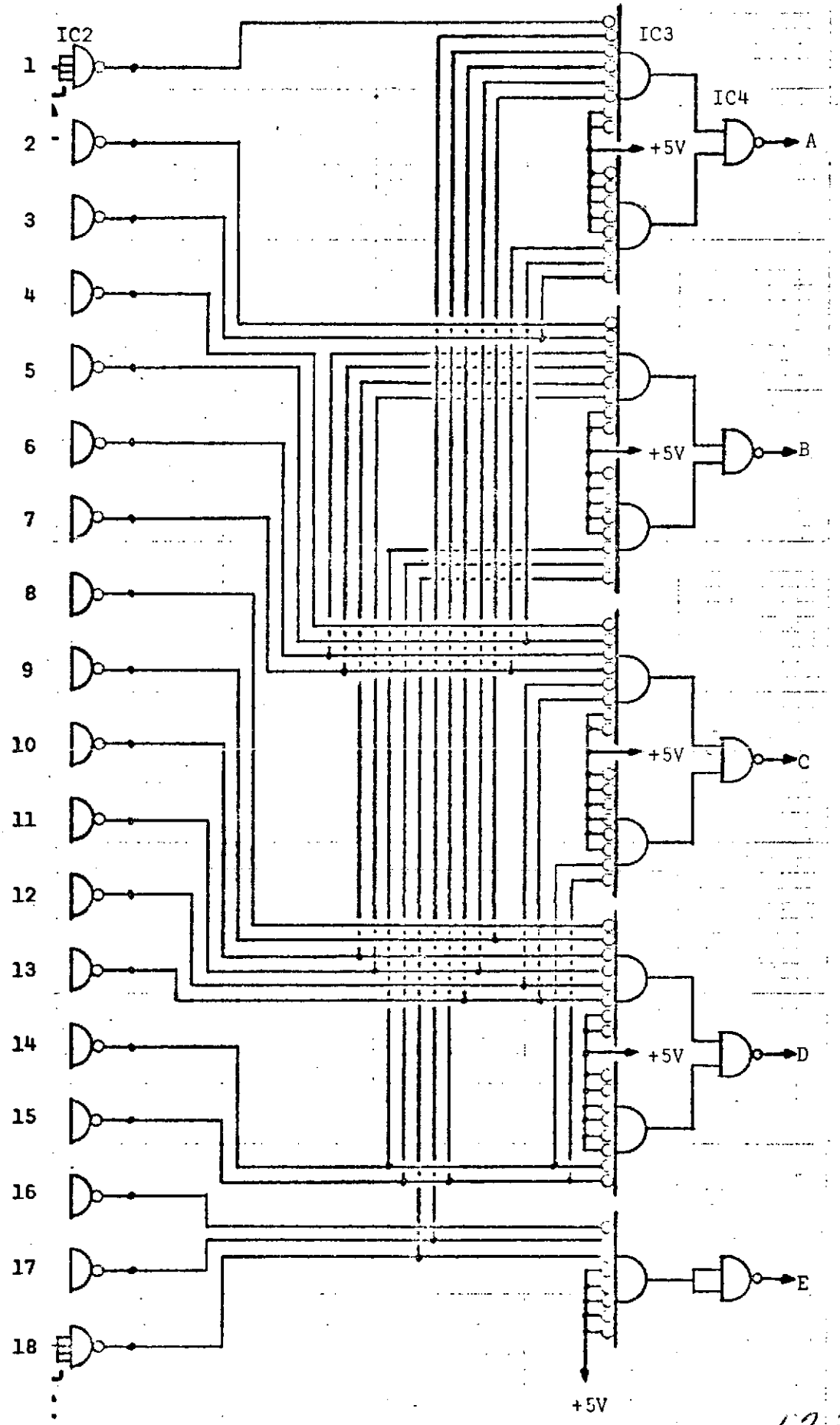

123

FIG. 2.5 18 INPUT TO 5 BIT BINARY CONVERTER

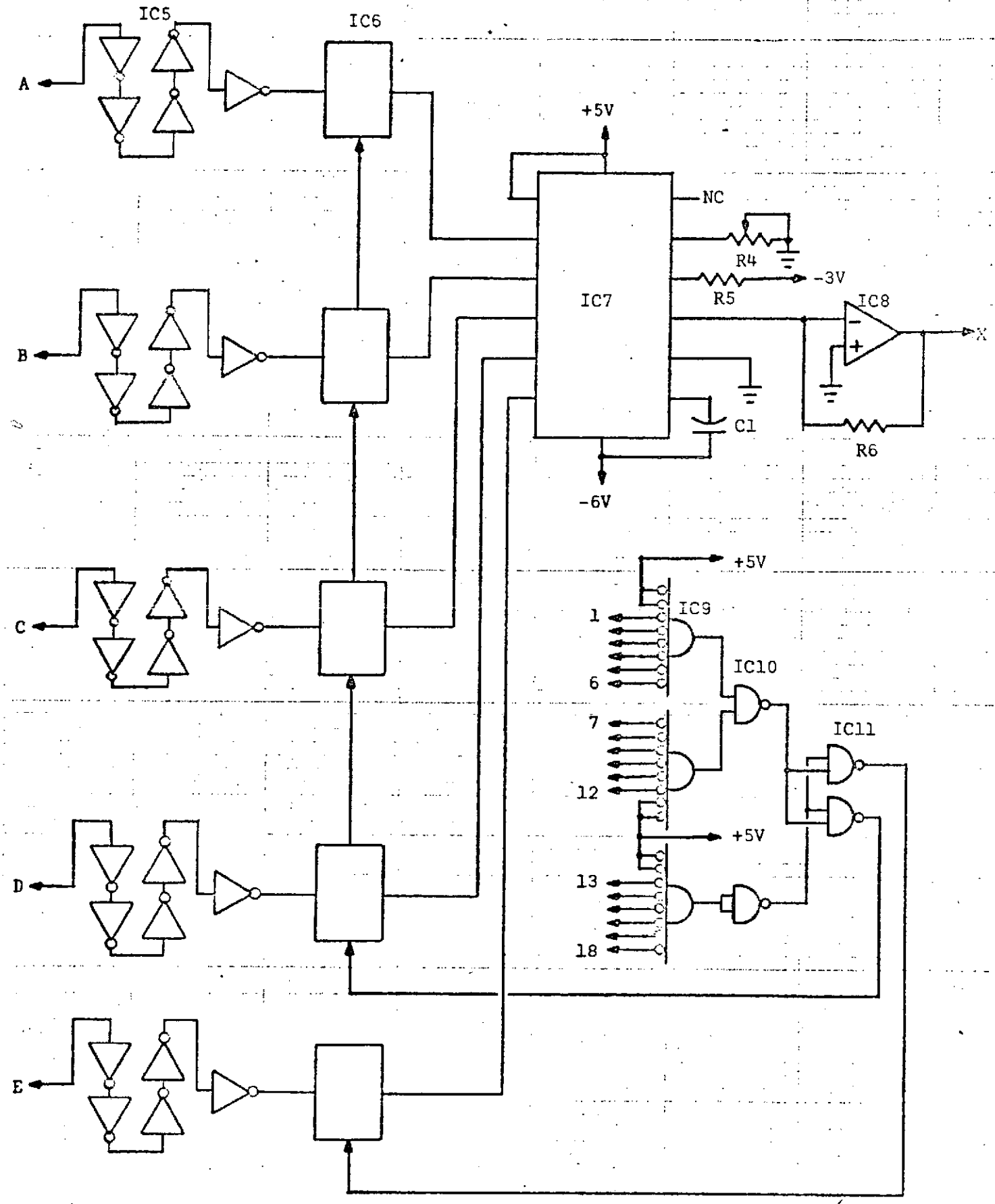

FIG. 2.6 5 BIT BINARY TO ANALOG CONVERTER

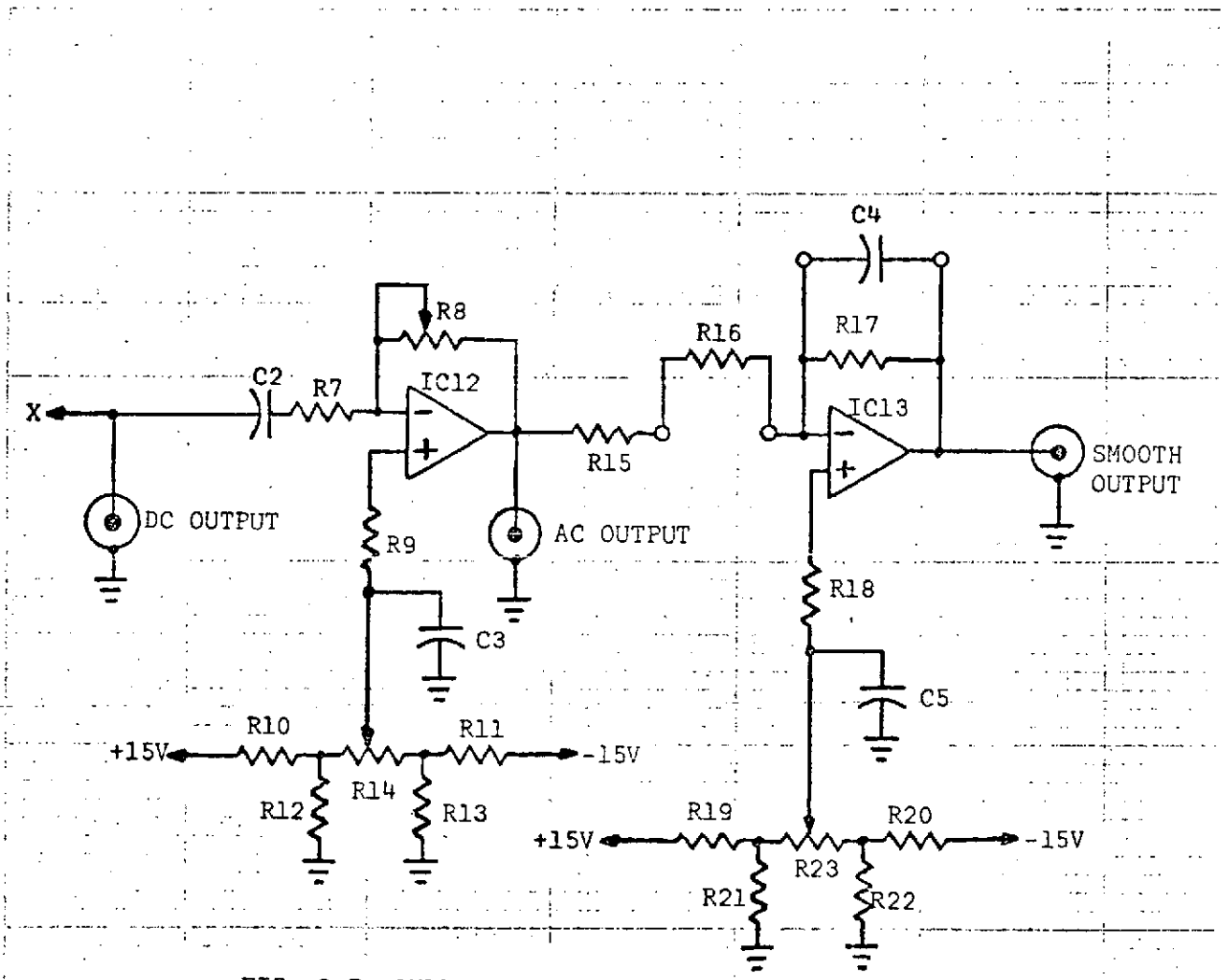

FIG. 2.7 OUTPUT AMPLIFICATION

FIG. 2.8 PRINTED CIRCUIT BOARD TEMPLATE

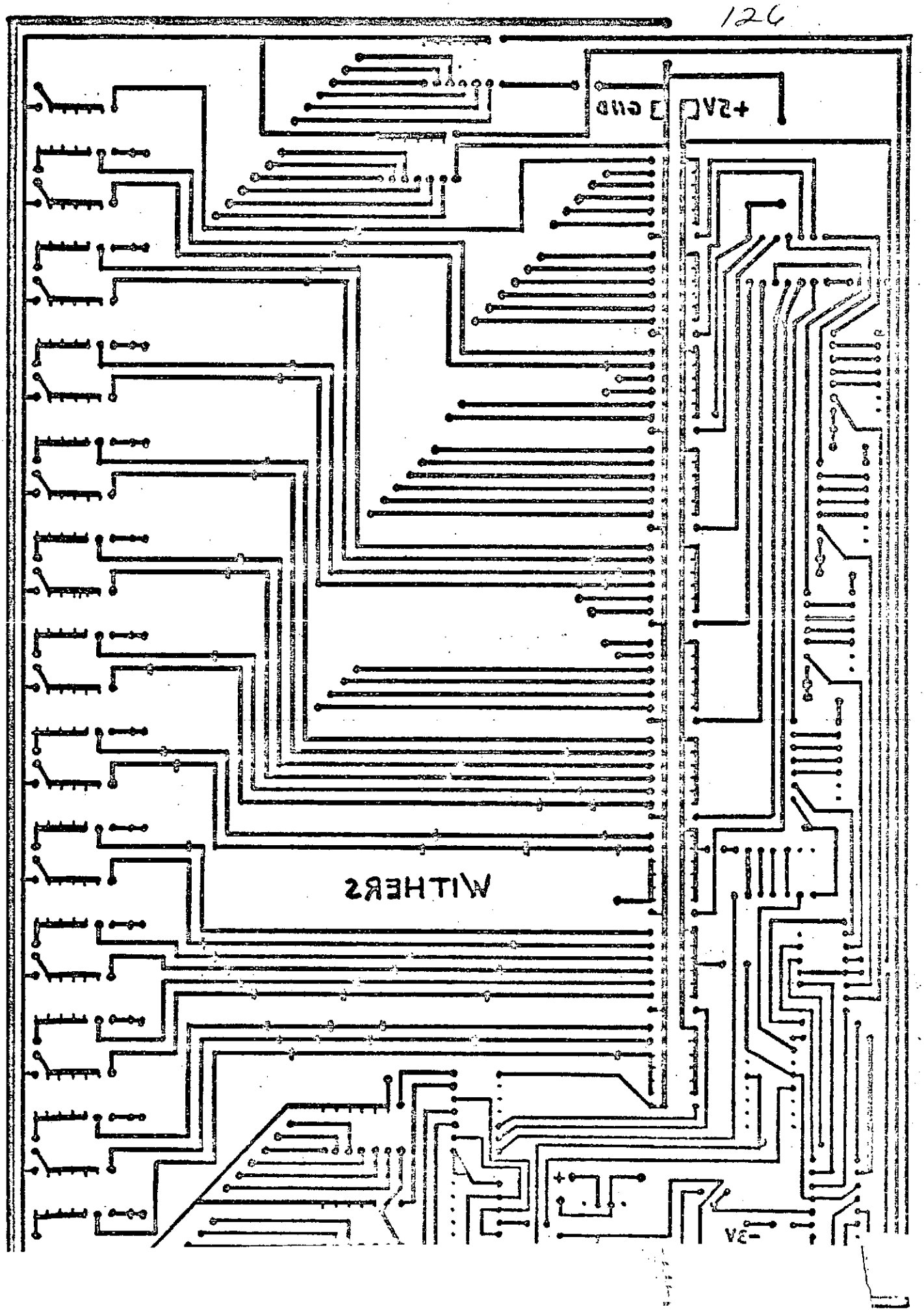

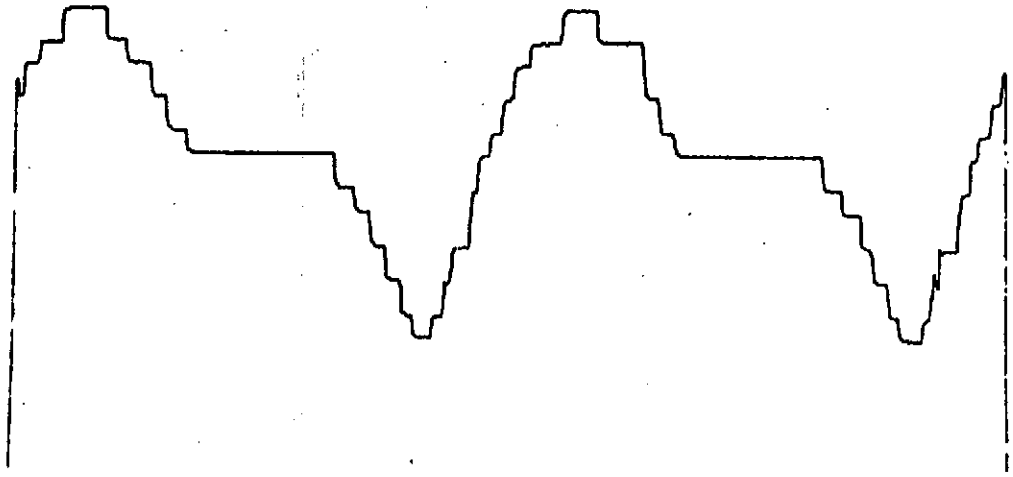

(A) Wave slope from the optical system

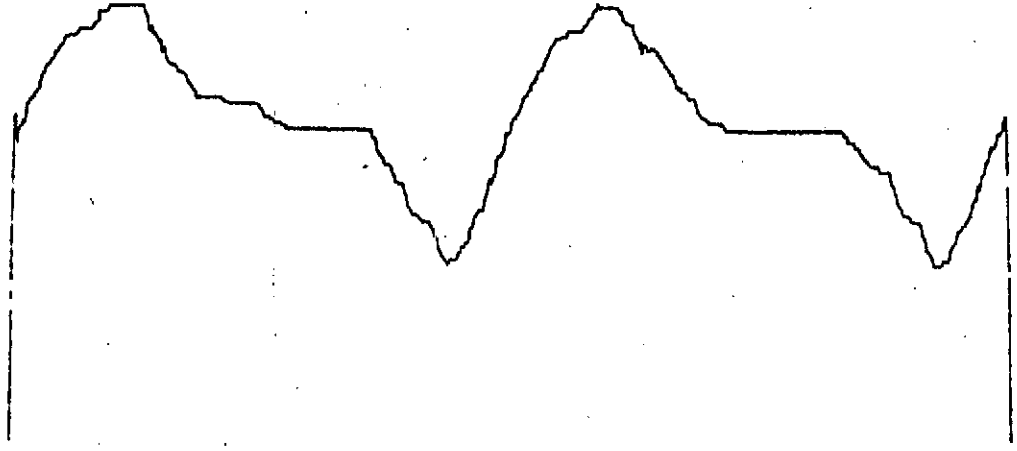

(B) Smoothed wave slope from the optical system

Fig. 2.9 Wave slope from the optical measuring system (vertical scales are not identical).

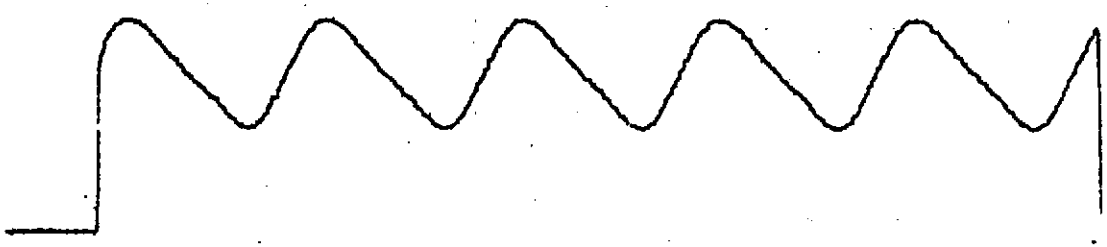

(A) Wave Height - measured by a capacitative probe

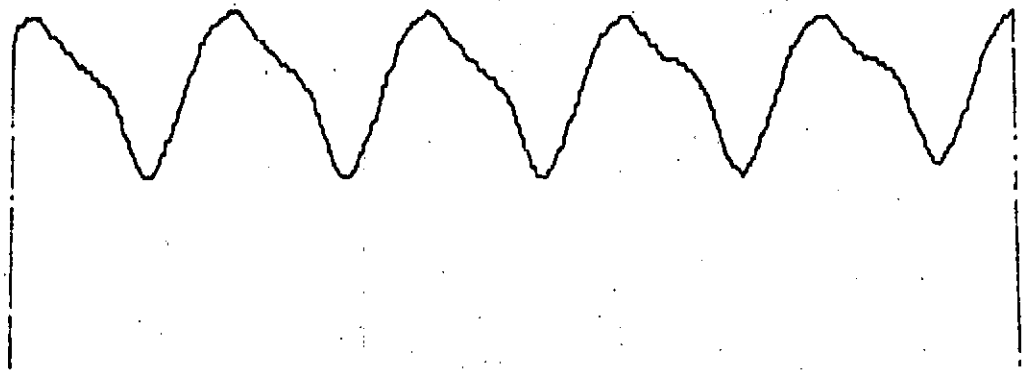

(B) Wave Height - by integrating wave slope

Fig. 2.10 Wave height as measured by a wave height probe and by the optical system (vertical scales are not identical).

3. Wave Decay Studies

3.1 Introduction

The investigation of capillary wave decay or attentuation rates on mean water currents has been nearly completed. Special attention was given to two separate conditions (1) when a constant mean water current is present and theoretical analysis predicts no energy transfer between the wave motion and the current, *i.e.*, there is no wave current interaction; and (2) when there is wave motion with a spatially varying current and wave-current interaction is expected from theoretical considerations (Phillips, 1966). Generally one expects an exponential decay of wave energy, and simple tests of wave decay confirm this. However, with capillary waves the presence of any film on the surface may contaminate the surface and although the decay is still exponential it may be greatly different than that predicted for clean surfaces. McGoldrick (1970) as well as Davies and Vose (1965) have reported results on this effect.

Because the effect of surface films can alter the results the present work includes extensive tests for the presence of surface films. This work indicates when these films can be expected, the effect of the surface film on wave damping, and how surface films can be avoided in laboratory experiments.

Another phenomena occurs in laboratory wave experiments, which is the occurrence of cross waves or waves that propagate perpendicular to the direction of the longitudinal wave under study. These waves are experienced in many wave studies when no currents are present and Mahony *et al.* (1972) have reported results from extensive cross wave experiments. The present study has also experienced cross waves under most conditions. Moreover the appearance and subsequent behavior of these cross waves is

not that expected, observed or predicted by previous work for waves motion when no current is present. The preliminary test results indicate that (1) cross wave current interaction can occur even when there is no energy transfer from the current to the longitudinal wave; and (2) the presence of a current can generate cross waves as the longitudinal wave decays. Both of these results have important applications in physical oceanography. The latter is especially important, because it indicates that a current can break up a regular longitudinal wave train into random motion even when there is no energy transfer from the current to the longitudinal wave train.

The importance of both film damping and cross waves in wave decay studies with application to physical oceanography has caused both to be investigated in detail. The results of these investigations are reported here.

3.2 Studies of the Effect of Surface Films

Numerous investigators have studied the problem of wave damping by viscosity and/or surface films. A recent example of this work is contained in a paper by Davies and Vose (1965) who measured the damping of capillary waves on both clean surfaces and those with controlled amounts of contaminations. In the absence of a surface film (clean surface), Davies and Vose observed that the damping of waves resulting from viscous energy dissipation in the bulk of the fluid could be accurately predicted by the relationship (one-dimensional)

$$E = E_o \exp\left[(-4\nu k^2/c_g)\, x\right] \tag{3.1}$$

where ν is the kinematic viscosity, k the wave-number, and c_g the wave

group velocity. This result is well known and can be obtained directly from a first order (linear) wave analysis (*e.g.*, Phillips, 1969). The wave energy E, also calculated from the linear analysis, is given by

$$E = \frac{\rho\sigma^2 a^2}{2k} \tag{3.2}$$

where ρ is the fluid density, a the wave amplitude (sinusoidal wave), and σ the radian frequency. In deep water ($d_w > \lambda/2$) σ can be expressed in terms of k by the relationship $\sigma^2 = gk + \gamma k^3$, where g is the acceleration of gravity and γ the kinematic surface tension. With this equation (3.2) can be rewritten in a more useful form

$$E = \frac{\rho(ak)^2\gamma}{2}\left(1 + \frac{g}{\gamma k^2}\right) = \frac{\rho(ak)^2\gamma}{2}\left(1+\beta\right) \tag{3.3}$$

where $\beta = g/\gamma k^2$ is dimensionless. The term ak is the maximum slope of the wave $\zeta = a \sin(kx - \sigma t)$, *i.e.*, $ak = (d\zeta/dx)_{max}$; furthermore it follows that $(ak)^2/2$ is equivalent to $[(d\zeta/dx)_{rms})]^2$ where rms is a root-mean square average of the wave slope. For short water waves ($\lambda < 1.7$ cm) β is less than one and in the limit as $\lambda \to 0$, $B \to 0$. For short capillary waves (in these experiments) $\lambda < 1$ cm and $\beta < 0.345$ equation (3.3) can be approximated by

$$E \doteq \rho\gamma \left(\frac{d\zeta}{dx}\right)^2_{rms} , \tag{3.4}$$

allowing equation (3.1) to be written as

$$E = \rho\gamma \left(\frac{d\zeta}{dx}\right)^2_{0\,rms} \exp\left[(-4\nu\, k^2/c_g)\, x\right] , \tag{3.5}$$

which implies

$$\left(\frac{d\zeta}{dx}\right)_{rms} = \left(\frac{d\zeta}{dx}\right)_{0^{rms}} \exp\left[\left(-2\nu\, k^2/c_g\right) x\right]. \tag{3.6}$$

Thus, for short capillary waves, one would expect to observe a wave with initial slope $(d\zeta/dx)_0$ decay at a rate given by

$$\Delta_v = \frac{2\nu\, k^2}{c_g} \quad , \tag{3.7}$$

which is the viscous attenuation coefficient. In view of this, a number of capillary wave decay studies were performed on tap water. Special care was taken to minimize the long term growth of a surface film (whose existence would invalidate the preceeding analysis). This was accomplished by a constant skimming process whereby water added to the bulk of the fluid was removed from the surface by a slightly submerged sharp-rimmed standpipe. The rate of surface runoff was maintained at approximately 10 cc/min.

In each instance the experimentally measured decay was exponential with a logarithmic decrement (attenuation coefficient) Δ_v as given by equation (3.7). The logarithmic decrement is defined as the natural logarithmic ratio of any two successive wave amplitudes (slopes) divided by the wave length $\Delta = \ell n(a_i/a_{i+1})/\lambda$ or simply $\Delta = \ell n(2)/d_2$ where d_2 is the distance required for the wave amplitude (slope) to decay to one-half the original amplitude (slope). The results of one of these decay trials are presented in Table 3.1 and Figure 3.1.

Table 3.1 Summary of wave conditions for decay data presented in Figure 3.1

Measured	Calculated
$T = 23^{\circ}$ C	$R_{\omega} = 321.59$
$\gamma = 71.29$ cm^3/sec^2	$\Delta_v = 0.0383$
$\lambda = 0.733$ cm	$d_2 = 18.1$ cm
$\tau = 28.21$ ms	$\Delta_f/\Delta_v = 3.17$
$c = 25.98$ cm/s	$c = 26.91$ cm/s
$\Delta = 0.0378$ cm^{-1}	$c_g = 36.11$ cm/s

Although the surface of the wave tank was constantly skimmed during all wave decay experiments, the possiblity of a surface film existed. A practical upper bound on film damping, which has been confirmed by experiment (McGoldrick, 1970), is that due to a rigid (inextensible or close packed) film acting in conjunction with viscous decay. The logarithmic decrement for this film is given by $\Delta_f = (\sigma\nu k^2/8)^{1/2}/c_g$ or a factor $2^{-5/2}\, R_w^{1/2}$ larger than Δ_v due to viscous dissipation alone. For all waves with $R_w > 32$, *i.e.*, capillary waves with $\lambda > 0.2$ mm and $\sigma < 10^5$, Δ_f is greater than Δ_v. For these experiments the Reynolds number R_w varies between 200 and 350 which implies $2.5 < \Delta_f/\Delta_v < 3.5$; thus the total decrement Δ_T would be $3.5\ \Delta_v < \Delta_T < 4.5\ \Delta_v$. McGoldrick (1970) experimentally obtained for unskimmed tap water a total decrement of $\Delta_T = 5.77\ \Delta_v$ for a wave Reynolds number $R_w = 450$, which is approximately what one would obtain from rigid film attenuation combined with viscous dissipation at this Reynolds number.

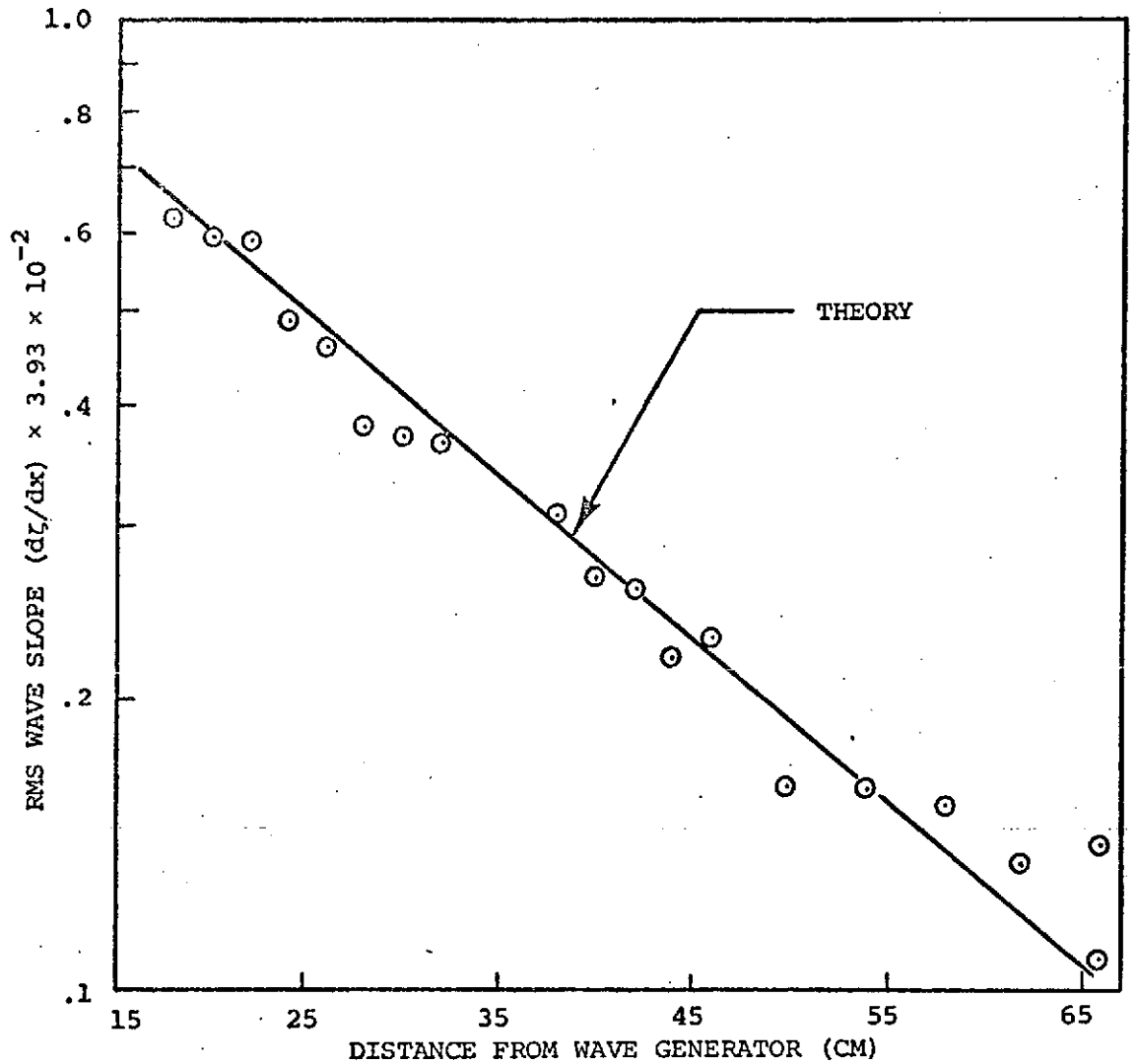

Figure 3.1 The measured decay of capillary waves on a static surface (U = 0) (the solid line is the theoretical prediction)

These calculations demonstrate that film damping, if present, should be easily observed experimentally in the form of increased damping. The data, however, show no such effect since within the experimental error (less than $\pm$ 10 percent) the measured decay rate was accurately predicted by viscous dissipation alone. Therefore, in view of the precautions taken to maintain a clean surface, *i.e.*, constant skimming, and no support in the decay data for increased damping, it was concluded that little or no surface film was present.

3.3 Data Acquisition Techniques

The data for these and all following experiments were obtained as follows. The wave slope was measured as described with our optical system. Changes in wave slope resulting from small variations in wave amplitude were minimized by averaging over several periods ($n > 10$) with a true rms voltmeter (DISA 55D35); wave maker period (τ) was measured by a digital counter (General Radio 1911) and static surface tension (T') by a du Noüy tensiometer. Wavelength was measured by comparing the phase of the water wave to that of the function generator (Wavetek 134) as viewed on a dual trace cathode ray oscilliscope (Tektronics 7704). The position of the incident light beam was set at a distance from the wave plunger where the phase of the measured water wave was judged by eye to be the same as that of the function generator. The light beam was then translated a total of five wavelengths (5λ) and the average value obtained was chosen as the actual wavelength. This averaging technique was needed because of the difficulty in determining when exactly 2π radians of phase shift had occurred; in other words, if the error in determining the endpoints of the phase comparison is spread

over several wavelengths, a more accurate measure of λ can be obtained. This averaging process was justified on the grounds that any small variation in λ over five wavelengths, as a result of a possible change in phase velocity, would be insignificant compared to an error in phase measurement, even though the measure of one wavelength might appear more desirable. The experimental phase velocity c was simply calculated from $c = \lambda/\tau$ and Δ the logarithmic decrement, measured from the slope of the experimental decay data when plotted on a semi-log scale.

The relationship between radian wave frequency $\sigma = 2\pi f$ and the radian wave-number $k = 2\pi/\tau$ for waves in deep water can be expressed as

$$\sigma^2 = gk + \gamma k^3 \tag{3.8}$$

Since the phase velocity is related to the frequency and wave number by $c = \sigma/k$, equation (3.8) gives the phase velocity as

$$c^2 = g/k + \gamma k \tag{3.9}$$

In addition to the phase velocity c, it is convenient at this point to compute the group $c_g = \frac{d\sigma}{dk}$. Thus the group velocity is

$$c_g = \frac{g + 3\gamma^2}{2} [gk + \gamma k^3]^{-1/2} \tag{3.10}$$

The calculated values of phase and group velocity (c and c_g, respectively) were obtained from equations (3.8) and (3.9) using the static experimental value of surface tension; the wave Reynolds number $R_w = (\frac{\sigma}{\nu k^2})$ was calculated from the measured wavelength and frequency ($\sigma = 2\pi/\tau$) and the tabulated value for viscosity at the measured temperature.

3.4 Capillary Waves on Constant Currents

Following these experiments a study of capillary wave dissipation on a constant current was undertaken. Modifications to the system required the addition of a recirculating pump and a section of the test channel with a reduced area 20 cm wide by 2 to 4 cm deep in order that current velocities as great as 30 cm/s could be obtained from moderate flow rates ($Q \leq 2$ L/s). The water current velocity was measured with a hot-film anemometer probe (developed by us) powered by a constant-temperature anemometer bridge (DISA 55D01). Within the resolution of the anemometer ($\pm$ 0.5 cm/s), the velocity profile in the reduced area test section was uniform. The usual mechanical wave maker was replaced by a pulsed air wave maker which produced waves without physically contacting the water surface. This device consisted simply of a narrow slit 2 mm wide and 20 cm long through which air pulses, generated by a large permanent-magnet loudspeaker, could be directed at the water surface. This change was necessary because a mechanical plunger stagnated the surface flow and generated a train of ripples, fixed on the oncoming stream, which interfered with the capillary waves under study.

With the modifications described above, wave decay measurements with constant velocity currents directed against the direction of wave propagation were carried out. In a majority of these trials, however, increased cross-wave content, which became more severe as one moved away from the wave generator, was observed. In addition, the ratio of cross-wave slope to progressive wave slope at any fixed point remained nearly constant over a wide range of wave generator amplitudes. This feature is not observed in wave decay studies on a static tank where a neutral

stability effect was observed. That is, there exists a wave generator amplitude which would not spontaneously generate cross-waves but would sustain (and amplify) externally introduced cross mode distrubances. Below this critical (and frequency dependent) amplitude cross-waves cannot be maintained, while above it cross-waves are always present. The existence of these points of neutral stability has been observed by other investigators and several theoretical and experimental papers have been written about cross-waves.

One of the most comprehensive studies to date is presented in a two-part paper by Mahony *et al.* (1972). Mahony surveyed previous theories and proposed that there are two modes of cross-wave generation one near and another more distant from the wave generator, while Barnard and Pritchard conducted experiments with cross-waves generated by a mechanical (flap type) wave generator on a still (zero current) surface. These experiments document a number of characteristics of cross-waves, including neutral stabilities and growth and decay rates. From this experimentalist's viewpoint, probably the most disturbing feature of cross-waves as reported by these investigators is that cross-waves are not stationary in either time or space. Rather they grow and decay at slow rates with time constants on the order of 75 seconds when the wave generator is producing longitudinal waves with a fundamental frequency on the order of 5 Hz.

When a mean current was present, no condition of neutral stability was observed. It was first hypothesized that the pulsed air or pneumatic wave generator was the source of this increased cross-wave content. This hypothesis was tested experimentally by measuring the cross-wave content (in two separate trials) of two identical trains of capillary waves (τ = 35.90 ms, λ = 0.928 cm) on still water, one generated by the mechanical

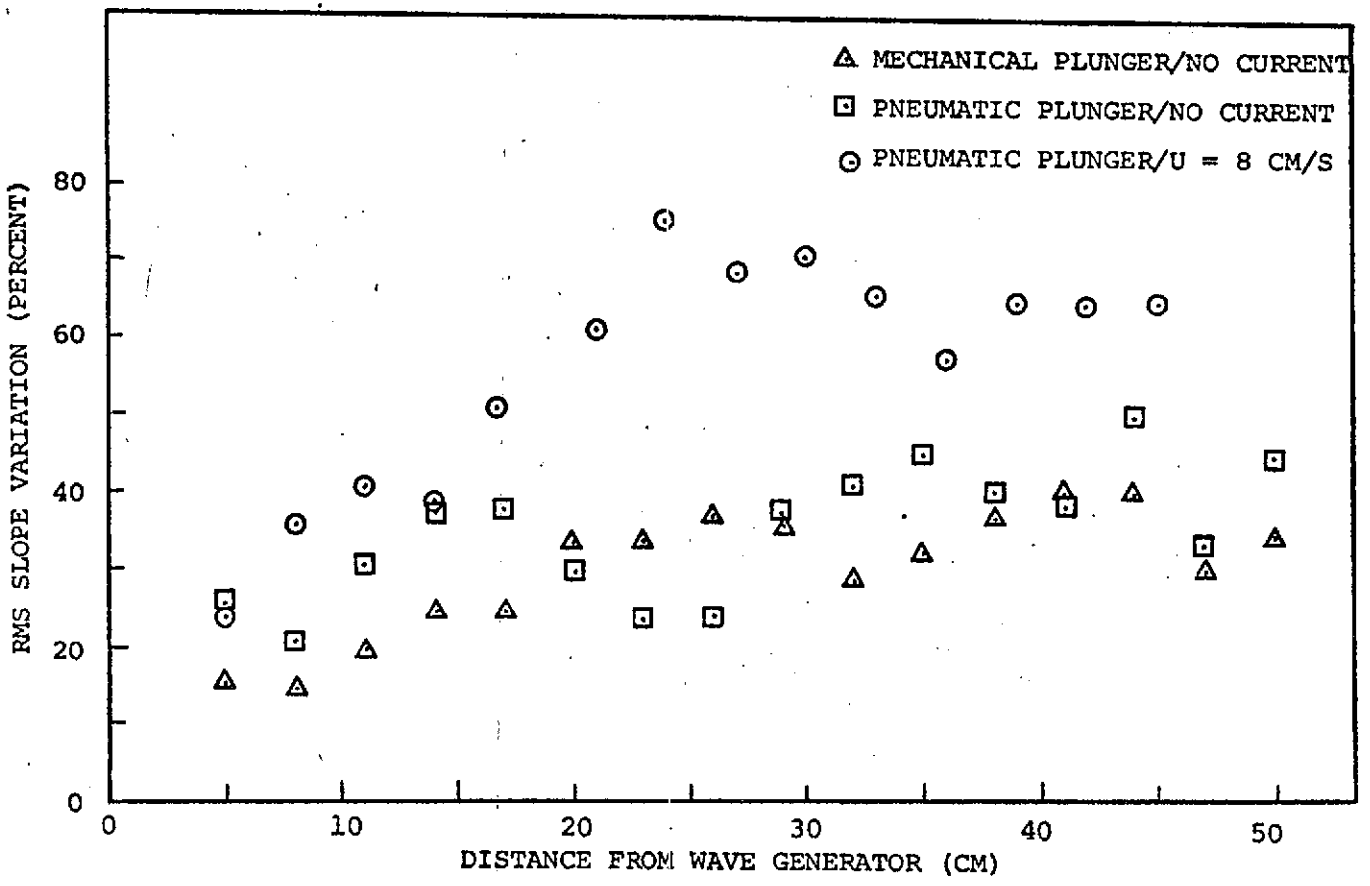

Figure 3.2 Growth of cross-mode wave content with respect to distance from the wave source

plunger and the other by the pneumatic generator. The amplitude of each generator was adjusted to give the same rms slope at a distance of 5 cm from the plunger and the variation in rms slope of the longitudinal wave was measured in the transverse direction (parallel to the wavefront) as a function of position from the wave generator. The results of these measurements, with the maximum transverse variation in wave slope expressed as a percent of the total wave slope, are presented in Figure 3.2. Initially the mechanical generator exhibits a lower percentage of slope variation in the transverse direction; however, after about 10 cm the percentage of cross modes from either of the generators is essentially the same with an equilibrium value between 30 and 40 percent. It is concluded, therefore, that the cross mode content initiated by either of the two generators is comparable, and that the increased cross mode wave content observed when a mean current is present cannot simply be attributed to the pneumatic wave generator. Rather it appears as if the current contributes to the growth of cross modes by some mechanism which is not presently understood. Figure 3.2 also presents a plot of the growth of cross modes when a current of -8 cm/s is present. The initial growth rate is nearly linear with distance with a final equilibrium value approximately double that observed on a static surface.

3.5 Wave Decay Measurements on a Constant Current

The apparent rate of wave decay is related to the cross mode content. When this content was low, the measured decay rate was that predicted by viscous dissipation alone. The decay was exponential with a logarithmic decrement $\Delta_v = 2\nu k^2/c_g$ based on the actual (local) wave-number (*cf.*, Section 3.5) and group velocity. A typical plot of one such run is

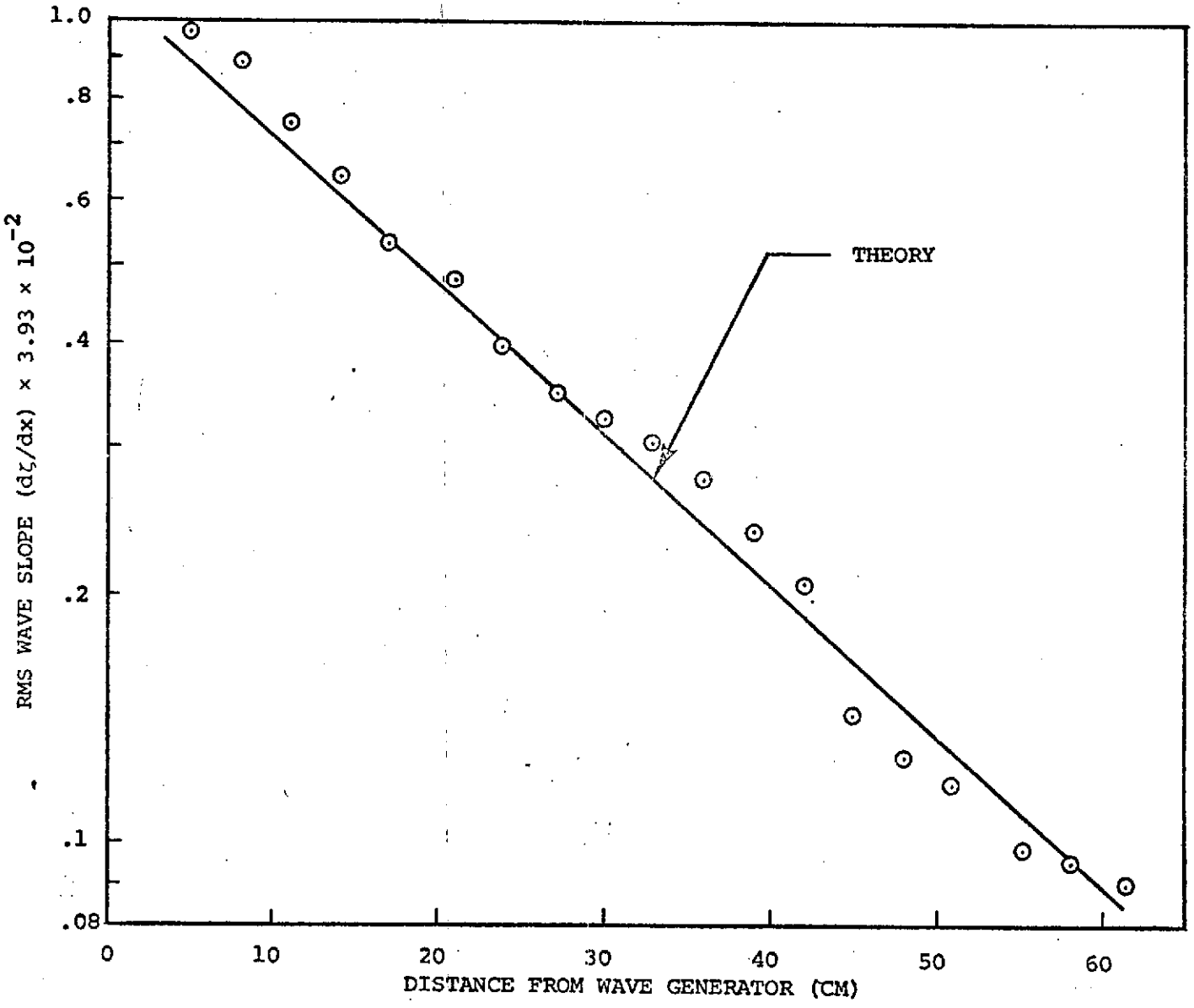

Figure 3.3 The measured decay of capillary waves on a current of -11.5 cm/s (cross-mode wave content is low)

presented in Figure 3.3 with accompanying Table 3.2. For the given conditions one concludes that film damping is not present by arguments previously outlined; *i.e.*, predicted film damping for $R_\omega = 210$ would be on the order of 2.5 times as great and the data do not support this fact. When cross mode content is high, the apparent decay rate is not exponential throughout. Rather, the decay rate is initially exponential in the vicinity of the wave generator, but about 20 to 30 wavelengths from the wave generator the decay data become erratic with large variations from the initial exponential decay rate (Figures 3.4, 3.5). However, from an observation of the data it appears that a lateral transfer of the progressive wave energy takes place; that is, an increase in energy at one traverse location (at a fixed distance from the wave source) is balanced by a decrease at another.

Table 3.2 Summary of wave conditions for decay data presented in Figure 3.3

Measured	Calculated
$T = 24.5°C$	$R_\omega = 210.6$
$\gamma = 71.3\ cm^3/s^2$	$\Delta_v = 0.041\ cm^{-1}$
$\lambda = 0.986\ cm$	$d_2 = 16.9\ cm$
$\tau = 80.42\ ms$	$\Delta_f/\Delta_v = 2.56$
$c = 12.26\ cm/s$	$c_i = 24.641\ cm/s$
$\Delta_{exp} = 0.0461\ cm^{-1}$	$U = c_i - c = 12.37\ cm/s$
$U = 11.5\ cm/s$	

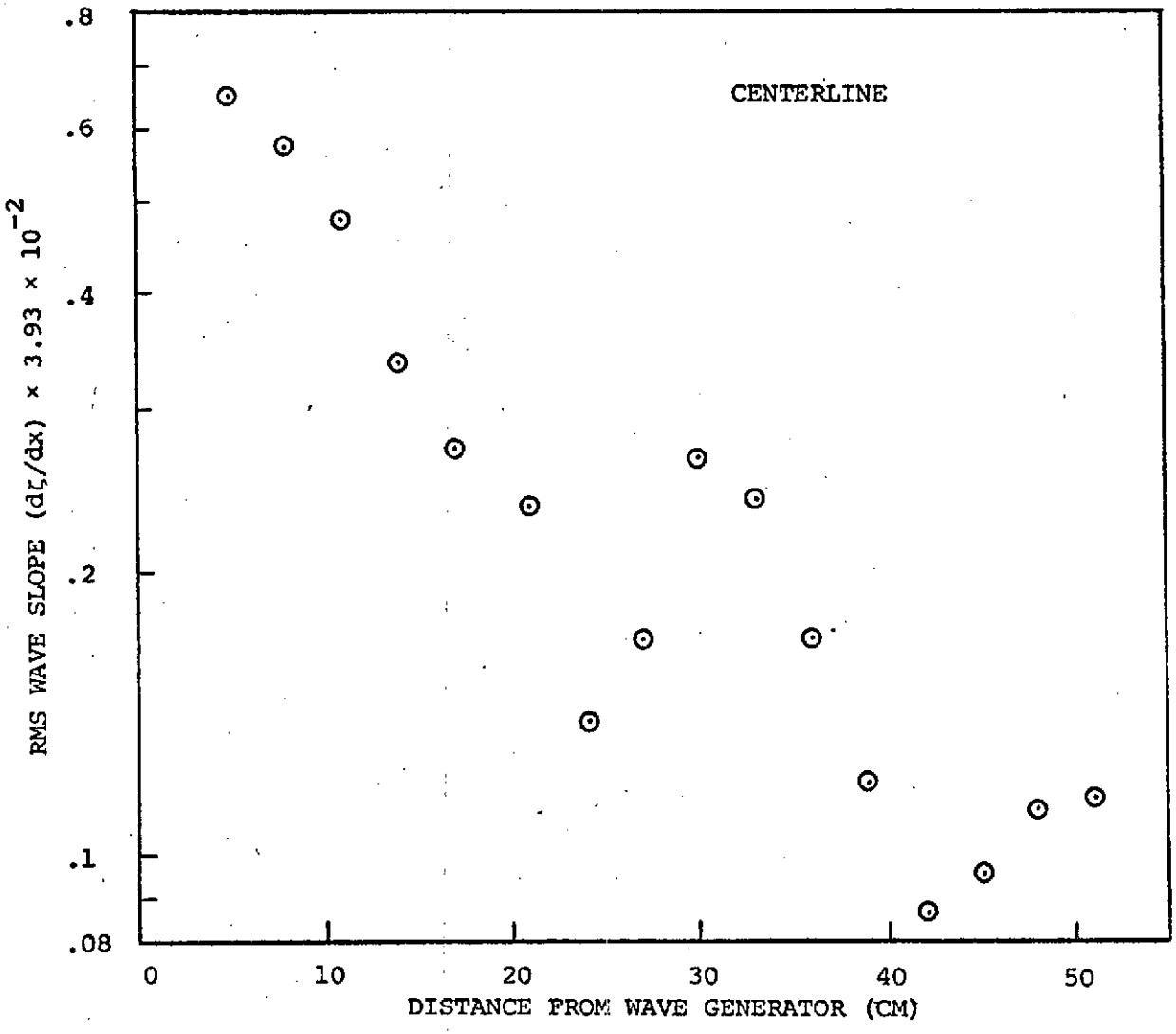

Figure 3.4 The measured decay of capillary waves along the tank centerline with a current of -8 cm/s (high cross-mode content)

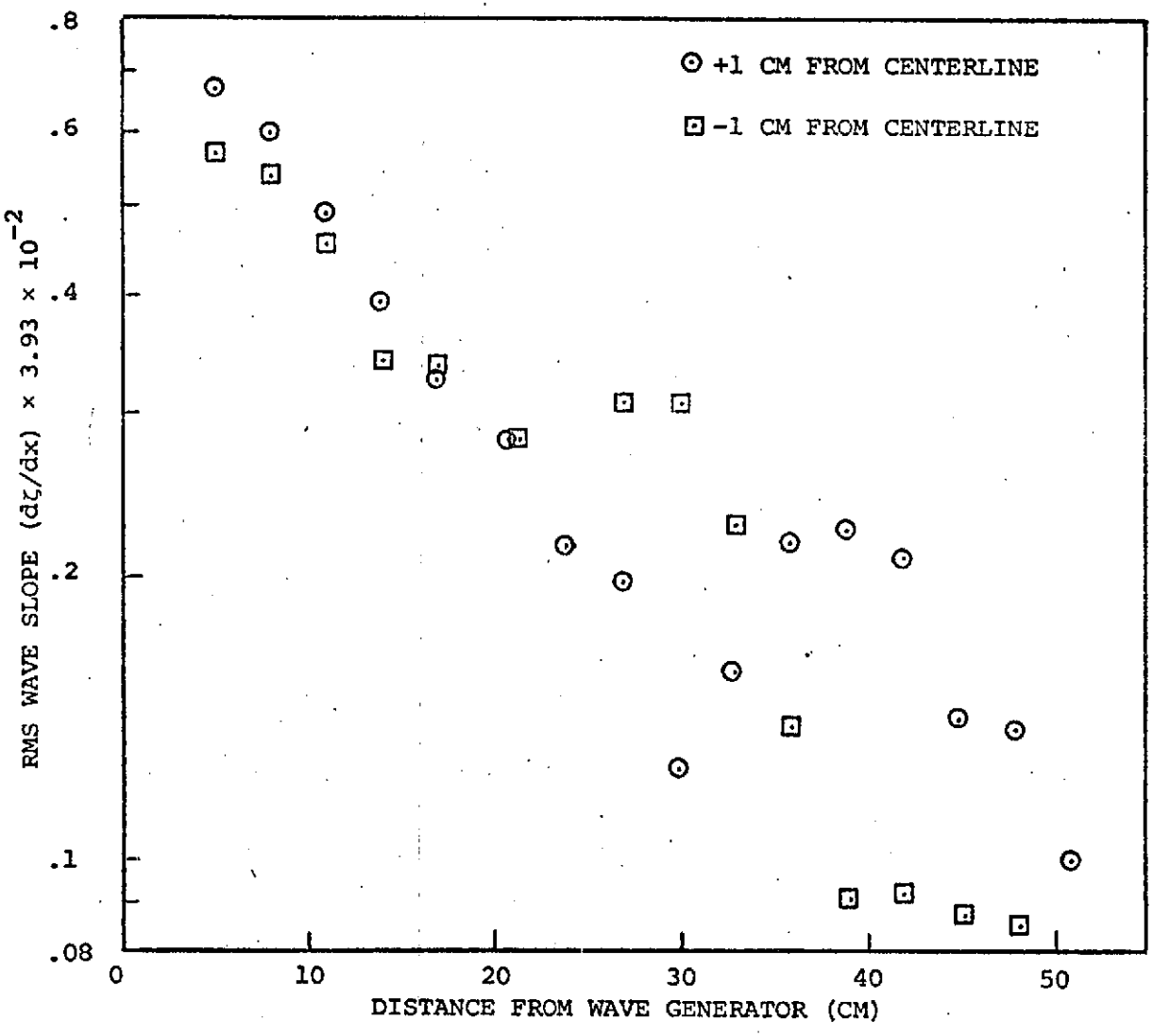

Figure 3.5 The measured decay of capillary waves one centimeter on either side of the tank centerline with a current of -8 cm/s (high cross-mode content)

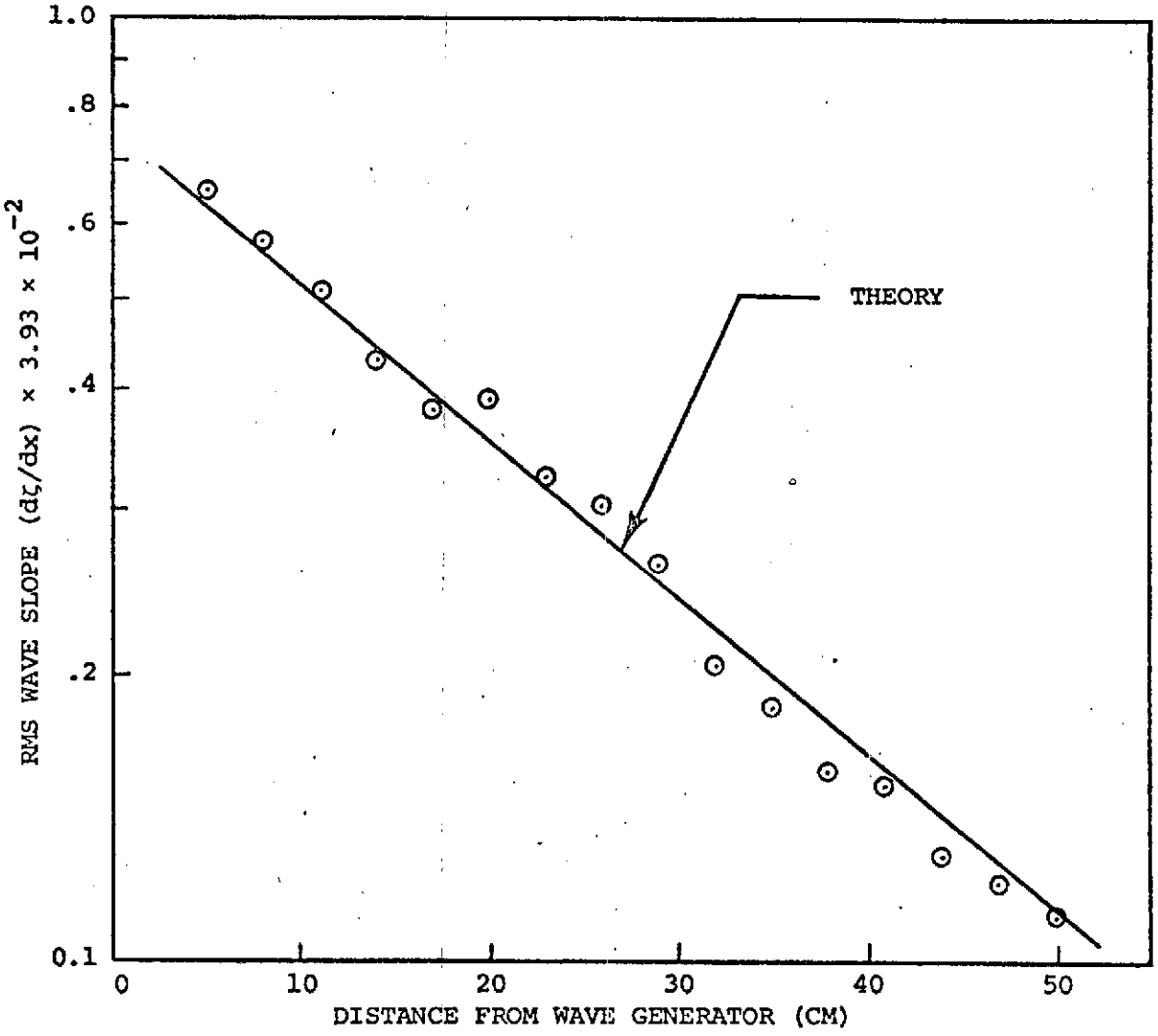

Figure 3.6 Decay of capillary waves on a current of -8 cm/s with high cross-mode wave content (the curve is the result of spatial averaging of seven traverses; Figures 3.4 and 3.5 are part of the set

Consequently, spatial averaging of the decay data in the transverse direction removed the individual peaks and troughs and resulted in a smooth exponential decay. In practice this was accomplished by measuring the wave slope as a function of distance from the wave generator at five or seven transverse locations across the tank. (Usually this was done symmetrically about the centerline). The tabulated values for slope at each position x from the wave generator were then averaged (arithmetic) to obtain the spatial average which was taken as the representative value of slope, and hence energy, at this value x. The results of one such trial are presented in Figures 3.4 and 3.5, which illustrate the peaking described above, and the results of spatial averaging of these data are given in Figure 3.6 and in the accompanying Table 3.3.

Table 3.3 Summary of wave conditions for decay data presented in Figure 3.6

Measured	Calculated
$T = 24°C$	$R_\omega = 264$
$\gamma = 71.4\ cm^3/s^2$	$\Delta_v = 0.0355\ cm^{-1}$
$\lambda = 0.026\ cm$	$d_2 = 19.5\ cm$
$\tau = 54.59\ ms$	$\Delta_f/\Delta_v = 2.87$
$c = 16.96\ cm/s$	$c_i = 25.04\ cm/s$
$\Delta_{exp} = 0.038$	$U = c_i - c = 8.08\ cm/s$
$U = 8\ cm/s$	

As a result one must conclude from these experiments, including the special case where U = 0, the following: (1) in the absence of surface

films the Kelvin dispersion equation (3.9) accurately relates phase velocity (or frequency) to wave-number; and, (2) the attenuation of waves occurs as a result of viscous dissipation as predicted by equation (3.6). In none of the cases, however, was energy transferred either to or from the current into the progressive (longitudinal) waves. However, Figure 3.2 indicates that energy is transferred from the current into the corss-waves or transverse modes.

3.6 Capillary Waves on a Variable Current

From theoretical considerations it has been suggested (Phillips, 1966) that wave energy transfer to or from a mean current, *i.e.*, wave-current interaction, should occur whenever waves propagate through regions where variable currents exist. This means that wave-current interactions depend on current gradients rather than simply the existence of a current. The previous experiments on constant currents support half of this argument, namely, when no current gradient is present no wave-current interaction occurs. To verify the second half of the argument, wave decay studies on a variable current were undertaken. In this section the results of the study are presented.

The measurement of capillary wave decay on a variable current proceeded in a manner indentical to that of the previous constant current experiments with the exception of wavelength measurements. These were obtained indirectly as follows. From equation (3.8) one obtains

$$\sigma_0^2 = (k_0\, c_0)^2 = gk_0 + \gamma k_0^3 \qquad (3.11)$$

where k_0, c_0, and σ_0 are the wave-number, phase velocity, and frequency of waves on a zero current.

From this it follows that

$$k_0 = (r + s)^{1/3} + (s - r)^{1/3} \quad , \tag{3.12}$$

where

$$r^2 = (\sigma^4/T'^2)/4 + (g/T')^3/27,$$

and

$$s = \sigma^2/2T' \quad .$$

The dispersion equation (3.9) can be used with an equation requiring the conservation of waves (*e.g.* Phillips, 1966) which for steady waves on deep water reduces to

$$\sigma_0 = \text{constant} = k_0 c_0 = kc = k(c_i + v) \tag{3.13}$$

These equations (3.9) and (3.13) are then solved simultaneously for wave number resulting in a cubic equation of the form

$$(k_0/k)^3 + a_1(k_0/k)^2 + a_2(k_0/k) + a = 0 \quad ,$$

where the coefficients, a_1, a_2, and a_3 depend only on the known quantities U, c_0, k_0, γ and g are given by

$$a_1 = -\left(\frac{2Uc_0 + g/k_0}{c_0^2}\right) \quad , \quad a_2 = (U/c_0)^2 \quad , \quad a_3 = \gamma k_0/c_0^2 \quad .$$

This equation is solved explicitly for k resulting in an expression of the form

$$k = k\ (k_0,\ c_0,\ U,\ \gamma,\ g) \quad . \tag{3.14}$$

Thus, for each value of current U, one can obtain a corresponding value for k and hence for the wavelength λ.

Figure 3.7 is an experimentally determined plot of the current used in the following wave decay study. By convention, the current is

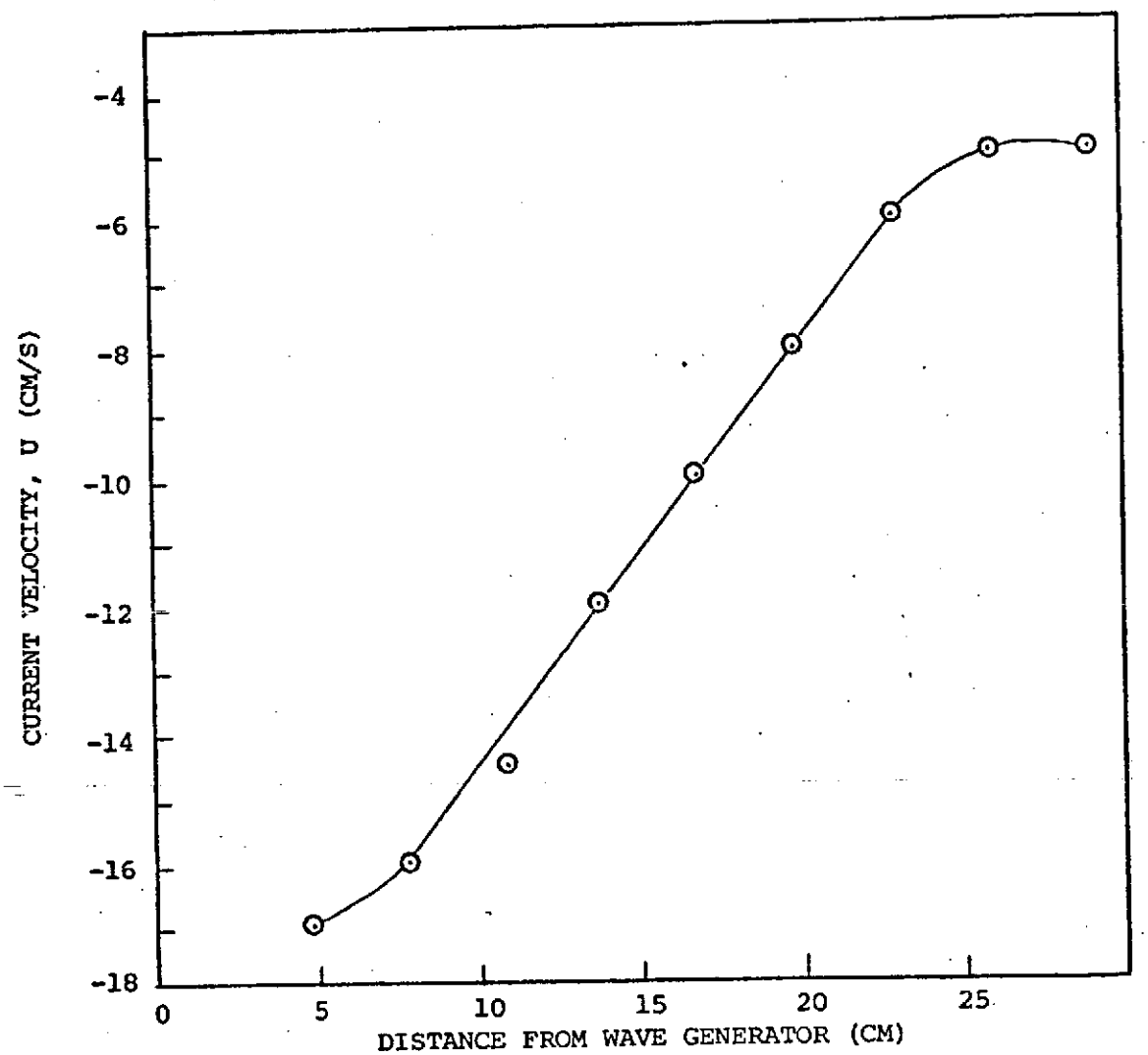

Figure 3.7 Experimentally measured velocity in the variable current test section (data taken with a hot-film anemometer)

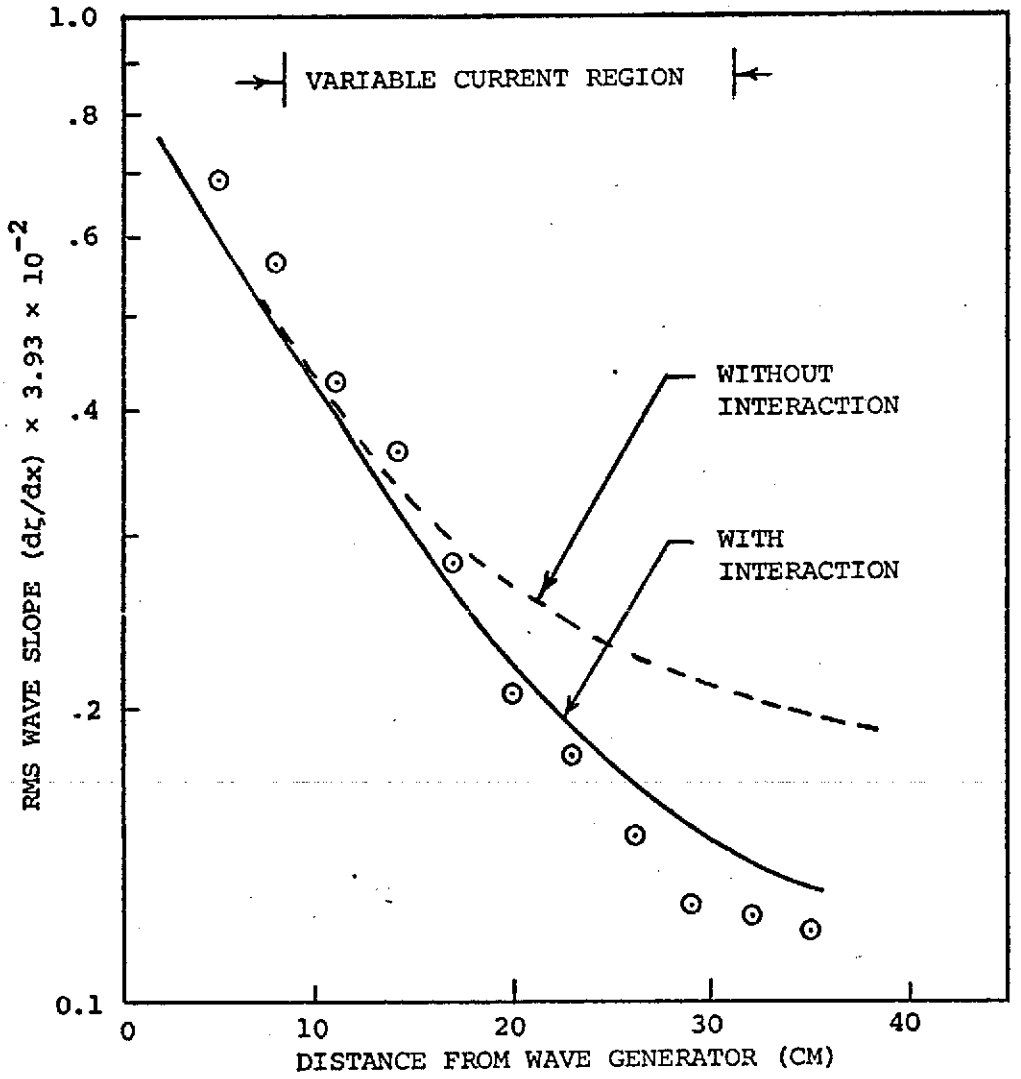

Figure 3.8 Decay of capillary waves on a variable current (*cf.*, Figure 3.7) (spatial averaging was required)

considered negative since it opposes the direction of wave propagation; also, the magnitude decreases linearly as one moves away from the wave generator (located at x = 0).

Waves with a period of 92.99 ms (10.73 Hz) were generated on the -17 cm/s current; the waves propagated through the variable current region and were finally dissipated in the -5 cm/s constant current region. The measured decay of these waves is presented in Figure 3.8.

The data presented are the spatial average of seven traverses of the test section as cross wave content was high due in part to the fast current and relatively short wave period.

The dashed line on Figure 3.8 represents the expected decay from viscous dissipation alone. This was obtained as follows. At each data point the wave-number k was calculated from equation (3.14) and the measured current velocity. This local wave-number was then used to compute the viscous decay decrement Δ_v at each point; the dashed line is the tangent of these local decay rates. It can be seen from the figure that the initial and final decay rates (slope of the dashed line) are tangent to the data. This is consistent with the previous findings for wave decay on constant currents since at either end of the variable current section constant current conditions exist. However, the over-all predicted rate of decay is too slow to explain the decay observed in the variable current region.

An analysis which includes the effect of a variable current on the wave energy is given by Phillips (1969). For a one-dimensional train of waves propagating in the x direction, he shows that the conservation of the fluctuating component of the wave energy can be expressed as

$$\frac{d}{dx}\left[E\,(U + c_g)\right] + S_{xx}\frac{dU}{dx} = -\varepsilon\ , \tag{3.15}$$

where E is the wave energy, U the current velocity, c_g the wave group velocity, S_{xx} the radiation stress in the x direction, and ε the rate of energy dissipation per unit volume due to viscosity. From a linear analysis, he also shows that $\varepsilon = 2\mu\gamma k^2\,(ak)^2 = 4\nu k^2 E$ and $S_{xx} = E\left(\frac{3+\beta}{2(1+\beta)}\right)$ where $\beta = g/\gamma k^2$ (introduced in equation (3.3)) is a dimensionless parameter. For this experiment β reaches a maximum value of 0.98 which implies that the acceleration of gravity is no longer negligible and must be included in the analysis. As a consequence the radiation stress S_{xx} and the group velocity c_g are expanded in a power series with β as an ordering parameter. Neglecting all but the linear terms, one obtains first order perturbation relations for S_{xx} and c_g given by

$$S_{xx} = E\,(3/2 - \beta) \tag{3.16a}$$

and

$$c_g = (3 - \beta/2)\,c/2. \tag{3.16b}$$

Thus equation (3.15) can be written as

$$\frac{d}{dx}\left[E(U + (3/2 - \beta/4)c)\right] + \left[(3/2 - \beta) + 4\nu k^2\right] E = 0\ . \tag{3.17}$$

Equation (3.17) can be put in the form

$$\frac{dE}{dx} + p(x)\,E = 0\ , \tag{3.18}$$

where

$$p(x) = \left[(5/2 - \beta)\frac{dU}{dx} + (3/2 - \beta/4)\frac{dc}{dx} + 4\nu k^2\right]/\left[U + (3/2 - \beta/4)c\right]\ . \tag{3.19}$$

Equation (3.18) has the general solution

$$E = E_0 \exp\left(-\int_0^x p(\omega)\, d\omega\right) , \qquad (3.20)$$

where E_0 is the wave energy at $x = 0$ and $p(x)$ represents a generalized decay coefficient for capillary waves on a current. It can be readily seen from equation (3.19) that when the current is constant dU/dx and dc/dx are zero, and $p(x)$ reduces to the constant $4\nu k^2/(U + (3/2 - \beta/4)\, c)$. Since capillary wave energy is proportional to rms slope squared, the decay decrement for wave slope is half the above or Δ_v where $U + (3/2 - \beta/4)\, c = c_g$, the group velocity.

For a variable current (3.19) is a function of $U(x)$ which must be determined experimentally. In view of the difficulty in obtaining a compact functional form for equation (3.19) and the approximations implicit in equation (3.17), no closed form integration of equation (3.20) was attempted. Rather, two graphical techniques were employed. In the first case $p(x)$ was plotted on a Cartesian scale, and the integral of $p(x)$ was simply obtained by counting squares under the curve. In this manner a table of values for the definite integral $\int_0^x p(\omega)d\omega$ was obtained. Subsequently, E/E_0 from equation (3.20) was evaluated at each data point and plotted on a semi-logarithmic scale.

Within a constant, the results of these calculations are presented as the solid line in Figure 3.8. Alternately, $p(x)$ was evaluated at the values of x corresponding to each data point. The value of $p(x)$ thus obtained corresponded to the energy logarithmic decrement or simply the slope of $E(x)/E_0$ at each data point. Thus, the solid line in Figure 3.8 can also be interpreted as the tangent to all the predicted decay rates

obtained from p(x). Table 3.4 summarizes the calculations involved to obtain p(x) given the experimentally measured values for the current.

Table 3.4 Numerical calculations involved in the evaluation of equation (3.19)

$U_{cm/s}$	c_i cm/s	$g/\gamma k^2 = \beta$	$4\nu k^2$	dU/dx	dc/dx	p(x)	$2\ell n2/p(x)$
-17	25.879	0.238	2.18	0.1	-0.9038	0.1119	12.379
-16	25.425	0.269	1.93	0.666	-0.25	0.1496	9.260
-14	24.625	0.341	1.52	0.666	-0.236	0.1259	11.00
-12	23.90	0.434	1.197	0.666	-0.19	0.108	12.829
-10	23.496	0.550	0.943	0.666	-0.117	0.0946	14.648
- 8	23.175	0.696	0.746	0.666	-0.10	0.0798	17.38
- 6	23.012	0.875	0.594	0.666	-0.011	0.0706	19.61
- 5	22.987	0.977	0.531	0.125	+0.0357	0.0665	20.86
- 5	22.987	0.977	0.531	0.0	0.0	0.0222	62.30

From the data in Figure 3.8 it can be seen that the decay rate throughout the variable current region is nearly constant, although the wave-number (k) and the current velocity (U) decreases rather rapidly. This effect can be explained by wave-current interaction theory through an examination of equation (3.19). It can be seen that the sum of three terms $(5/2 - \beta)\frac{dU}{dx}$, $(3/2 - \beta/4)\frac{dc}{dx}$, and $4\nu k^2$, jointly divided by the local group velocity, controls the rate of wave decay. At the beginning of the variable current region where U = -16 cm/s, the ratio of attenuation resulting from viscosity to that arising from the gradient

terms, *i.e.*, $R_{vg} = 4\nu k^2/[(5/2 - \beta)\frac{dU}{dx} + (3/2 - \beta/4)\frac{dc}{dx}]$ is $R_{vg} = \frac{1.93}{1.13} = 1.71$, so that for the shorter wavelengths encountered the rate of decay is controlled by viscous dissipation. As a current decreases, however, the wave-number decreases such that at U = -12 cm/s, $R_{vg} = \frac{1.20}{1.11} = 1.08$ which implies that the gradient terms account for nearly half of the apparent rate of decay. For u = -6 cm/s, the ratio $R_{vg} = \frac{0.595}{1.066} = 0.558$ and the effect of viscosity is overshadowed by the gradients. The net effect is that the sum of the three terms $(5/2 - \beta)\frac{dU}{dx}$, $(3/2 - \beta/4)\frac{dc}{dx}$, and $4\nu k^2$ remain roughly constant, and hence the rate of wave decay also remains constant. The data in Figure 3.8 support this observation.

It is important to note, however, that the increased rate of decay from the combined effects of wave-current interaction and viscous dissipation is actually apparent rather than real. That is, the action of the radiation stress is to transfer (conservatively) energy from the wave into the current rather than to dissipate it as is the case with viscosity. This can be shown for the case of pure capillary waves, *i.e.*, $\beta = 0$, by considering equation (3.17) without the term $(4\nu k^2)$ resulting from viscous dissipation, namely,

$$\frac{d}{dx}[E\,(U + 3/2\,c)] + \frac{3}{2} E \frac{dU}{dx} = 0. \qquad (3.21)$$

For pure capillary waves, equation (2.12) reduces to

$$c^2 = \gamma k^2 \quad . \qquad (3.22)$$

Combining equation (3.22) with (3.10), one obtains

$$\frac{c^3}{c_0^3} + \frac{U}{c_0}\,\frac{c^2}{c_0^2} - 1 = 0 \quad , \tag{3.23a}$$

from which it follows that

$$c^2 \frac{dU}{dx} = -2c\,(U + 3/2\ c)\,\frac{dc}{dx} \quad . \tag{3.23b}$$

Multiplying (3.21) by c^3 and combining with (3.23b), one obtains

$$c^3 \frac{d}{dx}\,[E(U + 3/2\ c)] - 3c^2E(U + 3/2\ c)\,\frac{dc}{dx} = 0 \quad , \tag{3.24a}$$

or

$$\frac{d}{dx}\,[E(U + 3/2\ c)/c^3] = 0 \quad . \tag{3.24b}$$

Thus, without viscous dissipation

$$\frac{E(U + 3/2\ c)}{c^3} = \text{const} = \frac{3}{2}\,\frac{E_0}{c_0^2} \tag{3.25}$$

where subscript (0) indicates conditions when $U = 0$.

For a single train of capillary waves, $E = \frac{1}{2}\rho\gamma(ak)^2$ (from equation (3.3)). Substituting into equation (3.25) results in

$$\frac{(ak)^2}{(a_0k_0)^2} = \frac{(\frac{c}{c_0})^3}{\frac{c}{c_0} + \frac{2}{3}\frac{U}{c_0}} = \frac{E}{E_0} \quad . \tag{3.26}$$

E/E_0 as a function of U/c_0 is plotted in Figure 3.9. It can be seen that the wave energy E decreases as $-U/c_0$ tends towards zero ($U/c_0 = 0$). Therefore, the energy is not dissipated as a result of the wave-current interaction. Rather it is simply transferred from the waves into the current. Thus, the vertical distance between the solid and dashed curves in

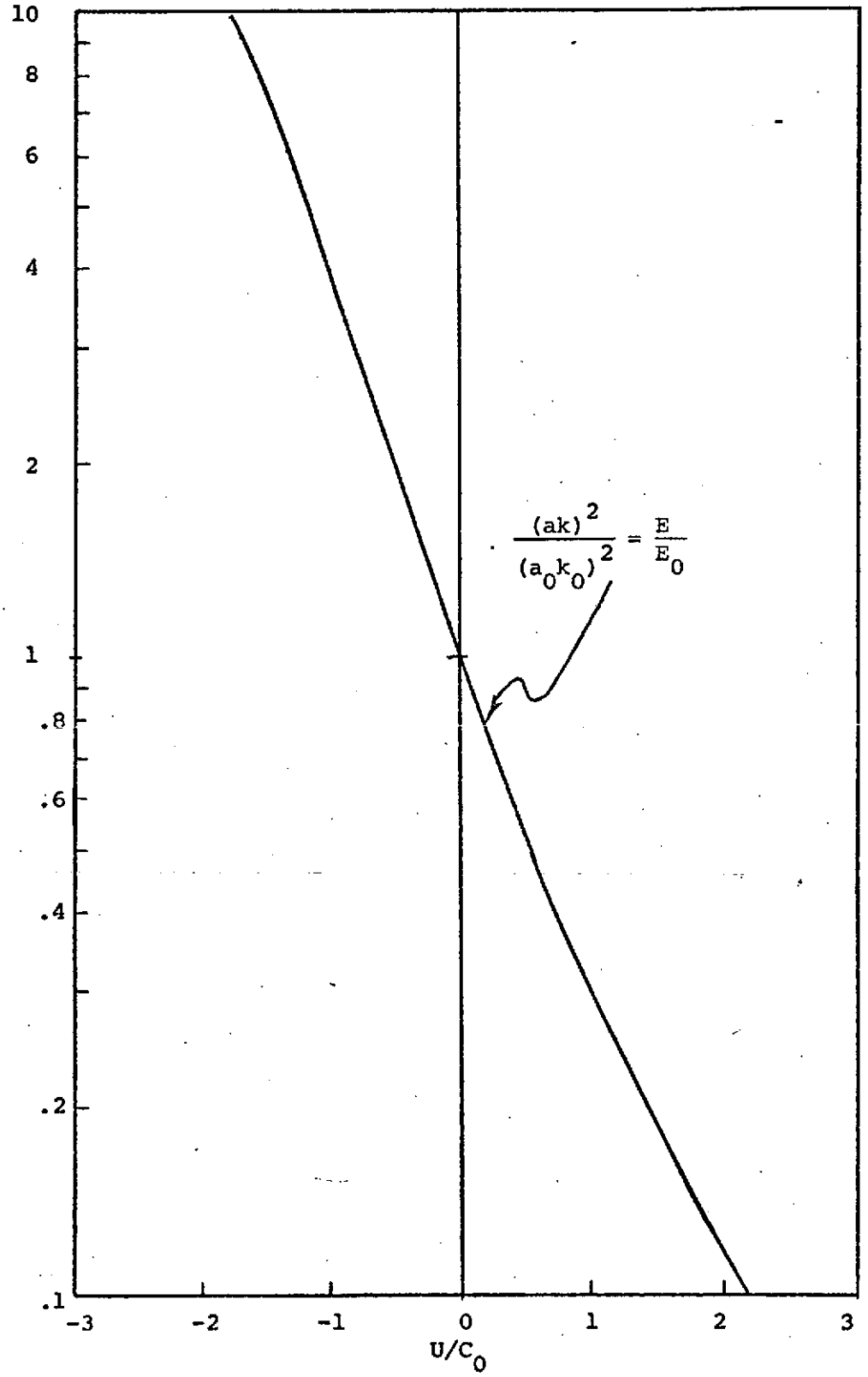

Figure 3.9 Calculated wave-current energy interaction based on current velocity (the curve is a plot of equation (3.26))

Figure 3.8 is a measure of the total energy transferred from the waves into the current. Ideally, if the starting current conditions could be re-established, this portion of the energy would be returned to the waves.

It is concluded that this detail investigation of wave-current interaction with variable currents confirms recent analytical predictions, that is the energy transfered from the wave to the current is exactly that predicted. However, it is probably more important to note that in a variable current the cross waves interact with the current to gain energy while the longitudinal waves interact with the current to loss energy. In physical oceanography one is concerned with the eventual wave state after propagation through a variable current region and these experiments that after a short period in many cases the cross waves will be almost as large as the longitudinal waves. This is considered to be quite an important observation.

4. Experimental Studies of Capillary-Gravity Wave Interaction

4.1 Introduction

In almost all remote sensing techniques a large part of the data (usually backscatter at some angle) occurs or is caused by the short wavelength waves on the ocean surface. Therefore attention must be given the shorter waves and how they effect the data that is obtained. Since these waves have much shorter wavelengths than the longer gravity waves, they may not be uniformly distributed on the longer waves, but may collect at the peak, trough, front or back of the gravity wave. In addition since the waves receive energy and decay at different rates, their relative amplitudes may change as the wave system propagates. Both of the factors, non-uniform distribution of the capillary waves and relative amplitude of the waves will alter the signal obtained by the sensing system. In the ocean there is, of course, a spectrum of wavelengths from the long gravity waves to the shorter capillary waves and thus we are considering the effect the gravity waves will have on the capillary waves. Any changes in the short wave distribution or amplitudes will alter a return signal from these waves.

In order to investigate this a simplified experiment was devised and undertaken. This was to generate a train of gravity waves at a single frequency or wavelength and superimpose on these long waves a uniform series of much shorter wavelength capillary waves (also at a single higher frequency). The composite wave system was measured near the plunger and then measured at various positions of increasing distance from the plunger in an effort to determine how the capillary waves interacted with the gravity waves. This data was analyzed to determine any non-uniformities in the capillary wave distribution and to see if any energy was being transfered between the wave systems. The experimental results are plots of composite wave height at various distances away from the generation source.

4.2 Experimental Technique

The waves were generated by a single plunger that was driven by a signal which was the addition of the two desired waves. Two sine wave generators were used, their signals added electronically and amplified to drive a large permanent magnet loudspeaker. The Speaker was connected to a plunger which was used to generate the waves. Figures 4.1a and 4.1b show a typical signal feed into the amplifier to drive the plunger. This particular signal has a lower frequency of 4 Hertz for the long wave and a frequency of 18 Hertz for the short wave. This signal record shown in Figure 4.1b is .51 sec. in duration and the longer scale Figure 4.1a is 1.25 sec. in duration. Note that the amplitude of the capillary waves is considerably larger than that for the gravity waves, the reason for this will be discussed later. This is the signal used to generate the data shown in Figures 4.3a to 4.3i. Figure 4.2 illustrates the speaker and plunger arrangement used to generate the waves. In order to assure that the plunger accurately reproduces the input signal to the amplifier a positive feedback circuit was employed. Figure 4.2 also shows this feedback circuit.

After generation the waves were measured by the optical wave slope system that we have developed, Sturm and Sorrell (1973). This system used the new electronic detection system and diode matrix that has been recently developed and was described in section two (2) of this report. This system measures wave slope directly and the signal must be integrated to provide wave height. The integrator used to accomplish this is also described in section two (2) and a discussion of the complete method may be found in the paper by Sturm and Sorrell (1973). One consequence of this procedure is that the amplitude scale is not the same for both waves, but varies directly with the phase speed of the wave. This presents no real error however, as the phase speeds are known and if the absolute

ratio of amplitudes is desired, they can be easily scaled. Moreover for the present experiments the amplitude scale was varied in order to show the waves as clearly as possible. Therefore, for all of the data presented, only the relative amplitude of the wave is presented and no absolute amplitudes are given.

Both waves are thus generated at the plunger and are observed at various distances away from the plunger. The waves require some distance from the plunger to reach equilibrium before viscous decay starts. This distance is greater for the gravity waves than the capillary waves, and the intermediate position of 7 cm from the plunger is the first observation point in all cases. By the time the capillary waves reach this distance there has been some decay, however the gravity waves have experienced no amplitude loss. This is the reason the plunger motion for the capillary waves (Figures 4.1a and 4.1b) is larger than that for the longer waves.

A complete discussion of the relevant theory is present in the previous section of the report. However some of the experimentally significant results of the theory are given here. Basically the theory predicts a stronger interaction, that is, the gravity wave will have a greater effect on the distribution and amplitude of the capillary waves, when the phase speed of the gravity wave C_1 is either equal to the phase speed of the capillary wave C_2 or when $C_1 = \frac{3}{2} C_2$. The greatest effect is expected when $C_1 = \frac{3}{2} C_2$ because the energy transfer is at the group velocity and the condition $C_1 = \frac{3}{2} C_2$ corresponds to equal group velocities. Table 4.1 gives the wavelength, frequency and phase speed for a range of capillary, gravity and capillary-gravity waves and is used to facilitate comparison of the wave systems. It is evident from this table that very high frequency capillary waves will be required to meet the condition $C_1 = \frac{3}{2} C_2$. The consequences of this will be considered later.

Table 4.1

Wavelength, Frequency and Phase Speed in the Range of Waves Considered

Wavelength λ (cm)	Frequency f (Hertz)	Phase Speed c (cm/sec)
30	2.28	68.6
20	2.80	56.1
15	3.24	48.7
10	4.01	40.1
8	4.51	36.1
5	5.90	29.5
4	6.80	27.2
3	8.30	24.9
2	11.6	23.2
1.8	12.8	23.07
1.6	14.4	23.07
1.4	16.6	23.26
1.2	19.8	23.74
1	24.7	24.65
.8	32.8	26.26
.6	48.4	29.1
.4	86.3	34.5
.3	131.3	39.4

2.3 Experimental Results

As previously mentioned the experimental results are plots of wave height verses time at increasing distances from the plunger. All data starts at an initial position 7 cm from the plunger. Data from 3 separate conditions is given. These conditions are:

	Gravity or long wave	Capillary or short wave
Run #1	$\lambda_1 = 10$ cm	$\lambda_2 = 1.6$ cm
	$f_1 = 4$ Hertz	$f_2 = 18$ Hertz
	$C_1 = 40$ cm/sec	$C_2 = 23.9$ cm/sec
Run #2	Gravity or long wave	Capillary or short wave
	$\lambda_1 = 5.1$ cm	$\lambda_2 = 1.1$ cm
	$f_1 = 6$ Hertz	$f_2 = 24$ Hertz
	$C_1 = 30$ cm/sec	$C_2 = 24.6$ cm/sec
Run #3	Gravity or long wave	Capillary or short wave
	$\lambda_1 = 5.1$ cm	$\lambda_2 = 0.86$ cm
	$f_1 = 6$ Hertz	$f_2 = 30$ Hertz
	$C_1 = 30$ cm/sec	$C_2 = 25.7$ cm/sec

The data for Run #1 is given in Figures 4.3a to 4.3i, for Run #2 in Figures 4.4a to 4.4e and for Run #3 in Figures 4.6a to 4.6c. A comparison of the present optical wave measurement system with a conventional wave height probe can be obtained from Figures 4.5a and 4.5b, as these data (Figures 4.5a and 4.5b) were taken with a wave height probe. The results are now discussed in more detail.

Run #1

The data were obtained at the following positions from the wave source (plunger).

4.3a	7 cm	4.3e	27 cm
4.3b	12 cm	4.3f	32 cm
4.3c	17 cm	4.3g	37 cm
4.3d	22 cm	4.3h	42 cm
		4.3i	47 cm

The wave system data in 4.3a, 4.3b, and 4.3c shows an even distribution and lends confidence that the waves were generated as expected. In Figure 4.3e there is some evidence that the waves are grouped more in the long wave trough, however 4.3f shows the waves grouped more on the long wave peak. Figure 4.3g and 4.3h show a similar result. At a position 47 cm from the plunger (Figure 4.3i) the capillary waves have almost completely decayed away. The capillary or short waves decay much faster with position than the long waves because they have traveled many more wave lengths in distance. This is another reason the capillary waves were generated with larger relative amplitudes.

The apparent shift in position of the capillary waves from the gravity wave trough to peak and back is believed to be caused by the difference in phase speed of the two wave systems. By the time the group of capillary waves propagate to the next position the gravity wave has propagated approximately 3.4 cm farther than the capillary wave. This places the small waves at a different position on the gravity wave. Indeed this illustrates that unless the gravity wave is sufficiently long for the capillary waves to die out between crests, a group of short waves will change position on the long wave unless the phase speeds are equal. The present wave tank permits wavelengths up to about 12 cm before tank size becomes a problem. Thus the phase speeds must be equal or else a grouping of short waves will shift relative position on the long wave.

Run #2

The figures show data obtained at the following positions from the wave generation source.

4.4a	7 cm	4.4d	17 cm
4.4b	12 cm	4.4e	22 cm
4.4c	17 cm		

Both the long wave and the short wave are at higher frequencies in an attempt to generate waves with the phase speeds more nearly equal. The main feature here is the rapid decay of the capillary waves, and by the time they have traveled 17 cm from the plunger they have nearly vanished. Figure 4.4d is with an expanded time scale to verify this. Data given in 4.4e, which is 22cm from the wave source, contains virtually no short waves.

Because detection of the short waves is marginal at a position 15.5 cm from the source, (Figures 4.4c and 4.4d), this data taken by the optical system was compared with that obtained from a conventional wave height probe. Figure 4.5a and Figure 4.5b (expanded time scale) shows data at identical conditions of Run #2 15.5 cm from the wave source. These data were taken with a capacitive wave height probe which had a probe diameter of 0.25 mm. In these data the capillary wave is completely obscured by the probe. This shows the high resolution of the optical system and the inherent difficulties associated with using a probe system to measure capillary waves.

Run #3

This condition has an even higher capillary wave phase speed in an attempt to determine if the waves group on the long wave peak or trough. Data are shown for three positions:

4.6a	7 cm
4.7b	12 cm
4.6c	17 cm

Figure 4.6a demonstrates that the waves are generated as desired and that there is ample capillary wave content. Figure 4.7b shows considerable capillary wave decay, and at a distance 17 cm from the wave source the capillary waves are no longer observable. This demonstrates the inherent problem with attempting to generate both a long wave and a short wave with the same phase speed. As the short wave length is

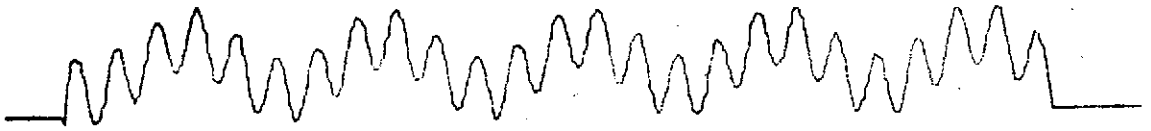

(a) Trace duration = 1.28 sec

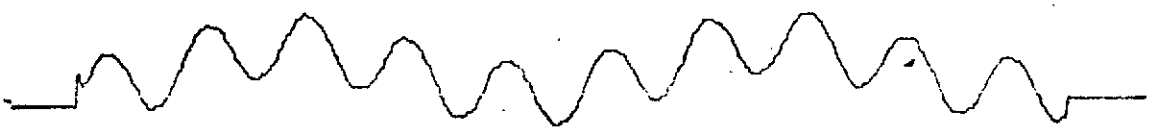

(b) Trace duration = 5.1 sec

Figure 4.1 Input to wave generator Run #2, $f_1 = 4$, $f_2 = 18$.

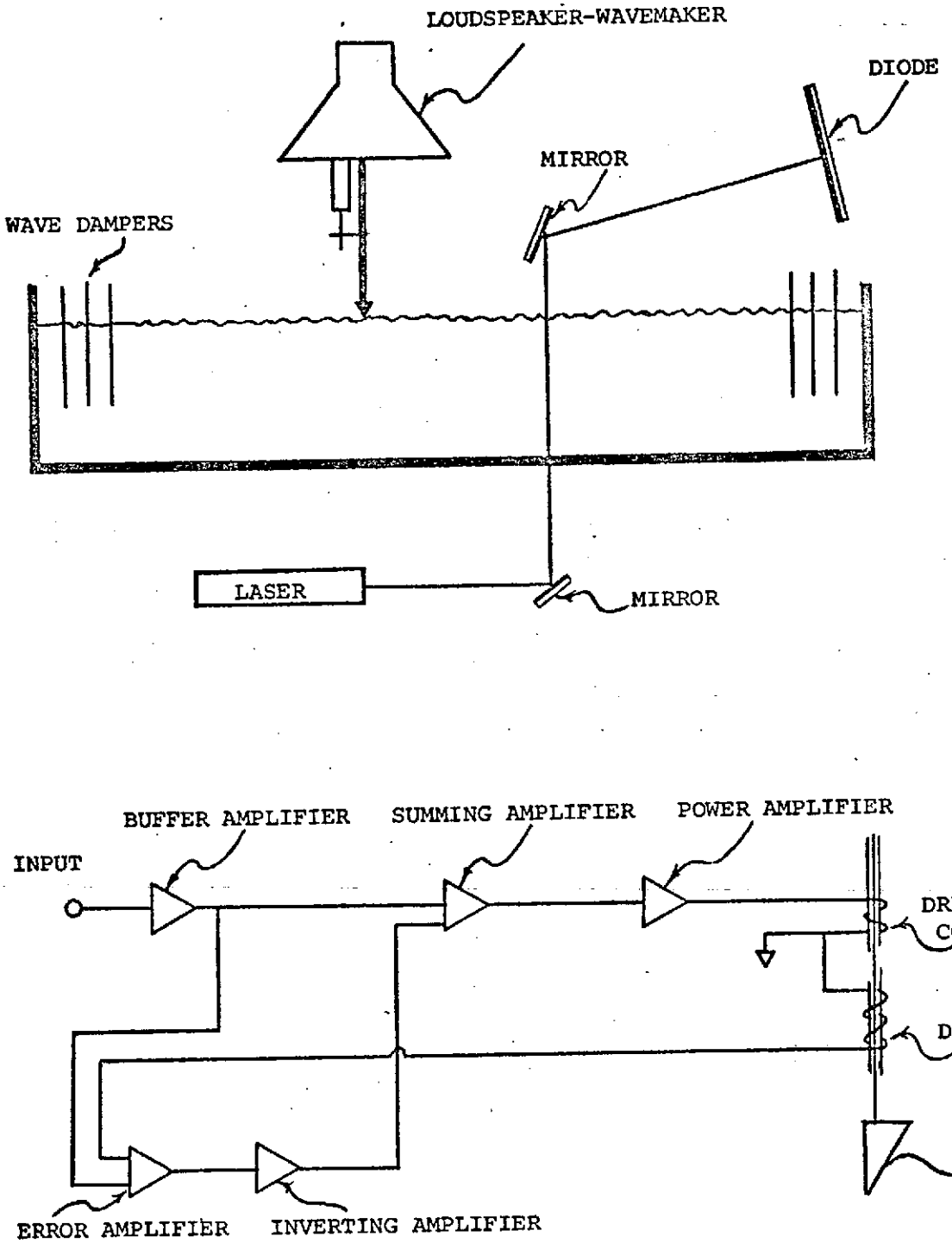

Figure 4.2 Schematic representation of the experimental facility and wavemaker control circuit

(a) 7 cm from wave source

(b) 12 cm from wave source

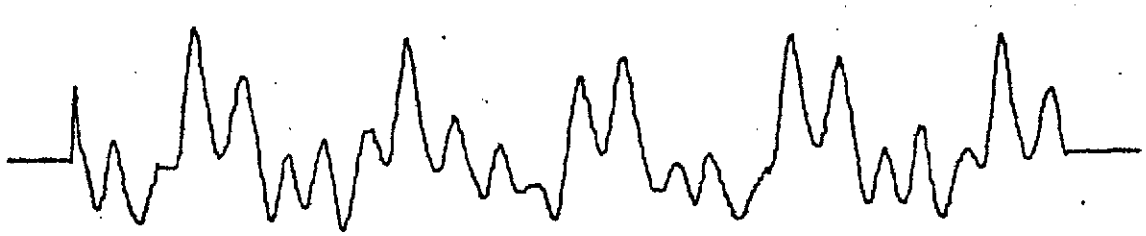

(c) 17 cm from wave source

Figure 4.3 Data from Run #1

(d) 22 cm from wave source

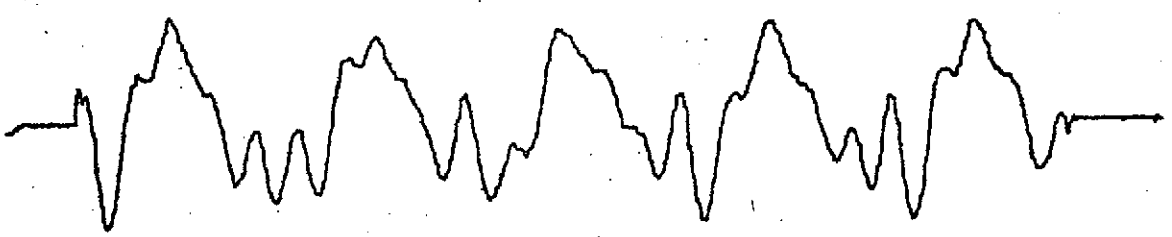

(e) 27 cm from wave source

(f) 32 cm from wave source

Figure 4.3 (cont.) Data from Run #1

(g) 37 cm from wave source

(h) 42 cm from wave source

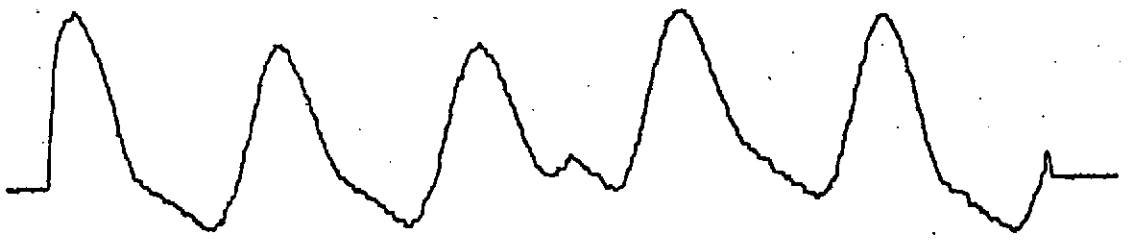

(i) 47 cm from wave source

Figure 4.3 (cont.) Data from Run #1

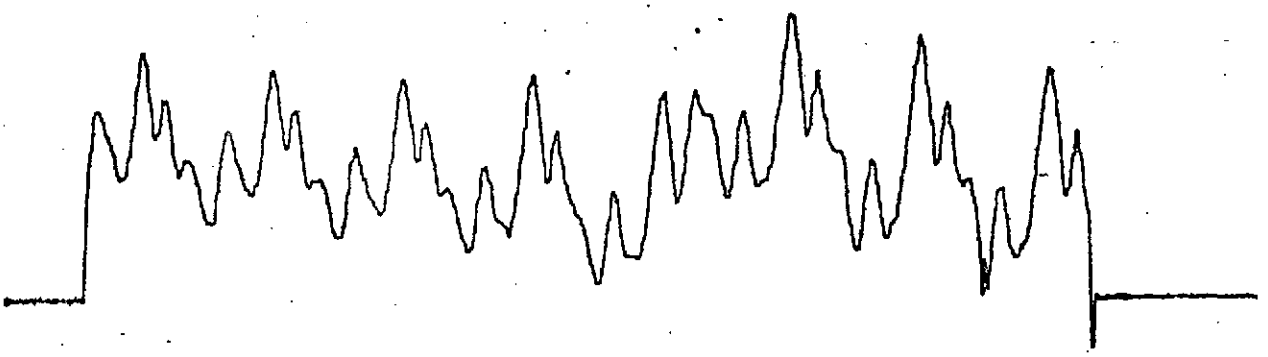

(a) 7 cm from wave source

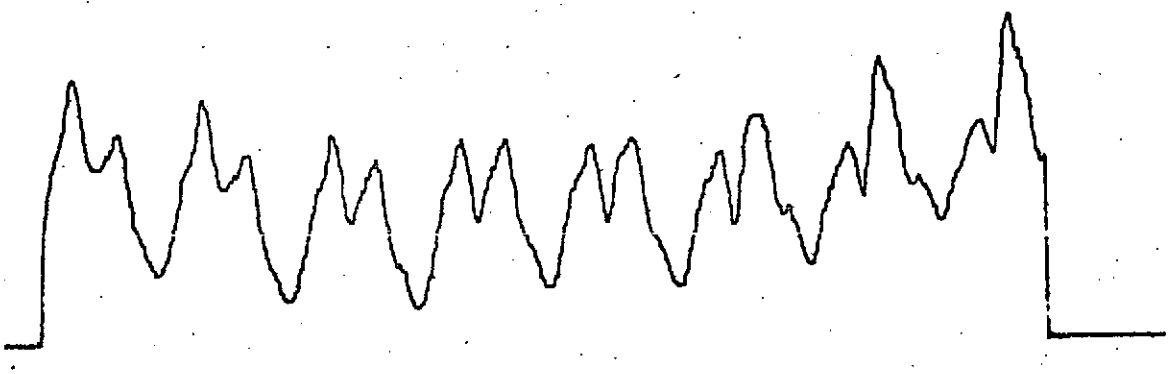

(b) 12 cm from wave source

(c) 15.5 cm from wave source

Figure 4.4 Data from Run #2

(d) 15.5 cm from wave source
expanded time scale

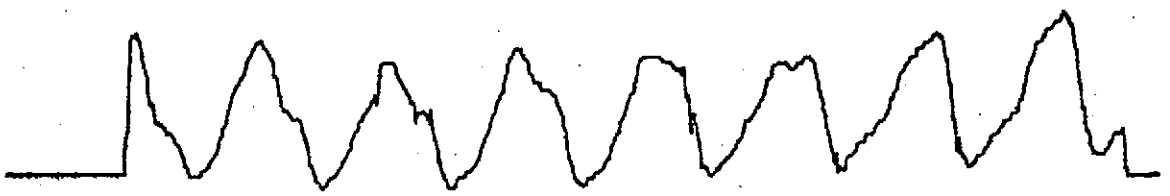

(e) 17 cm from wave source

Figure 4.4 (cont.) Data from Run #2

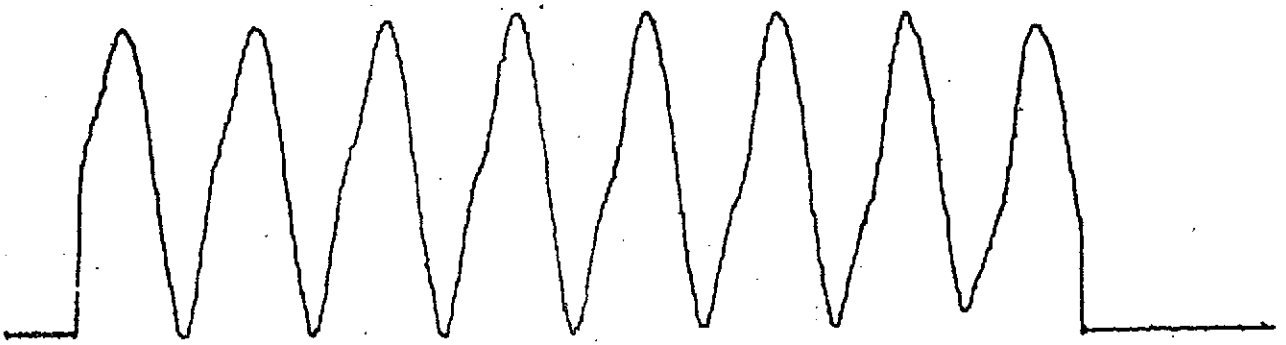

(a) Trace duration = 1.28 sec

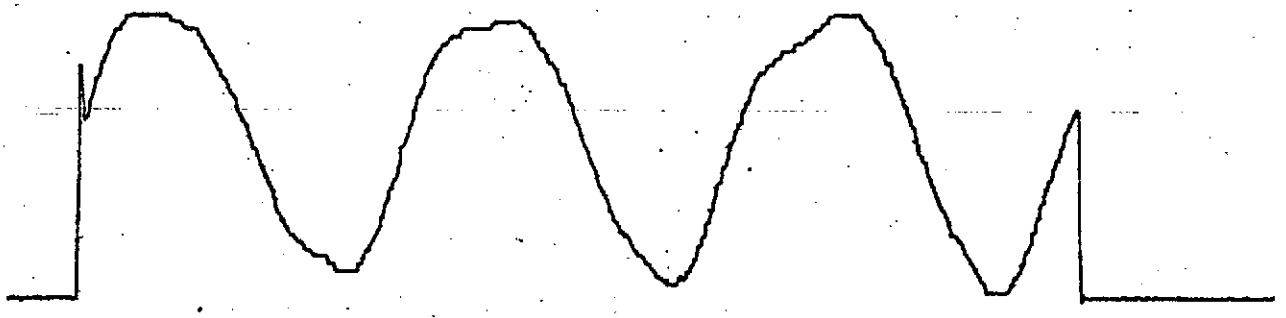

(b) Trace duration = 5.1 sec

Figure 4.5 Data from wave height probe Run #2, 15.5 cm from source

(a) 7 cm from wave source

(b) 12 cam from wave source

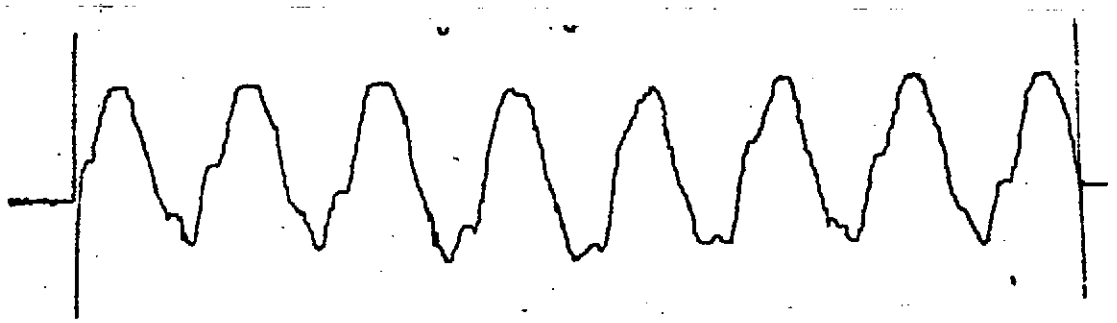

(c) 17 cm from wave source

Figure 4.6 Data for Run #3

reduced in order to increase the phase speed, the wave decays very rapidly. If an attempt is made to produce shorter long waves with lower phase speeds, the distinction between long and short waves is lost.

4.4 Summary and Conclusions

A simple experiment was undertaken to investigate the interaction between long gravity waves and much shorter capillary waves. The experiment was to generate both wave systems and to observe the effect of the long wave on the shorter capillary wave. Run #1 shows the difficulty in analyzing the results when phase speeds of the two wave systems are different. Run #2 indicates the rapid decay of the shorter waves with increasing frequency and compares the present optical system for data acquisition with the conventionsl wave height probe. This illustrates the necessity of using the optical system. Run #3 verifies the rapid decay of high frequency capillary waves and shows that it is probably not possible to generate a distinct long wave and short wave with the same phase speed and have the composite wave system last for any appreciable length of time or distance of propagation.

For these observations it appears that a system of wind driven waves, or possibly plunger and wind driven waves are necessary for the experiments. If the short waves are wind generated, then it should be possible to continuously add energy to the short waves so they do not decay or at least do not decay so rapidly. With this approach the long waves could be plunger generated and the short wave generated and sustained by the wind. Under these conditions it should be possible to generate and measure long waves and short waves which have the same phase speed.

5. Preliminary Wind-Wave Measurements

5.1 Introduction

The previous sections present the results of measurements of waves generated by a wave maker or plunger. Waves generated in this manner have definite periods or wave lengths, and thus it is meaningful to describe the wave by these characteristics. However, wind generated waves are random and thus the only meaningful data are some form of wave statistics or average properties of the waves. Because radar backscatter is primarily influenced by surface roughness and also because the high frequency components are important, results in the form of wave slope spectra are the most useful. These data can be obtained with the optical wave measurement system described in Part 2 of this section. Preliminary results of wave slope spectra for different conditions of current and wind speed are given in Figures 5.1, 5.2, 5.3, and 5.4. These results demonstrate a strong relation between current and slope spectra.

5.2 Data

The data for the accompanying figures was obtained in the wind-wave tank at N. C. State University. This tank is 2 ft. x 3 ft. in cross section and has a fan capable of generating winds to 40 m/sec. In addition a pump system has been installed to produce mean water currents. This system permits the generation of wind waves and the investigation of changes in wind-wave statistics due to a current.

The data were obtained by recording the output of the optical wave measurement system on magnetic tape. The tape system has a FM record and playback mode so that low frequency waves can be recorded. Data are recorded for a length of time sufficient to obtain the desired amount and then played back through an audio spectrum analyzer. Because the analyzer requires frequencies above

20 Hertz (audio frequency) the tape speed is increased by a factor of 16 when played back into the spectrum analyzer. This gives a low frequency limit of 1.25 Hertz in the slope spectra. The output of the spectrum analyzer is then recorded on an x-y plotter. The data given in 5.1, 5.2, 5.3, and 5.4 are the analyzer output as plotted. These spectra shows considerable fine scale structrue. In order to get a better picture of this structure several spectra are plotted on top of each other. This shows the repeatibility of the spectra and also shows if a particular fine structure characteristic of the spectra or random. These slope spectra are basically plots of the relative magnitude of the RMS slope within specified frequency bands. They are taken with a wind speed of 2 m/sec at zero water current and with a mean water current of 10 cm/sec in the direction of the wind. Figures 5.1 and 5.2 are wave slope spectra down the channel, that is, slope spectra in the direction of the wind or current. The shift of the spectrum is in quantitative agreement with the theory developed by Huang, et. al. (1972). Generally it shows that a positive current shifts the wave energy toward the lower frequencies. The data given in Figures 5.3 and 5.4 are slope spectra across the channel. These have less energy content and, in addition, both the downwind and cross wind spectra with the positive current show less energy transfer from the wind than when there is no current. Therefore it is not meaningful to compare the relative total energy content of the two spectra. The data show the expected strong dependence of wave spectra on current.

Reproduced from best available copy.

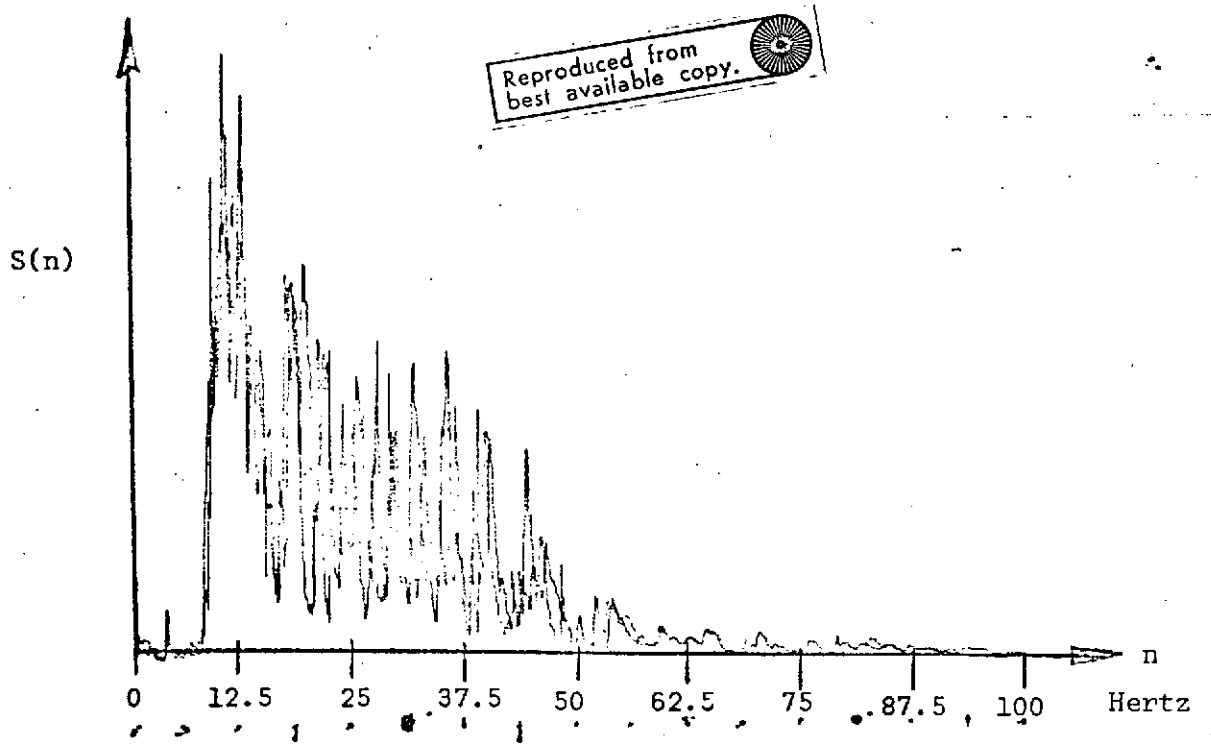

Figure 5.1 Downwind slope spectra
Wind = 2 m/sec Current = 0 cm/sec

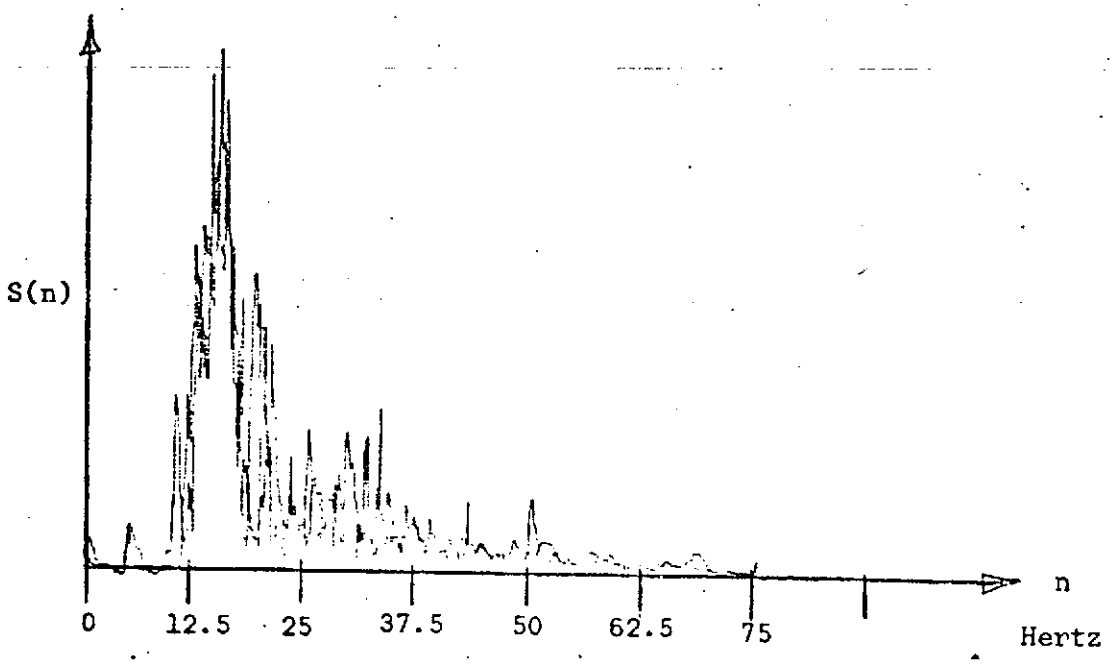

Figure 5.2 Downwind slope spectra
Wind = 2 m/sec Current = 10 cm/sec

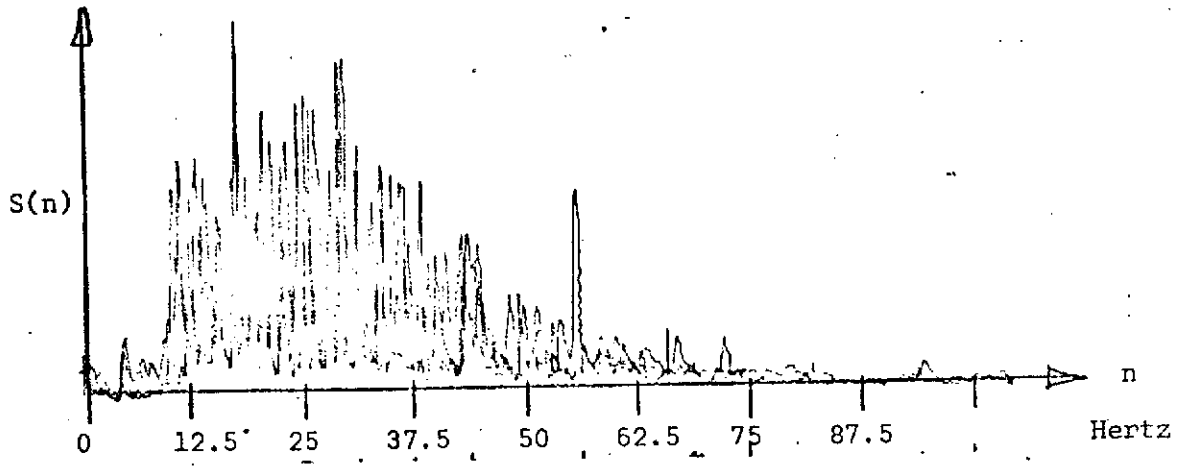

Figure 5.3 Crosswind slope spectra
Wind = 2 m/sec Current = 0

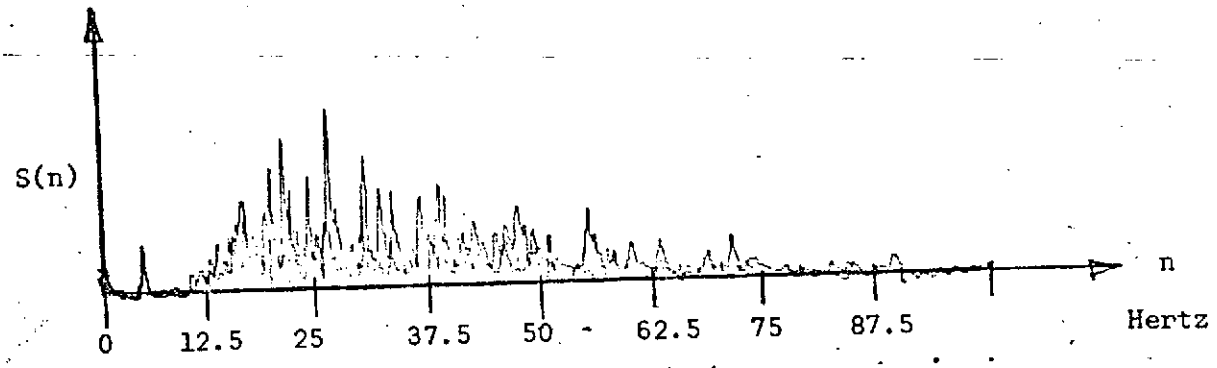

Figure 5.4 Crosswind slope spectra
Wind = 2 m/sec Current = 10 cm/sec

REFERENCES

1. Cox, C. S. (1958). "Measurements of Scopes of High Frequency Wind Waves," Jour. of Marine Research, Vol. 16, p. 199-225.

2. Cox, C. S., and W. H. Munk (1954). "Measurement of the Roughness of the Sea Surface from Photographs of the Sun Glitter," Jour. Opt. Soc. of Amer., Vol. 44, p. 838-850.

3. Davies, J. T., and R. W. Vose (1965). "On the Damping of Capillary Waves by Surface Films," Proc. Royal Soc., London A286, p. 218.

4. Hunag, Norden E., Dvaidson T. Chen, Chi-Chao Tung, and James R. Smith (1972). "Interactions Between Steady Non-Uniform Currents and Gravity Waves with Applications for Current Measurement," J. Phy. Oceanography, Vol. 2, p. 420.

5. Hulburt, E. O. (1934). "The Polarization of Light at Sea," Jour. of Opt. Soc. of America., Vol. 24, p. 35-42.

6. Mahoney, J. J, B. J. S. Barnard, and W. G. Pritchard (1972). "Cross Waves, Part 1 and Part 2", J. Fluid Mech., Vol 55, p. 229.

7. McGoldrick, L. F. (1970). "An Experiment on Second-Order Capillary-Gravity Resonant Wave Interactions," J. Fluid Mech., Vol. 40, p. 251.

8. McGoldrick, L. F. (1971). "A Sensitive Linear Capacitance-to-Voltage Converter, with Applications to Surface Wave Measurements," Rev. Sci. Instruments, Vol. 42, p. 359.

9. Phillips, O. M. (1966). The Dynamics of the Upper Ocean, Cambridge Univ. Press, London, England.

10. Prettyman, C. E., and M. D. Cermak (1969). "Time Variation of the Rough Ocean Surface and its Effect on an Incident Laser Beam," IEEE Trans. Geo. Sci. GE-7, p. 235-243.

11. Schooley, A. H. (1954). "A Simple Optical Method for Measuring the Statistical Distribution of Water Wave Slopes," Jour. Opt. Soc. of Amer., Vol. 44, p. 34-40.

12. Sturm, G. V., and F. Y. Sorrell (1973). "Optical Wave Measurement Technique and Experimental Comparison with Wave Height Probes," Applied Optics, Vol. 12, No. 8, p. 1928-1933.

13. Tober, G., R. C. Anderson, and O. H. Shemdin (1973). "Laser Instrument for Detecting Water Ripple Slopes," Applied Optics, Vol. 12, p. 788-794.